INFORMATION TO USERS

This manuscript has been reproduced from the microfilm master. UMI films the text directly from the original or copy submitted. Thus, some thesis and dissertation copies are in typewriter face, while others may be from any type of computer printer.

The quality of this reproduction is dependent upon the quality of the copy submitted. Broken or indistinct print, colored or poor quality illustrations and photographs, print bleedthrough, substandard margins, and improper alignment can adversely affect reproduction.

In the unlikely event that the author did not send UMI a complete manuscript and there are missing pages, these will be noted. Also, if unauthorized copyright material had to be removed, a note will indicate the deletion.

Oversize materials (e.g., maps, drawings, charts) are reproduced by sectioning the original, beginning at the upper left-hand corner and continuing from left to right in equal sections with small overlaps.

Photographs included in the original manuscript have been reproduced xerographically in this copy. Higher quality 6" x 9" black and white photographic prints are available for any photographs or illustrations appearing in this copy for an additional charge. Contact UMI directly to order.

Bell & Howell Information and Learning
300 North Zeeb Road, Ann Arbor, MI 48106-1346 USA
800-521-0600

Université d'Ottawa • University of Ottawa

PETROGRAPHIC AND GEOCHEMICAL STUDIES OF THE ALTERATION ZONES ASSOCIATED WITH GOLD MINERALIZATION AT THE HOLLOWAY MINE, SOUTHWESTERN ABITIBI GREENSTONE BELT, CANADA

by

Jean Claudia Ropchan

A thesis submitted to the School of Graduate
Studies in partial fulfillment of the requirements
for the degree of M. Sc. in Earth Sciences

OTTAWA-CARLETON GEOSCIENCE CENTRE
UNIVERSITY OF OTTAWA

ABSTRACT

The Holloway mine is an Archean lode gold deposit hosted within the southwestern Abitibi greenstone belt. Rocks hosting the deposit are bounded by two main branches of the Destor-Porcupine fault zone and belong to the Destor Porcupine Complex. The Destor Porcupine Complex is correlated along strike with pre-Timiskaming age meta-volcanic rocks and Timiskaming meta-sediments.

Meta-volcanic rocks of the Destor Porcupine Complex were tested using the Treuil method and shown to belong to a tholeiitic suite that differentiated via fractional crystallization producing three distinct groups: tholeiitic meta-basalts, Fe-tholeiitic meta-volcanic rocks, and variolitic meta-volcanic rocks. The least evolved tholeiitic meta-basalts have flat-lying REE profiles approximately equal to 10 times chondrite. Tholeiitic meta-basalts are characterized by Fe/Mg = 2, and relatively higher compatible elements such as Al, V, and Ni. Intermediate Fe-tholeiitic meta-volcanic rocks differentiated via 70-80% fractional crystallization of a tholeiitic meta-basalt magma source. The Fe-tholeiitic meta-volcanic rocks are characterized by Fe/Mg = 8, relatively high concentrations of incompatible elements such as Th and Zr, and flat-lying REE profiles around 50 times chondrite values. 85-92% fractional crystallization of the tholeiitic magma source produced highly evolved 'felsic' meta-volcanic rocks with flat-lying REE profiles equal to 100 times chondrite values. The variolitic meta-volcanic rocks have the highest concentration of incompatible elements and Fe/Mg = 8.

Alteration at the Holloway deposit consists of a silicified and albitized core surrounded by halos of sericite and carbonate alteration. Carbonate alteration is composed mainly of ankerite and appears pervasive due to many overlapping hydrothermal events. The silicified-albitized core of the hydrothermal system is centred on the variolitic meta-volcanic rocks at the ultramafic-mafic footwall contact. Sericite alteration is expressed in the ultramafic rocks as fuchsite, and in the mafic rocks it clearly defines foliation. Sericite alteration corresponds to elemental increases of CO_2, K_2O, Rb, Ba, Cs, Sb, and sometimes Au, S, As, and W.

Lightning Zone mineralization is the earlier of two gold mineralizing events. It is associated with fine-grained disseminated pyrite and hosted by silicified and albitized variolitic meta-volcanic rocks having variolitic and hyaloclastite textures. A non-mineralized cross-cutting dyke places an upper age limit for Lightning Zone mineralization at 2672 Ma. The second mineralizing event, vein-type mineralization, is vein-associated and commonly occurs within massive Fe-tholeiitic meta-volcanic rocks. Results from statistical factor analysis show that gold-bearing hydrothermal fluids contain S, W, and sometimes As. Both episodes of gold mineralization only occur within meta-volcanic rocks that have a Fe/Mg = 8.

SOMMAIRE

La mine Holloway est un gisement filonieu d'or Archéen, hébergé dans la ceinture de Roches Vertes du Sud-Ouest de L'Abitibi. Les roches hôtes sont limitées par les deux ramifications principales de la faille destor Porcupine, et appartiennent au complexe Destor Porcupine. L'Orientation de ce complexe est identique à celle des Roches métavolcaniques de Kidd-Munro et celle des méta-sédiments de Timiskaming.

Les Roches méta-volcaniques du complexe Destor Procupine ont été analysé grâce à la méthode Treuil et montrent leur appartenance à une suite tholeiitique differenciée via une cristallisation fractionnée qui a produit 3 groupes distincts: des méta-basaltes tholéiitiques, des roches méta-volcaniques fe-tholéiitiques et des roches méta-colcaniques variolitiques. Les mèta-basaltes les plus differenciés possédent des profils REE plats et sont aproximativement égaux à 10 fois celui de la chondrite. Les mèta basaltes tholéitiques sont caracterisés par Fe/Ng=2, et possédent une plus haute abondance en éléments tels que Al, V et Ni.

Les Roches mèta-volcaniqes Fe-tholeitiques intermèdiaires ont été differencié par 70.80 % de cristallisation fractionnée d'une source magmatique mètabasaltique tholéiitique.

Les roches métavolcaniques Fe-tholéitiques sont caractérisées par Fe/Ng=8, et possédent des abondances relativemeut élevées en élements incompatibles tels que Th et Zr, et leurs profils REE correspondent à peu près á 50 fois les valeurs de la chondrite.

85 à 92% de cristallisation fractionnée du magma tholéiitique source a produit un fort développement de roches métavolcaniques 'felsiques' avec des profils REE égaux à 10 fois les valeurs de la chondrite. Les roches méta-volcaniques variolitiques ont la plus haute concentration en éléments incompatibles et possèdent un Fe/Mg=8.

L'Altération du gisement filonieu Holloway consiste en un coeur silicifié et albitisé par des halos d'altération carbonatée est composée principalement d'Ankerite et apparaît pènètrante due aux nombreux systemes hydrothermaux successifs. Le coeur silicifié-Albitisé du système hydrothermal est centré sur les roches mèta-volcaniques variolitiques au niveau du contact métamafique-mafique.

L'Alteration en sercite (= la sèricitisation) est expimée dans les roches ultra mafiques telles que la fuchsite, et dans les roches mafiques, cette altération définit clairement une foliaton. La séricitisation correspond à une augmentation en éléments CO_2, K_2O, Rb, Ba, Cs, et parfois en Au, S, As, et W.

La zone minéralisée est la première de 2 événements de minéralisation d'or. Elle est associée à des grains fins de pyrite disséminés et contenus dans les roches méta-volcaniques variolitiques avec des textures hyaloclastiques.

Un dyke non minéralisé en travers se met en place a un âge supérieur limité par la zone minéralisé à 2672Ma. Le second èvènement de minéralisation, de type minéralisation filonienne, est associé aux roches métavolcaniques fe-tholéiitiques massives. Les résultats d'une analyse statistique montrent que les fluides hydrothermaux permettant la mineralisation en or, contiennent S, W et parfois As. Les deux épisodes de minéralisation d'or se sont déroulés seulement dans les roches méta-volcaniques qui possèdent un rapport Fe/Mg=8.

TABLE OF CONTENTS

LIST OF TABLES

LIST OF FIGURES

LIST OF PLATES

CHAPTER ONE: INTRODUCTION

Gold showings are abundant along Highway 101 between Matheson, Ontario and the Quebec border. The Holloway mine is located on the north side of Highway 101, approximately 15 kilometres west of the Quebec border opposite the Holt-McDermott mine on the south side of Highway 101. Holloway mine is 700 kilometres north of Toronto, 720 kilometres northwest of Ottawa, 130 kilometres east of Timmins, and 65 kilometres north of Kirkland Lake (figure 1.1). It is not uncommon in the region to have two gold deposits in such close proximity, however, the contrasting styles of mineralization are noteworthy. Ore zones at the Holt-McDermott mine are centered on dykes within and outside faults, whereas ore zones in the Holloway mine are located along lithologic contacts and intrusive rocks are rare (Couture & Robert, 1997). The dominant types of alteration minerals at Holt-McDermott include albite and ankerite (Couture & Robert, 1997). Holloway ore is hosted within quartz-albite-pyrite-altered Fe-tholeiitic meta-volcanic rocks surrounded by haloes of sericite and ankerite alteration. Also in contrast to Holt-McDermott, wherever hematite alteration occurs at the Holloway mine, ore grades are insignificant.

There is little outcrop in the study area, and recent mapping by Berger (1997) relied on the use of diamond drill core. Topography in the area is gentle with a maximum relief of 3-4 metres over 50 metre horizontal distance. Overburden is 10-15 metres thick and consists of lacustrine varved clays overlying a basal sandy to bouldery till (Broughton *et al.*, 1991). Vegetation in the area is a mixed forest of poplar, birch, black and white spruce and balsam, with low ground consisting of tag alder swamp.

1.1 REGIONAL GEOLOGY

The Superior Province is the largest Archean craton in the world, comprising an area of 1,572,000 km^2 (Thurston, 1991). It is unique because it contains linear, fault-bounded subprovinces that are divided into four tectonostratigraphic classifications: volcanic-plutonic

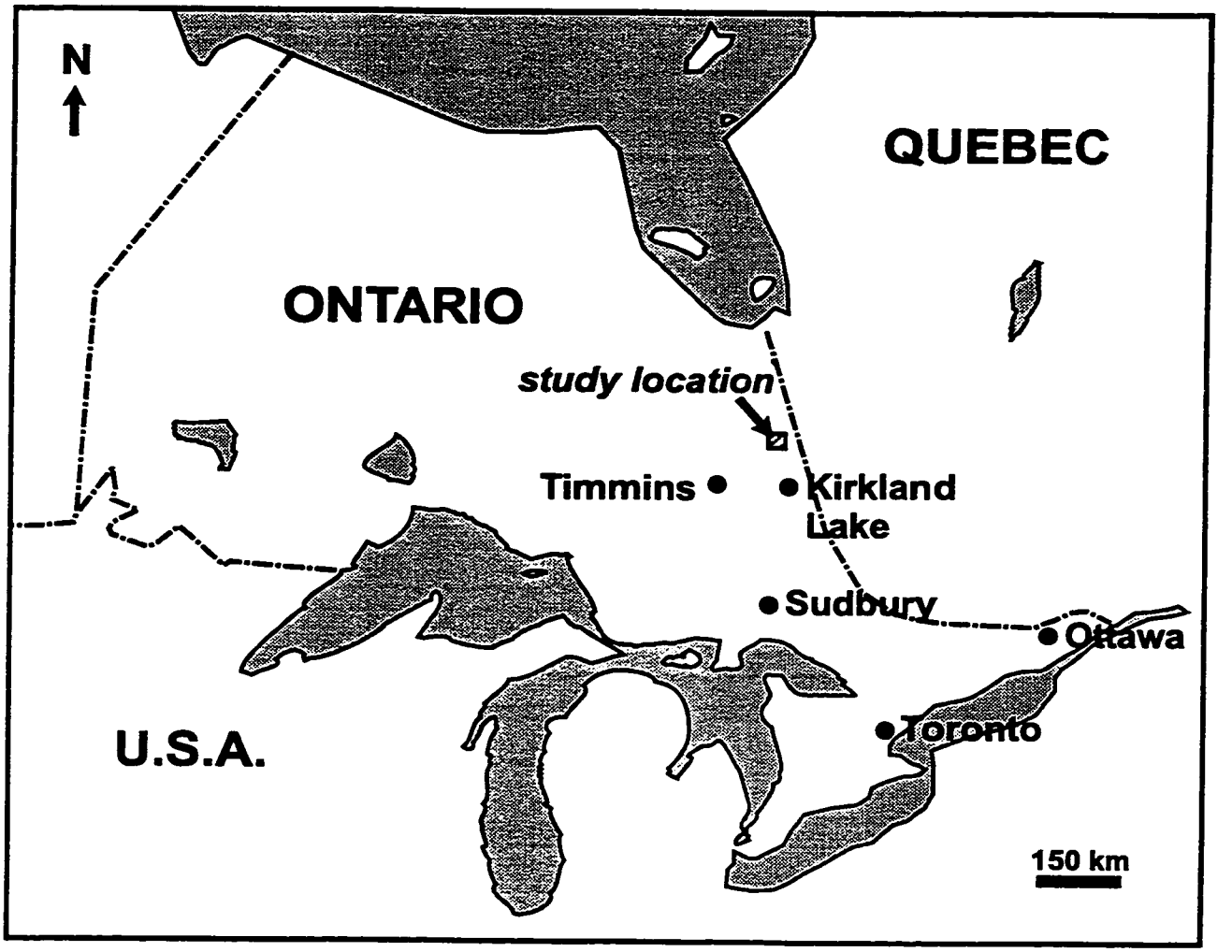

Figure 1.1: Location map for the Holloway deposit.

(greenstone belts), meta-sedimentary, plutonic and high-grade gneiss (Thurston, 1991). The Holloway deposit is located in the southwestern Abitibi greenstone belt. The study of Archean rocks is important because they host many economic ore deposits. Identifying, describing and interpreting Archean rocks is essential to the field of exploration geology. In the early 1990's, the southwestern Abitibi greenstone belt was the most intensely explored greenstone subprovince in Canada (Thurston, 1991).

The Superior Province is special because the greenstone belts contain a diversity of supracrustal environments, and a notable feature of the southwestern Abitibi greenstone belt is that it contains a high proportion of supracrustal rocks compared with intrusive rocks relative to other subprovinces (Thurston, 1991; Corfu, 1993). Regional metamorphism in the Abitibi subprovince generally reached only lower and middle greenschist facies except in some locations, near major faults and batholiths, where fluid flow and contact metamorphism have further increased the grade of metamorphism. Regional deformation zones, including the Cadillac-Larder Lake and Destor-Porcupine fault zones, separate east-west trending lithostratigraphic units (Jensen & Langford, 1985). Intrusions of felsic porphyries and mafic dykes are concentrated along the fault zones (Broughton *et al.*, 1991). The Holloway deposit, along with several other gold showings, occur along these fault zones (figure 1.2).

Jensen and Langford (1985) adhered to early vertical tectonic models for the development of the Archean Abitibi greenstone belt in the Kirkland Lake area. They attributed the stratigraphy to volcanic cycles that were subsequently folded and faulted into their current configuration. Later, Corfu (1993) dated Abitibi greenstone belt development between 2750 to 2670 Ma and divided the time into periods based on dominant tectonic activity. Jackson *et al.* (1994) further contributed to Corfu's classification scheme by dividing the southwestern Abitibi greenstone belt into five principal supracrustal assemblages: IRON-, THOLKOM-, INTFEL-, TURB- and, ALUFLU-types. These later tectonic models rely heavily on plate tectonic models, and describe microplate interactions to account for diverse formational environments prior to accretion. Most recently, Heather (1998) interpreted that the original

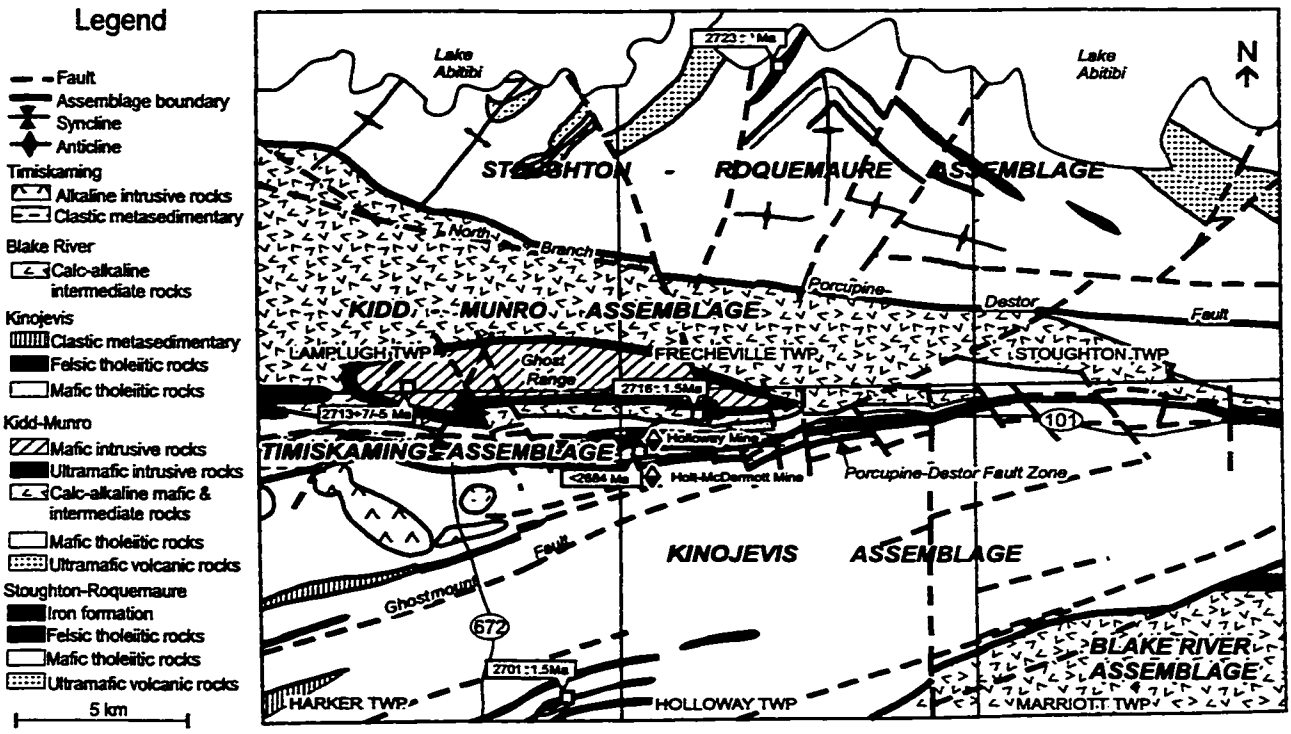

Figure 1.2: Geologic map of the southwestern Abitibi greenstone belt (Ayer *et al.*, 2000).

'vertical' tectonic model is more valid, where assemblages are erupted in situ and later folded and faulted. The succession of rocks in the area of the Holloway deposit belong to the north limb of a large (75 X 150 km), east-plunging synclinorium (Jensen & Langford, 1985). Figure 1.3 features an idealized stratigraphic column for rocks in the north, central and south segments of the southwestern Abitibi greenstone belt.

The Hunter Mine group (Jensen & Langford, 1985), now redefined as the Kidd-Munro assemblage (Ayer *et al.*, 1999), comprises the oldest rocks in the mine area, cropping out north of the Holloway deposit (figure 1.2). Mortensen (1987) dated a quartz-feldspar porphyry dyke from the Hunter Mine assemblage about 30 kilometres east of the Holloway mine, in Quebec, at 2730 ±1.5 Ma. This part of the Hunter Mine group is now re-defined as part of the Deloro assemblage, and is comprised of calc-alkaline rocks that conformably underlie the Stoughton-Roquemaure assemblage (Ayer *et al.*, 1999). Dostal and Mueller (1996) found that Hunter Mine meta-basaltic rocks display subduction-related characteristics with a negative Nb anomaly and enrichment of LILE and LREE and that they are enriched in Ti, Ni and Cr relative to typical volcanic arc tholeiitic basalts. Dostal and Mueller (1996) characterize the Hunter Mine group as a deep-water felsic-dominated edifice resting on the sea floor.

The Stoughton-Roquemaure, Kidd-Munro, and Kinojevis assemblages belong to Jackson *et al.*'s (1995) THOLKOM-type of supracrustal assemblage. Tholeiitic meta-basalt and/or meta-komatiite rocks dominate THOLKOM-type assemblages which vary widely in the proportion of tholeiitic meta-basalt, meta-komatiite, mafic-ultramafic intrusions, and intermediate to felsic meta-volcanic rocks (Jackson *et al.*, 1994). These THOLKOM-type assemblages were deposited between 2720-2700 Ma, which Corfu (1993) describes as a period of extensional magmatism with compositions of komatiite, tholeiite and calc-alkaline affinity. The rocks of this assemblage are interpreted by means of geochemistry to have formed in an ensimatic environment (Jackson *et al.*, 1994). Modern analogues would be mid-ocean ridges and back-arc basins. According to the tectonostratigraphic model of

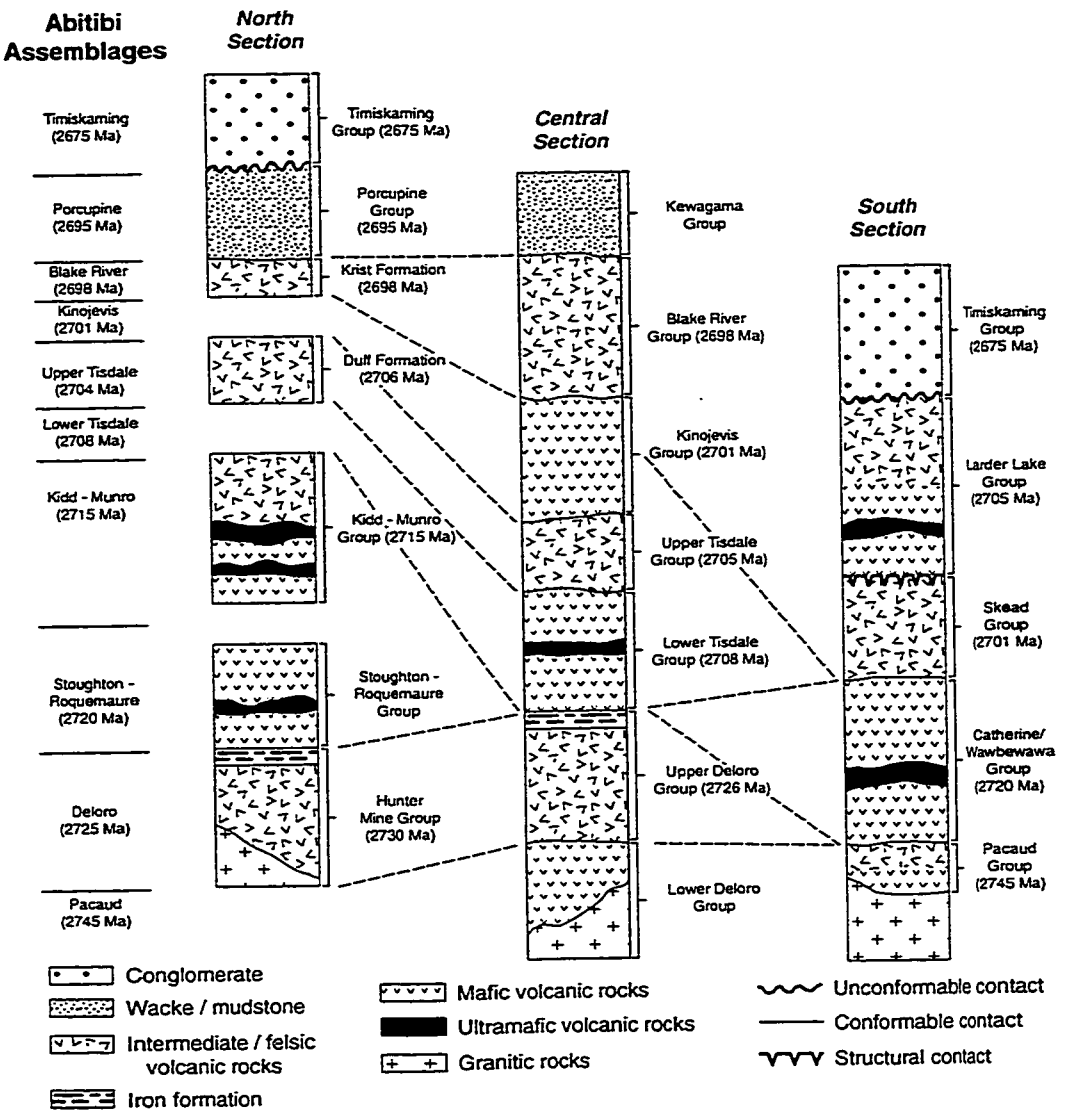

Figure 1.3: Idealized stratigraphic column for rocks of the north, central, and south sections of the southwestern Abitibi greenstone belt (Ayer *et al.*, 1999).

Jackson *et al.* (1994), tholeiitic basalt to komatiite rocks are found at axial sites of extension, while felsic plus intermediate rocks are believed to have formed in a thicker crustal environment at off-axis sites of extension (Jackson *et al.*, 1994). Lesher *et al.* (1986) state that felsic rocks in this assemblage are likely due to partial melting of existing crust.

The Stoughton-Roquemaure assemblage is characterized by Mg- and Fe-tholeiitic meta-basalt sequences with localized meta-komatiites and felsic meta-volcanic units. Ayer *et al.* (1999) give the Stoughton-Roquemaure an age of 2720 Ma. A concordant U-Pb zircon age date of 2714 ±2 Ma was obtained for a rhyolite at the base of the Kidd-Munro about 50 km west of the mine in Beatty Township (Corfu *et al.*, 1989).

The Kidd-Munro (2715 Ma) assemblage is re-defined by Ayer *et al.* (1999) to include a Mg- and Fe-tholeiitic meta-basalt to meta-komatiite suite and a calc-alkaline suite of intermediate to felsic pyroclastic rocks. Berger and Amelin (1999) report a concordant U-Pb zircon age date of 2716 ±1.5 Ma for a calc-alkaline tuff breccia sampled less than 2 km north of the Holloway deposit from drill core.

The Kinojevis (2701 Ma) assemblage is characterized by tholeiitic mafic meta-volcanic rocks with thin felsic flows near the upper portion of the assemblage (Ayer *et al.*, 1999). A flow banded rhyolite correlated with the Kinojevis assemblage collected from Harker Township, about 10 km southwest of Holloway deposit, gives a concordant U-Pb zircon age of 2701 ±1.2 Ma (Berger & Amelin, 1999).

The Blake River (2698 Ma) assemblage is characterized by calc-alkaline mafic to felsic meta-volcanic rocks in Ontario and includes tholeiitic meta-basalt and FIII-type rhyolite in Quebec (Ayer *et al.*, 1999). The Blake River assemblage conformably overlies the Kinojevis assemblage (Ayer *et al.*, 1999). A porphyritic rhyolite from Pontiac Township, about 20 km southeast of the Holloway deposit, gives a concordant U-Pb zircon age date of 2701 ±2 Ma (Corfu *et al.*, 1989). According to Jackson *et al.*'s (1994) classification, the Blake River

assemblage belongs to the INTFEL-type where intermediate to felsic rocks dominate and have a calc-alkalic affinity. Dominant INTFEL-units are fragmental and/or effusive and likely subaqueous due to their association with pillowed flows (Jackson *et al.*, 1994). A modern tectonic analogue for INTFEL-type assemblages is island-arc complexes where more evolved (ensialic) volcanic rocks are formed due to subduction zones (Jackson *et al.*, 1994).

The Porcupine (2695 Ma) assemblage is also re-defined by Ayer *et al.* (1999) and belongs to Jackson *et al.*'s (1994) TURB-type supracrustal assemblage. TURB-type assemblages are characterized by meta-sandstones to meta-mudstones and matrix-supported conglomerates (Jackson *et al.*, 1994). This assemblage includes a variety of facies associations from well-graded distal turbidites to coarse, proximal, poorly sorted conglomerates (Jackson *et al.*, 1994). Notably, there are no interlayered meta-volcanic rocks found in TURB-type assemblages (Jackson *et al.*, 1994). TURB-type meta-sediments represent older sediments in the southwestern Abitibi greenstone belt (Jackson *et al.*, 1994). These distal deposits are tectonically interpreted to be related to an emerging collisional orogen (Jackson *et al.*, 1994). Corfu (1993) described 2700-2688 Ma as a period of compression, expressed by folding and thrusting. During this period turbidites were deposited and calc-alkaline plutons were intruded.

The Timiskaming assemblage has an age of *ca.* 2675 Ma (Ayer *et al.*, 1999) and belongs to Jackson *et al.*'s (1994) youngest supracrustal assemblage, ALUFLU-type. ALUFLU-type assemblages are identified by the presence of dominant alluvial-fluvial facies meta-sedimentary rocks, including clast-supported conglomerates and cross-bedded sandstones plus alkalic meta-volcanic rocks and syenitic intrusions (Jackson *et al.*, 1994). Angular unconformities and regional shear zones are commonly associated with the ALUFLU-type assemblage (Jackson *et al.*, 1994). The tectonic environment for the ALUFLU assemblage is interpreted as the final emergence of an arc-continent collision, including braided stream and alluvial fan settings (Jackson *et al.*, 1994). According to the tectonostratigraphic model, ALUFLU-type meta-sediments were deposited and/or preserved beside steep escarpments

formed by steeply dipping reverse faults (Jackson *et al.*, 1994). Alkalic meta-volcanic rocks and co-magmatic syenite intrusions are also thought to be derived in same the arc-continent collision that created the steeply dipping reverse faults (Jackson *et al.*, 1994).

A distinctive feature of the Superior Province is the presence of sedimentary subprovinces and Timiskaming-type sequences of alluvial-fluvial sedimentary rocks and alkalic to calc-alkalic meta-volcanic rocks within greenstone belts (Thurston, 1991). Timiskaming-type deposits consist of conglomerates in unconformable contact with pre-2700 Ma volcanic successions in the Superior Province (Thurston & Chivers, 1990). Mueller and Corcoran (1998) found that sediments in Timiskaming basins show the characteristics of late orogenic or strike-slip basins that develop adjacent to major crustal-scale structures. Evidence supporting tectonic influence on sedimentation in Timiskaming basins include rapid lithofacies changes, cyclic repetition of units, high sediment accumulation rates, basin margin and intrabasinal unconformities, coarse clastic debris at basin margins with shallow-water deposits in the center, thick stratigraphy relative to basin size and, basin margin faults (Mueller & Corcoran, 1998). Interpreted crustal-scale structures, such as the Porcupine-Destor Fault Zone, induced Timiskaming-type sedimentation, and are considered important pathways for gold-bearing fluids (Mueller & Corcoran, 1998).

1.2 Gold Mineralization in Archean Environments

World-wide, lode gold deposits are typically Late Archean or Early Proterozoic in age and hosted by assemblages of mafic volcanic rocks with significant ultramafic and sedimentary (greywacke and shale) rocks (Roberts, 1988; Kerrich & Cassidy, 1994). Hodgson (1993) reports that most mining camps with large deposits in belts dominated by volcanic rocks are characterized by the spatial conjunction of three rock assemblages: (1) high-magnesium mafic-ultramafic volcanic and intrusive rocks, in Archean belts comprising komatiite- and variolitic basalt-bearing volcanic sequences, (2) sedimentary rock belts, particularly those containing fluviatile sequences that unconformably overlie the volcanic rocks, and (3) felsic

intrusions. Pyrite is the dominant sulphide in this environment (Roberts, 1988).

High-magnesium rocks may have anomalously high gold values and could represent gold-source rocks (Hodgson, 1993). Sedimentary rock belts represent sedimentation during crustal-scale faulting, at which time the faults served as conduits for ore-forming fluids. Corfu (1993) described deposition between 2681-2676 Ma as Timiskaming-type consisting of alluvial-fluvial sequences and predominantly alkalic magmatism. After Timiskaming deposition, compression was renewed between 2676-2670 Ma resulting in polyphase folding and thrusting. Kerrich (1983) surmised that there is an association of quartz feldspar porphyries (QFP) with gold deposits. The role of the QFP would have been to heat hydrothermal fluids and circulate them by focusing them through fractures in the rock.

The timing of gold mineralization in the Abitibi greenstone belt is controversial. Two distinct mineralizing events are proposed for the southwestern Abitibi greenstone belt (Couture *et al.*, 1994). The early mineralizing event (>2690 Ma) shows different age relationships to deformation, and contrasting crosscutting relationships with intrusions when compared to the late mineralizing event (<2684 Ma) (Couture *et al.*, 1994). Kerrich and Cassidy (1994) link early lode-gold mineralization to tectonomagmatic events whereby mineralization typically occurs <10 to ~40 million years post terrane accretion. Corfu (1993) gives an age between 2630-2580 for hydrothermal minerals associated with the late gold mineralizing event.

Robert *et al.* (1997) define 16 common types of bedrock gold deposits based on geological environment, nature of mineralization and hydrothermal alteration. A conceptual model is proposed by Robert *et al.* (1997) where many types of gold deposits are related to the same large syenite-centered hydrothermal systems. Holloway's main ore zone is lithologically-bounded, lacking proximal intrusive rocks. The Holloway deposit corresponds to Robert *et al.*'s (1997) non-carbonate stockwork-disseminated type, whereby the group is defined by volcanic-hosted submarine basalts having a stockwork-disseminated form and a geochemical

signature of Na- and K-silicates plus As, Bi, and Te.

Volcanic-hosted mesothermal gold deposits generally occur near regional faults or "breaks" (Hodgson, 1993; Roberts, 1988). The Holloway gold deposit, along with several other deposits such as the Francoeur 3 deposit (Couture & Pilote, 1993), occur along major faults. Mineralization is controlled by fault splays because splays are more conducive to dilation than large and straight major faults (Hodgson, 1993). Sibson *et al.* (1988) describe the fluid pumping mechanism whereby a fault-valve (located in a first order fault) is responsible for the deposition of gold. When the valve is closed, fluids enter gold source rocks; when valve is open, fluids reverse and enter second order faults that have favorable gold deposition characteristics. Hodgson (1993) states that the gold-Timiskaming-type association is thought to be structural, such that the gold and sedimentary rocks are genetically related to crustal-scale faults superimposed on the large-scale thrusts and associated folds related to accretion. Hodgson (1993) adds that arsenopyrite is more common in deposits along the major structural breaks than in deposits away from these areas. Arsenopyrite is present in vein-type gold mineralization in the Holloway gold deposit.

Huanzhang and Guoxiang (1996) compiled a list of potential ore-forming fluids:

- silicate-dominated magmas or derived oxide, carbonate, sulphide-rich magmatic liquids,
- water-dominated hydrothermal fluids that separate from magmas,
- meteoric waters,
- seawater,
- formation (connate) water,
- fluids associated with metamorphic processes, and
- hydrothermal fluids derived from modern seafloor vents and from hydrothermal springs.

They determined that shear zone fluids have no well-defined source and that the ore-forming

fluids could be derived from metamorphic, magmatic, mantle degassing, and/or lower crustal granulization and deeply recycling groundwater. Huanzhang and Guoxiang (1996) support the opinion that ore-forming fluids in shear zones have a magmatic hydrothermal origin due to elevated concentrations of LILE. Rocks in shear zones and magma hydrothermal solutions are rich in LILE (Huanzhang & Guoxiang, 1996).

Gold (in lode gold deposits) is transported as a thio-complex in neutral solutions with low concentrations of total sulphur (Seward, 1984; Roberts, 1988). Mikucki's (1998) recent review suggests that a wide range of Archean lode gold deposits are formed within vertically extensive, crustal-scale hydrothermal systems. It is further suggested that gold is transported as $Au(HS)_2^-$ over a range of metamorphic conditions and crustal depths (Mikucki, 1998). Gold is precipitated by oxidation of the solution, change in pH, decrease of temperature, or by lowering the activity of reduced sulphur (Seward, 1984; Roberts, 1988). The activity of sulphur can be reduced by boiling, dilution, oxidation or, reaction with iron in the host rock to precipitate iron sulphide (Seward, 1984; Roberts, 1988). Mikucki (1998) determined that fluid-rock interactions, in particular wall rock sulphidation, is the most important type of precipitation mechanism. Gold deposition occurs through coupled reactions of the type:

$$FeO_{rock} + 2H_2S^0 = FeS_{2\,(pyrite)} + H_2O + H_{2\,(g)}$$

and

$$Au(HS)_2^- + H^+ + \tfrac{1}{2}H_{2\,(g)} = Au + 2H_2S^0$$

Wall rock alteration associated with Archean lode gold deposits typically includes zones of carbonate, albite, sericite, and locally K-feldspar alteration (Robert, 1997; Roberts, 1988). Roberts (1988) summarizes that the major components added to altered rocks include CO_2, K, S, H_2O, Au, B, As, Rb, W, Mo, Ba, and Sb. Alteration zones at the Holloway deposit consist of carbonate, sericite, and quartz-albite.

1.3 History of Mine Property

The history of Holloway's property is summarized from Broughton *et al.*'s (1991) technical report and Satterly's (1951) early report on the geology of Harker Township. Prospecting in the Holloway mine area began in 1907-08 and the earliest gold discovery was made by Cochenour and Willans in 1917. In 1922, W. S. Seagers staked claims north of the Teddy Bear Creek and coarse native gold was discovered in the quartz veins at Seagers Hill, approximately 500 metres south of the surface projection of Holloway's Lightning Zone. Seagers Hill geology consists of quartz veins within a shear zone. Two shafts were sunk on the Seagers Hill deposit by Abitibi Mines, Ltd. which formed in 1924. In 1929 a new company, Teddy Bear Valley Mines, Ltd., was formed through the amalgamation of Abitibi Mines Ltd. with the Teddy Bear Valley Syndicate group. In 1934 a shaft was sunk on the site of the old No. 2 Abitibi shaft. In 1935 a second shaft was sunk and diamond drilling was carried out. Additional diamond drilling was carried out in 1942 and in 1947 a magnetic survey was made. Between 1947 and 1980, the property laid idle.

Holloway's Lightning Zone was discovered in 1986. The Lightning Zone is characterized by disseminated pyrite and quartz-albite alteration along the lithologic contact between the footwall meta-komatiites and hanging wall mafic meta-volcanic rocks. Holloway's property is located on three claim groups: the Mining Corporation, Cadden, and Teddy Bear. In 1989, Noranda acquired ownership of the Hemlo Gold-Freewest property (60:40 joint venture) comprising the Mining Corporation and Cadden claims. In 1991, Hemlo-Freewest-Newmont had 60% interest and Teddy Bear Valley Mines Ltd. had 40% interest in the Holloway property. Hemlo acquired Battle Mountain Gold adopting their world renowned name. Battle Mountain Gold has an 84.7% interest in the Holloway Joint Venture; Teddy Bear Valley Mines Ltd. has the remaining 15.3% interest. Construction of Holloway mine began in 1994.

Previous studies on the Holloway mine property include a technical report by Broughton *et*

al. (1991) and a M. Sc. thesis by Guy (1996). The report by Broughton *et al.* (1991) describes the exploration history, property geology, structural geology, alteration and mineralization. Guy (1996) expands on Broughton *et al.*'s (1991) descriptions, providing detailed petrographic and structural information on the Holloway deposit. Current work includes this alteration study using extensive geochemical data, and a Ph. D. thesis by Luinstra (in progress) detailing the structural geology of the deposit and area. The objectives of this thesis are summarized below, and will be addressed throughout the thesis.

1.4 OBJECTIVES

1. The fundamental objective of this study was to sample the Holloway gold deposit for geochemical and petrological data in order to characterize the Holloway deposit. Petrological descriptions are presented in Chapter 2, and geochemical data are analyzed and interpreted in Chapter 4.

2. In Chapter 2, the timing and relationship between alteration and mineralization types is described. In addition, to describing the alteration and mineralization events, Chapter 2 outlines which alteration types are related to mineralizing events.

3. Upon determining the relationship between alteration and mineralization, another goal of this study is to characterize productive alteration types. In Chapter 4, geochemical techniques are employed to qualitatively describe alteration of the Holloway gold deposit.

4. Another objective of this study is to unravel the alteration events and investigate the nature of the rocks prior to mineralization. Certain lithologies are known to be favourable hosts for gold mineralization.

5. Lastly, it is desirable to determine favourable lithologies for ore deposition in order

to define a model for further exploration in the area. Descriptions of three meta-volcanic lithologies that occur in the Holloway deposit are detailed in Chapter 4.

1.5 ACKNOWLEDGMENTS

This study was made possible by the collaboration of the University of Ottawa, the Ontario Geological Survey, and Battle Mountain Gold Ltd., representing a positive trend toward government and industry involvement in post-secondary education. Foremost, I would like to thank my supervisor, Dr. Tony Fowler, who without his encouragement and assistance, none of this would have been possible. Priceless technical and administrative support were provided by John Loop, Ron Hartree, Ron Labelle, Sylvie Thériault, and Hélène De Gouffe. The Ontario Geological Survey managed to fulfill their mandate to educate (under increasing budget cuts), and provided a portion of the financial support necessary to undertake a geochemical study; thanks to John Ayer, Ben Berger, Dave Crabtree, and my field assistant, Sean Nattress. Battle Mountain Gold also provided funding (not easy to do when gold is around $300/oz), and the experience of Roger Dahn, Roman Gadzala, Richard Labine, Pat Mohn, and other mine/exploration geologists. Geochemical data arrived through the efforts of John Loop (see above), Eric Hoffman (ACTLABS), Peter Bélanger & Conrad Grégoire (GSC - Analytical Chemistry Laboratory), and Dr. Ted Appleyard (UW, SOMA). Lastly, thanks to those who rode the pendulum of my mood swings (period dependant on impending deadlines).

CHAPTER TWO: PETROLOGY OF THE HOLLOWAY GOLD DEPOSIT

2.1 HOLLOWAY MINE STRATIGRAPHY

The Holloway mine is located on Highway 101, 15 kilometres west of the Ontario-Quebec border. The Destor-Porcupine fault zone (DPFZ) consists of two main branches in the Holloway mine area (figure 2.1). The central branch of the DPFZ separates the Kidd-Munro assemblage from those of the Destor Porcupine Complex (DPC). Intermediate to felsic calc-alkaline volcanic rocks of the Kidd-Munro assemblage represent the oldest rocks in the area and outcrop north of the DPFZ's central branch (Broughton *et al.*, 1991). The south branch of the DPFZ separates the Destor Porcupine Complex from the Kinojevis assemblage. The DPC is a fault bounded block of komatiitic and tholeiitic meta-volcanic rocks with intermixed meta-sedimentary rocks (Broughton *et al.*, 1991). Rock units of the DPC (table 1) have been correlated along strike with Kidd-Munro assemblage meta-volcanic rocks and Timiskaming meta-sediments. Blake River calc-alkaline volcanic rocks overlie the Kinojevis assemblage to the south (Jensen & Langford, 1985).

The scope of this thesis is to provide a detailed geochemical characterization of the alteration zones of the Host Iron-Tholeiitic meta-volcanic rocks (unit V). Broughton *et al.* (1991) and Guy (1996) provide comprehensive descriptions of the remaining units that comprise the Destor Porcupine Complex. Figure 2.2 illustrates a typical cross section through the Destor Porcupine Complex.

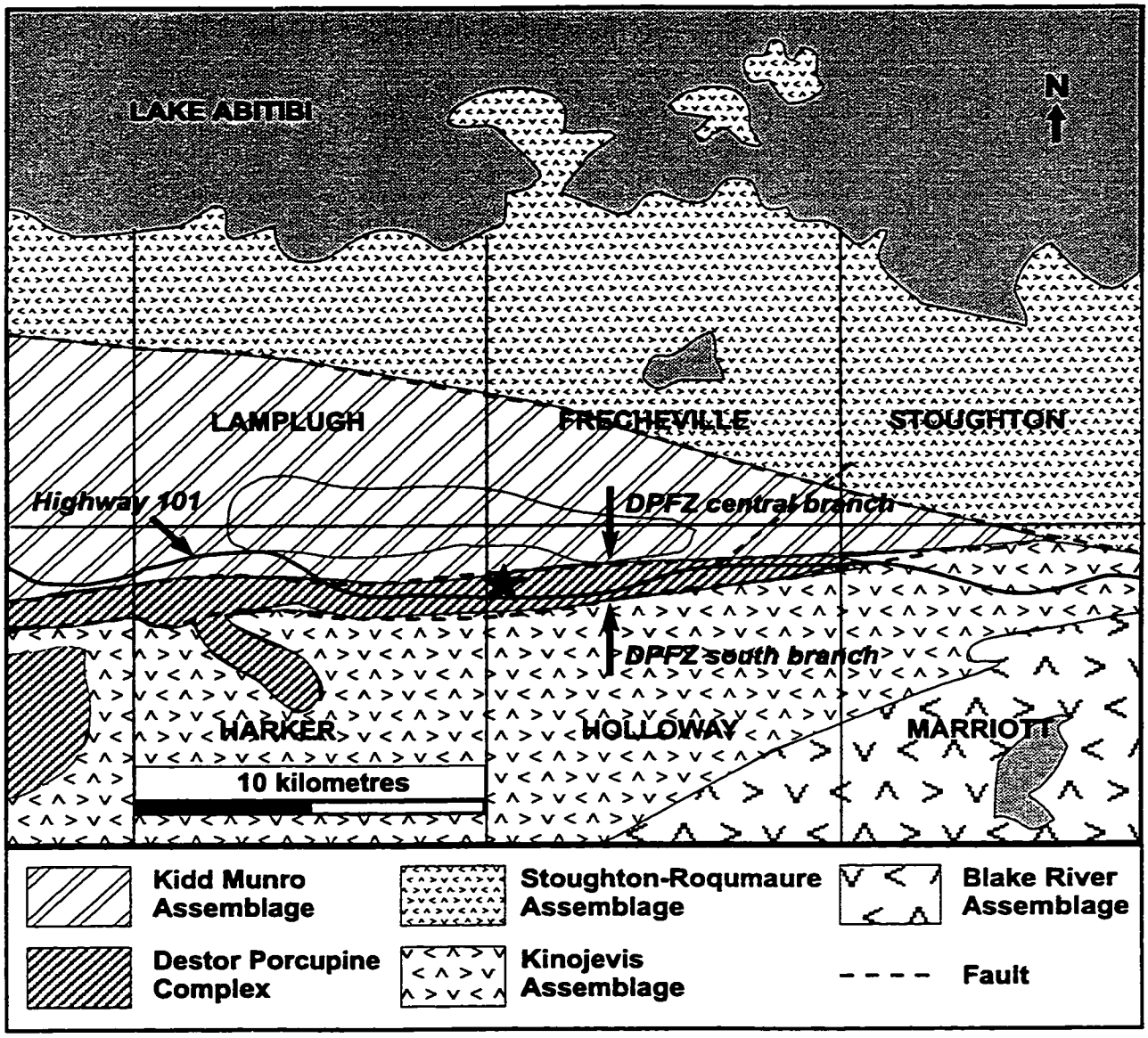

Figure 2.1: Geology of the Holloway mine area (modified from Broughton *et al.*, 1991 & Ayer *et al.*, 1999). The star indicates the location of the Holloway mine within the Holloway Township.

Table 1: Stratigraphy of the Destor Porcupine Complex from south to north (Broughton *et al.*, 1991).

DPC Unit	Lithology	Thickness (m)
I	Greywacke/argillite	<500
II	Fe- and Mg-tholeiite flows (Seagers Hill Tholeiites)	70-200
III	Polymictic jasper-bearing conglomerate/arkosic sandstone (Timiskaming)	70-170
	FAULT CONTACT	
IV	Greywacke/argillite	45-120
V	Fe-tholeiite flows, local interfingered basaltic komatiite flows (Host Iron-Tholeiites)	30-150
VI	Komatiite flows, interfingered Fe- and Mg-tholeiite flows, minor interflow sediments	30-130
VII	Conglomerate, greywacke-argillite	100-120
VIII	Komatiite and minor tholeiite flows	>100

2.2 Host Iron-Tholeiitic Meta-Volcanic Rocks

The Host Iron-Tholeiitic meta-volcanic unit consists of a 30-150 meter thick sequence of meta-basalt flows that strike approximately 090° and dips 60° to the south (Broughton *et al.*, 1991). Flow morphology of the meta-volcanic rocks consist of all flow facies including massive and pillowed flows plus flow breccias, hyaloclastite, and/or auto-brecciated flow. All of the flow facies are locally variolitic. Jensen and Langford (1985) report the primary mineral assemblage of relatively unaltered Fe-tholeiitic rocks from the Holloway area as 40-50% dark green to black augite, 30-40% plagioclase (An_{40}-An_{60}), 5-10% Ti-magnetite, and 2-8% quartz.

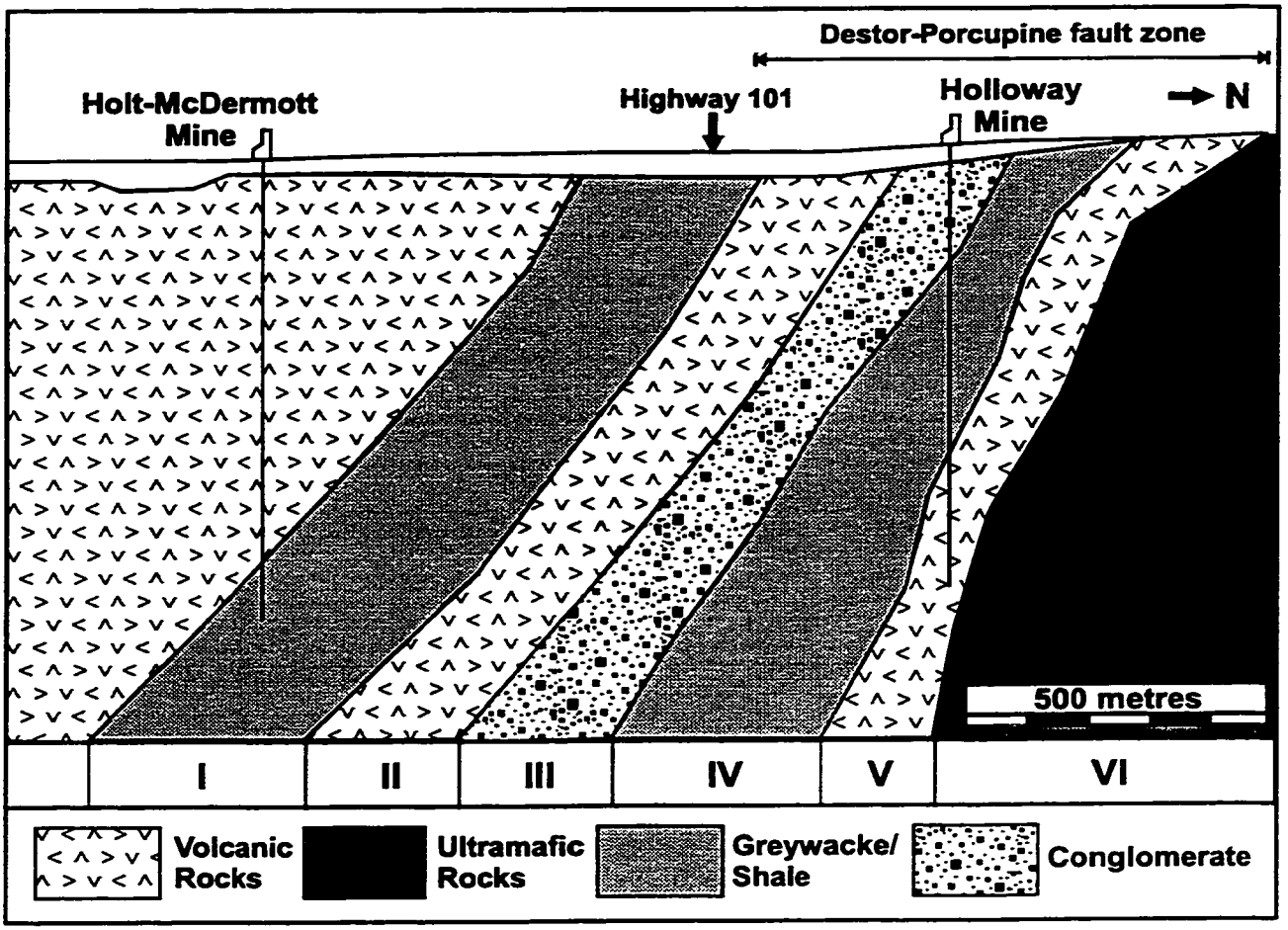

Figure 2.2: Generalized cross section through the Destor Porcupine Complex in the vicinity of the Holloway deposit (after Talbot, 1998). The roman numerals correspond to the units of the Destor Porcupine Complex. Ore zones at the Holloway deposit are located at the lithologic contact between units V and VI, within the variolitic meta-volcanic rocks.

2.2.1 Massive and Pillowed Flows

Least altered massive and pillowed flows from the mine area are metamorphosed to greenschist grade. They are medium to dark green, fine-grained rocks, consisting of an assemblage of chlorite, plagioclase, carbonate, and oxide minerals. Carbonate, sericite, and hematite alteration is common within these flows. The details of alteration petrography are further discussed below. Weathered surfaces are rusty due to aerial oxidation of pervasive ankerite alteration. Beige spots of mm-sized leucoxene are a common alteration product of titaniferous magnetite. Leucoxene is a mineral aggregate consisting of rutile and titanite; leucoxene replaces ilmenite and titanomagnetite in the mafic host rocks (Mueller & Groves, 1991). Pillowed flows tend to be more foliated than massive flows, such that the pillows are stretched beyond the point where tails are preserved, and only chloritic selvages indicate that they were pillows. Consequently, relict pillows can not be used for top determinations in the mine area.

2.2.2 Variolitic Flows

Variolitic texture is the mafic equivalent of spherulitic texture and is readily identified by the presence of round globules of a felsic mineral. Varioles, in this instance, are composed of radiating crystals of plagioclase that form under conditions of substantial undercooling (Fowler *et al.*, 1987). Variolitic flows are dominated by the presence of varioles, sometimes agglomerated to comprise 90% of the rock. Typically, variolitic flows are light gray rocks with a fine-grained matrix (plates 1 & 2). Varioles are commonly 1-2 cm in diameter, lighter in colour than the matrix, and in some cases are cherty white. Jones (1992) showed that evolved variolitic suites have complex mineral assemblages of albite, Fe-Ti oxides and pyrite, whereas less evolved flows have a simpler assemblage of carbonate minerals.

Plate 1: Photograph of a silicified-albitized variolitic rock. This sample was collected from the 415 metre level of the west mine workings. Chalk white coloured varioles are mm- to in size, and have been fractured by deformational events. The sample is light gray in colour and has many quartz-albite veins cutting through it. Disseminated pyrite hosts gold mineralization at pyrite-pyrite grain boundaries and within grain fractures.

Plate 2: Photograph of a sericitized variolitic rock. This sample was collected from drill hole U650-31 in the east mine workings. The matrix hosting the mm- to cm-sized chalk white varioles has been sericitized, and a pyrite stringer vein runs parallel to the foliation. The varioles were fractured and filled by quartz-albite alteration prior to the major sericitization event.

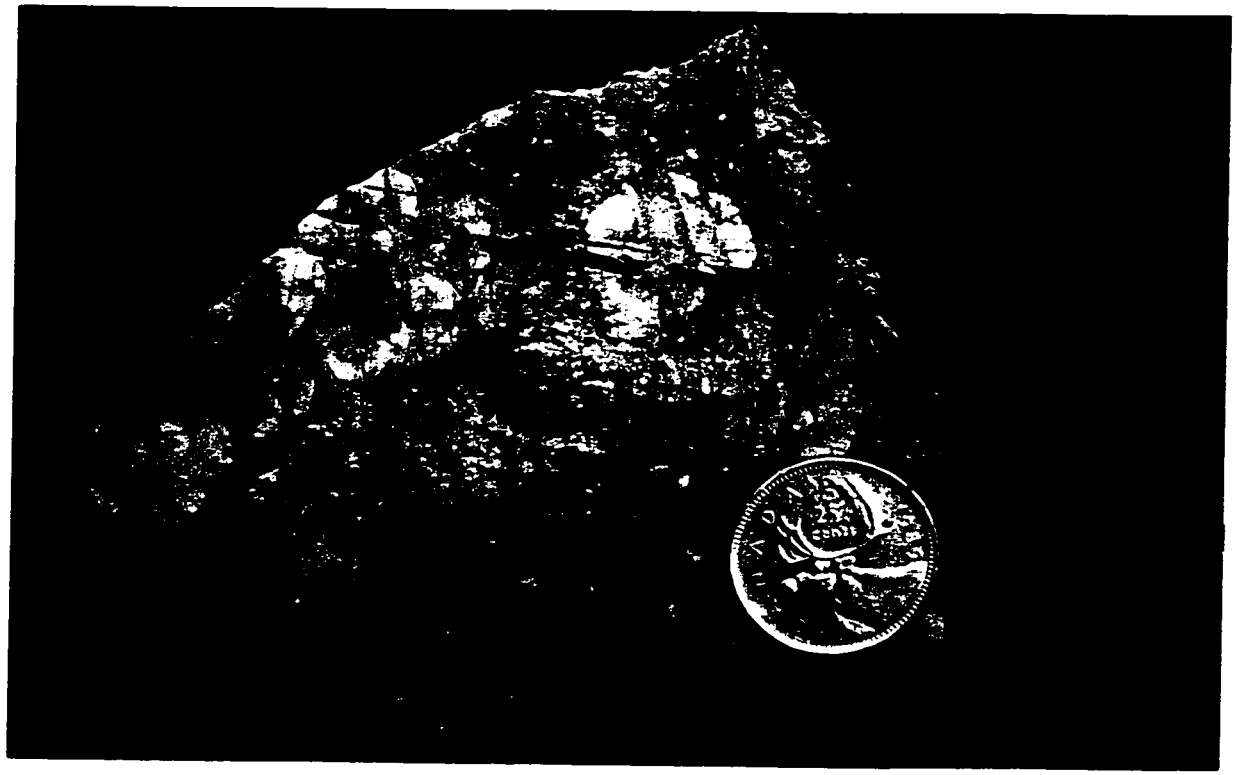

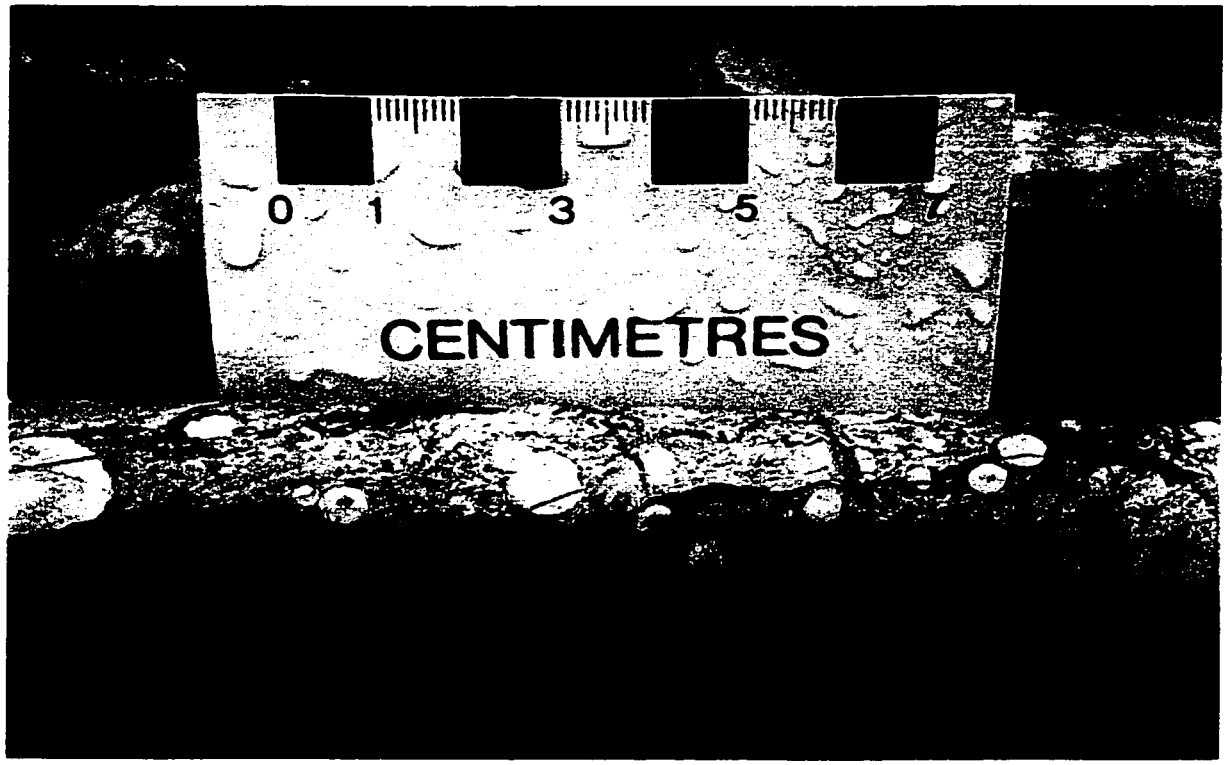
0
1
3
5
CENTIMETRES

Three types of alteration are observed within the variolitic flows: sericite, quartz-albite, and hematite. The details of alteration petrogenesis are further described below. Sericitized variolitic rocks tends to have lower gold concentrations (Au < 4.5 g/t or 4500 ppb) than their silicified-albitized equivalents (Au < 46 g/t or 46,000 ppb).

The origin of some Archean felsic volcanic rocks has been attributed to different mechanisms: fractional crystallization from a basaltic precursor (Fowler & Jensen, 1989), partial melting of crust (Gélinas & Ludden, 1984), and liquid immiscibility (Gélinas *et al.*, 1976). Fowler and Jensen (1989) showed that Kinojevis Group rhyolite sequences, containing abundant variolites, represent the most evolved stages of fractional crystallization of high iron-tholeiitic basalts. Gelinas (1976) found that variolitic rocks are enriched in high field strength elements (HFSE), rare earth elements (REE) and Si relative to Fe-tholeiitic basalts. Some relatively undeformed blocks of variolitic rock show what appears to be primary flow-banding with spherulites aligned along the banding (plates 3 & 4).

2.2.3 Heterolithic Breccia (3D-CG)

One of the thesis objectives was to describe the mine's 3D-CG heterolithic breccia unit and determine its origin. 3D-CG is Holloway mine terminology for a mafic volcanic heterolithic flow breccia. The 3D-CG heterolithic breccia (unit V of the DPC) has a fine-grained dark gray matrix supporting mainly mafic clasts (plate 5). Clasts range in size from a few millimetres to decimetres. Clast compositions include leucoxenitic mafic volcanic and fine-grained light to dark coloured meta-volcanic rocks. A sample of the 3D-CG was collected from near the base of the 3D-CG unit, structurally above the mineralized variolitic rocks for radiometric age determination. Pillowed basalt flows lie structurally above the 3D-CG unit.

In thin section, clasts from the 3D-CG unit have a similar mineralogy to the matrix consisting of carbonate, quartz, albite, chlorite, and leucoxene (plate 6). The mineral assemblage represents seawater and hydrothermal alteration plus greenschist metamorphism.

Plate 3: Photograph of a flow-banded felsic clast within a hematized heterolithic breccia unit. This sample was collected from the 550 metre level of the east mine workings. The flow-banded clast is a 10 cm wide block located just above the scale in the photograph.

Plate 4: Close-up photograph of a felsic clast showing probable flow-banding. The spherules are sub mm-sized and aligned parallel to flow-banding in the clast. Also, the flow-banding is defined by pyrite and quartz-feldspar layers

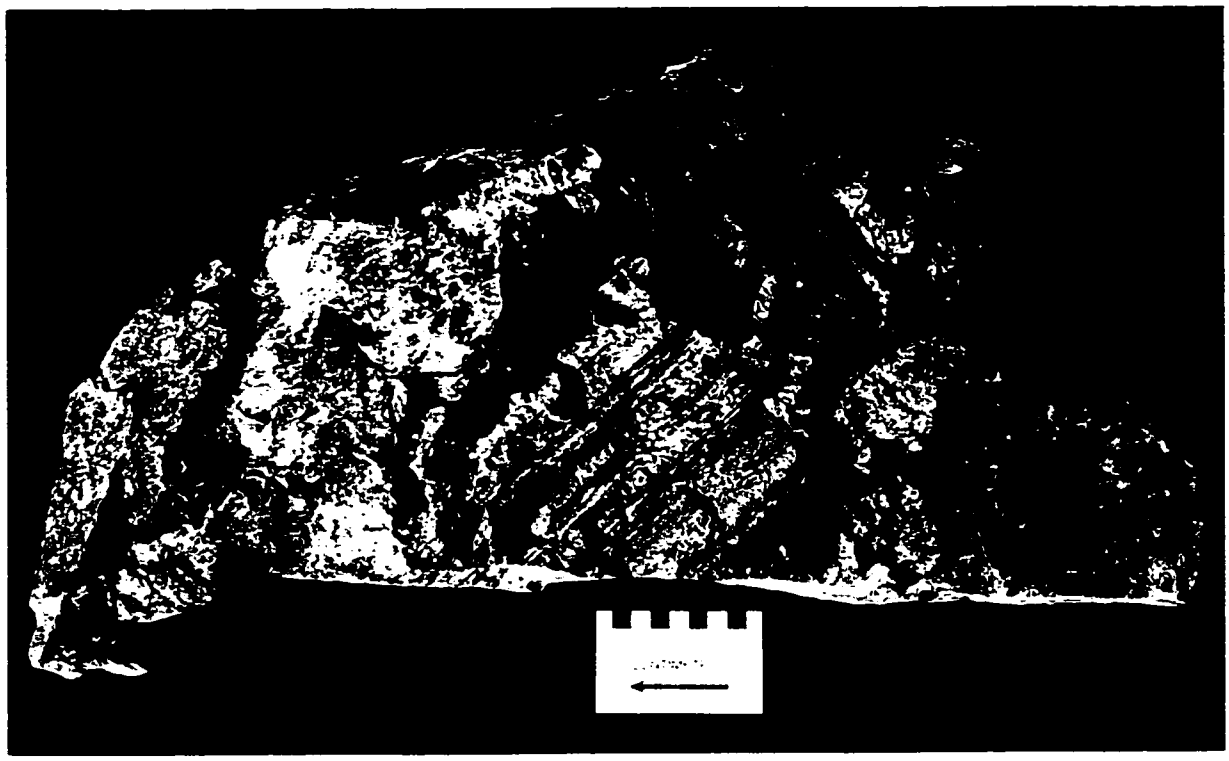

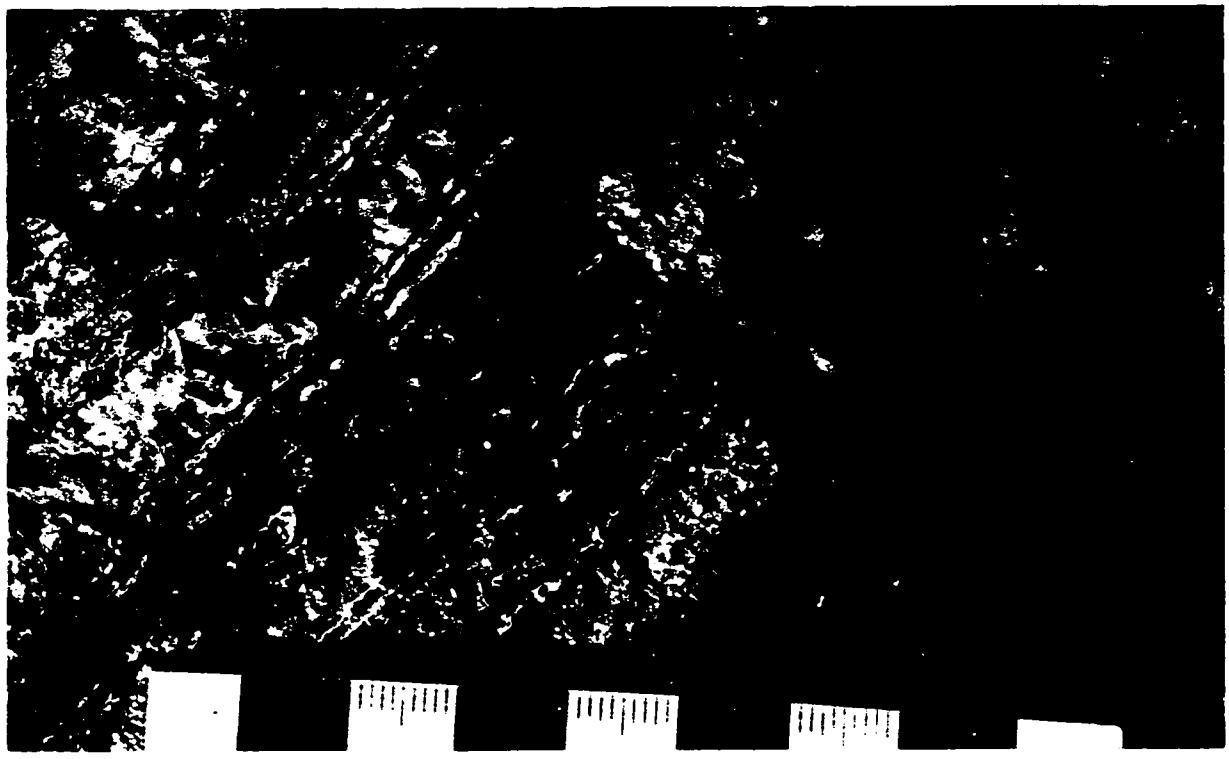

Plate 5: Photograph of the 3D-CG mafic meta-volcanic heterolithic breccia unit. This sample was collected from drill hole U650-24 in the east mine workings. The dark gray rock contains leucoxenitic mafic meta-volcanic clasts that are nearly indistinguishable from the fine-grained matrix.

Plate 6: Photomicrograph of the 3D-CG heterolithic breccia. Sample 520-131, PPL, field of view = 2 mm. The left side of the photomicrograph shows well developed foliation in the fine-grained matrix. Compositionally, there is little difference between the matrix and the leucoxenitic clast at the right side of the photomicrograph. The boundary between the matrix and clast is defined by a change in grain size.

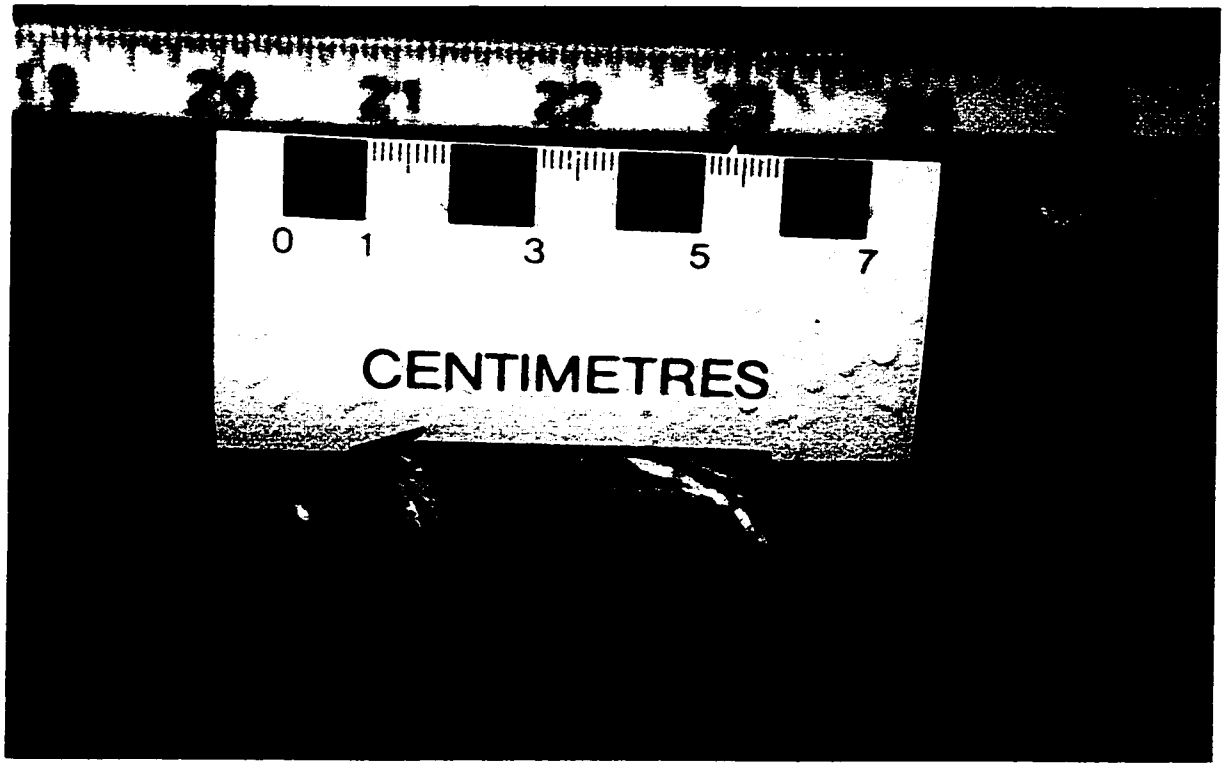
0 1 3 5 7
CENTIMETRES

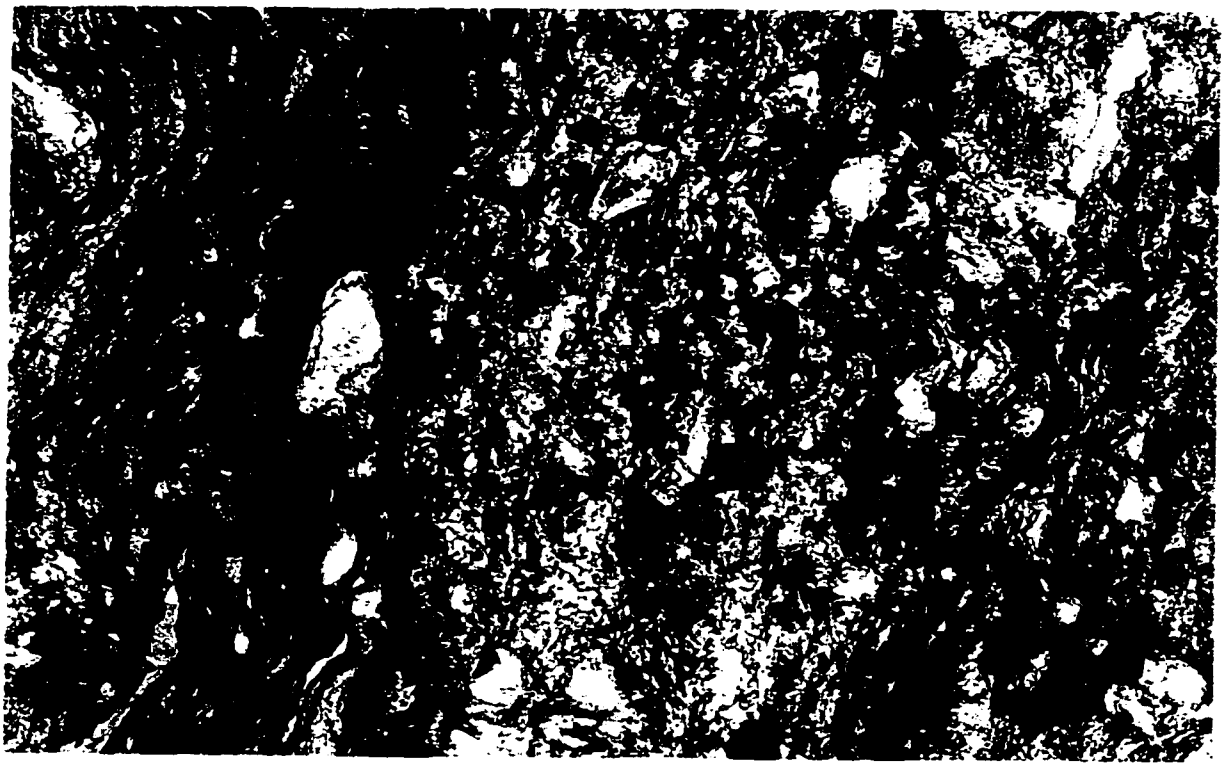

Leucoxenitic clasts are distinguished from the matrix by grain size. The fine-grained matrix is strongly foliated and crenulated, and contains peculiar rounded quartz phenocrysts. The rounded quartz grains are commonly observed in thin sections of other mafic meta-volcanic rocks in the mine sequence.

Potential origins for the 3D-CG heterolithic breccia include hydrothermal brecciation, epiclastic deposition or submarine debris flows. If the 3D-CG unit was formed via hydrothermal brecciation, the rock should be dominated by angular clasts. Instead the 3D-CG unit is matrix-dominated with relatively few rounded mafic meta-volcanic clasts. REE data, presented in section 4.2, provides certain clues to the origin of the 3D-CG unit. Holloway's meta-volcanic rocks have flat-lying REE profiles, but the 3D-CG unit has LREE-enriched profiles similar to nearby meta-sediments. Epiclastic deposition would expectantly have a uniform grain size. Through the process of elimination, it is reasonable that the 3D-CG unit represents a submarine debris flow.

2.3 ALTERATION

Powell *et al.* (1995) determined that regional metamorphism in the nearby Rouyn-Noranda area occurred between 2677 and 2643 Ma. A sericitized and carbonatized crosscutting intermineral dyke at the Holloway deposit is dated at 2672 Ma indicating that rocks in the Holloway mine area were subjected to alteration prior to the greenschist-grade metamorphism in the Rouyn-Noranda area. Least altered rocks at the Holloway deposit are characterized by mineral assemblages of chlorite, epidote and carbonate. Greenschist metamorphism overprints several episodes of alteration proximal to the deposit. Indications of alteration are readily observed by the presence of sericite, quartz±albite±ankerite veins, and rusty weathering of pervasive ankerite. Alteration is apparently concentrated on the Komatiite-Host Iron-Tholeiite contact (units V and VI of the DPC), equivalent to the "footwall contact" of Guy (1996). The core of the hydrothermal system was dominated by quartz and albite alteration, surrounded by an envelope of sericite alteration and a wider

envelope of carbonate alteration. Also, hematite alteration occurs as patchy zones throughout the deposit.

2.3.1 QUARTZ AND ALBITE

Guy (1996) determined that the first episode of alteration in the mine sequence is represented by the silicified-albitized zone. Albite alteration zones represent the core of large hydrothermal systems (Mueller & Groves, 1991). At the Holloway deposit, the silicified-albitized alteration zone is defined by sharp boundaries and has the highest proportion of veining. Albite alteration is cherty in appearance and was initially mistaken for silicification. In fact, quartz and albite are ubiquitously intermingled in the silicified-albitized alteration zone, such that in thin section it is often difficult to discern the two. Variolitic hyaloclastites host the most intense albite alteration and are the most common setting for Lightning Zone mineralization (Broughton *et. al.*, 1991). Albite alteration is expressed as small disseminated euhedral grains or as fine-grained radiating to fan-shaped spherulitic clusters of albite. Relict variole textures are typically granular (plate 7), having been largely destroyed by alteration. The radiating texture (plates 8 & 9) of some plagioclase may be formed by the metasomatic replacement of the original mineral assemblage by albite.

Silica precipitates as an alteration mineral when hydrothermal fluids that are saturated with respect to quartz begin to cool (Kerrich, 1983). Likewise, the hydrolysis reaction of albite to muscovite (sericite) consumes K from the hydrothermal fluid, lowering the K/Na such that when temperatures decrease, gangue albite ±paragonite is formed (Kerrich, 1983). Thus during cooling of a hydrothermal fluid, both quartz and albite can precipitate which may account for the flooding of quartz and albite in albite-altered samples.

Plate 7: Photomicrograph of relict variole texture displaying granular texture. Sample 520-126, CPL, field of view = 2 mm. The core of this variole is centred near the bottom right corner of the photomicrograph. Radial alignment of the minerals is faint due to strong alteration. The rim of the variole is marked by sericite.

Plate 8: Photomicrograph of albite alteration showing the radiating texture of albite. Sample 485-113, CPL, field of view = 2 mm. Coarse grained plagioclase is radially aligned and displays 'undulose extinction' due to the different orientations of the individual grains. Late carbonate alteration is pervasive throughout the thin section in the form of small euhedral grains that crystallized as the hydrothermal system was beginning to wane.

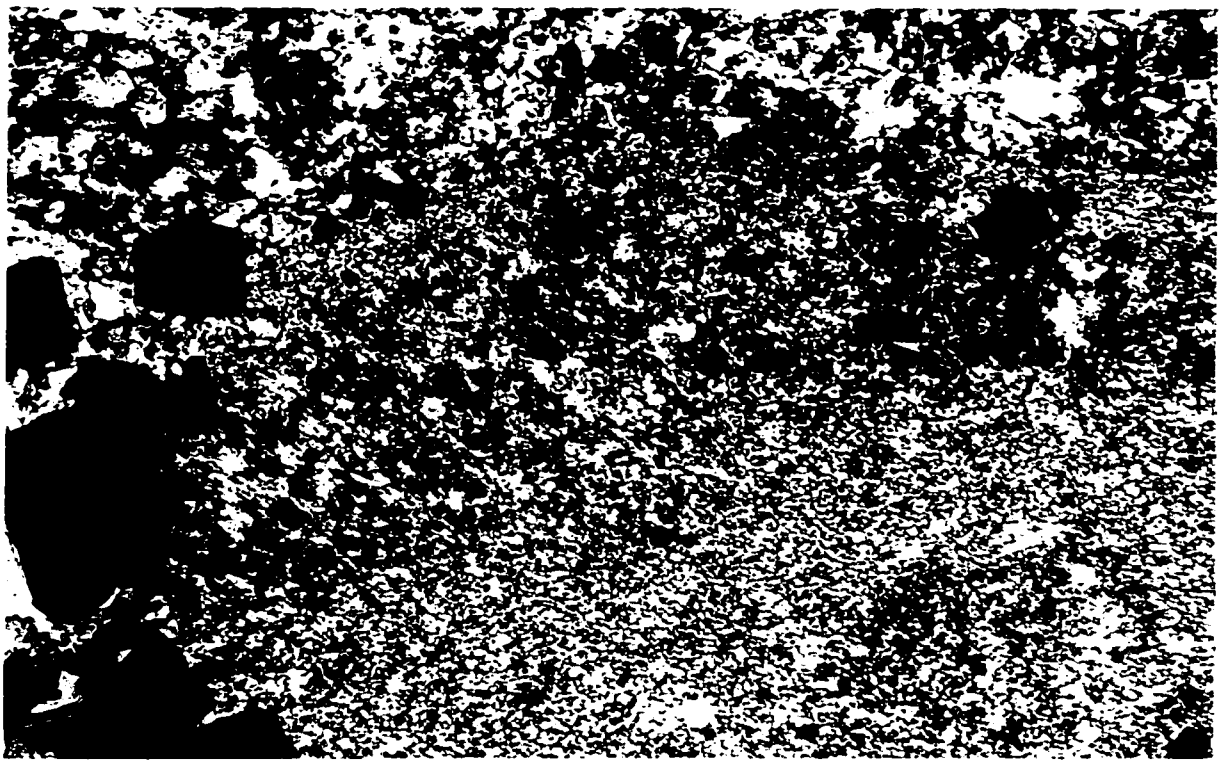

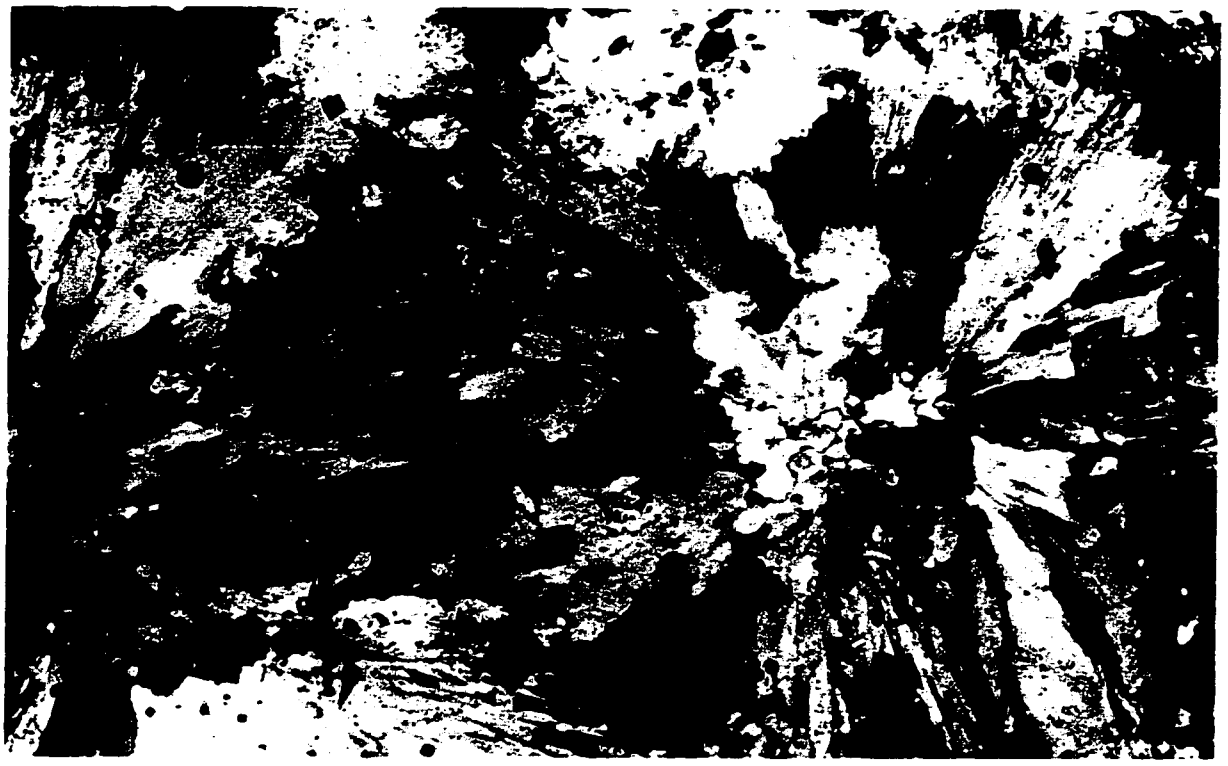

Plate 9a: Photomicrograph of relict hyaloclastite texture. Sample 445-09, PPL, field of view = 2 mm. Fe-Ti oxide minerals reveal the dusty outline of a primary hyaloclastite texture.

Plate 9b: Photomicrograph of overprinting radiating albite texture. Sample 445-09, CPL field of view = 2 mm. Same position as plate 9a, but under cross nicols, coarse-grained radial plagioclase overprinst the relict hyaloclastite texture, indicating its hydrothermal origin.

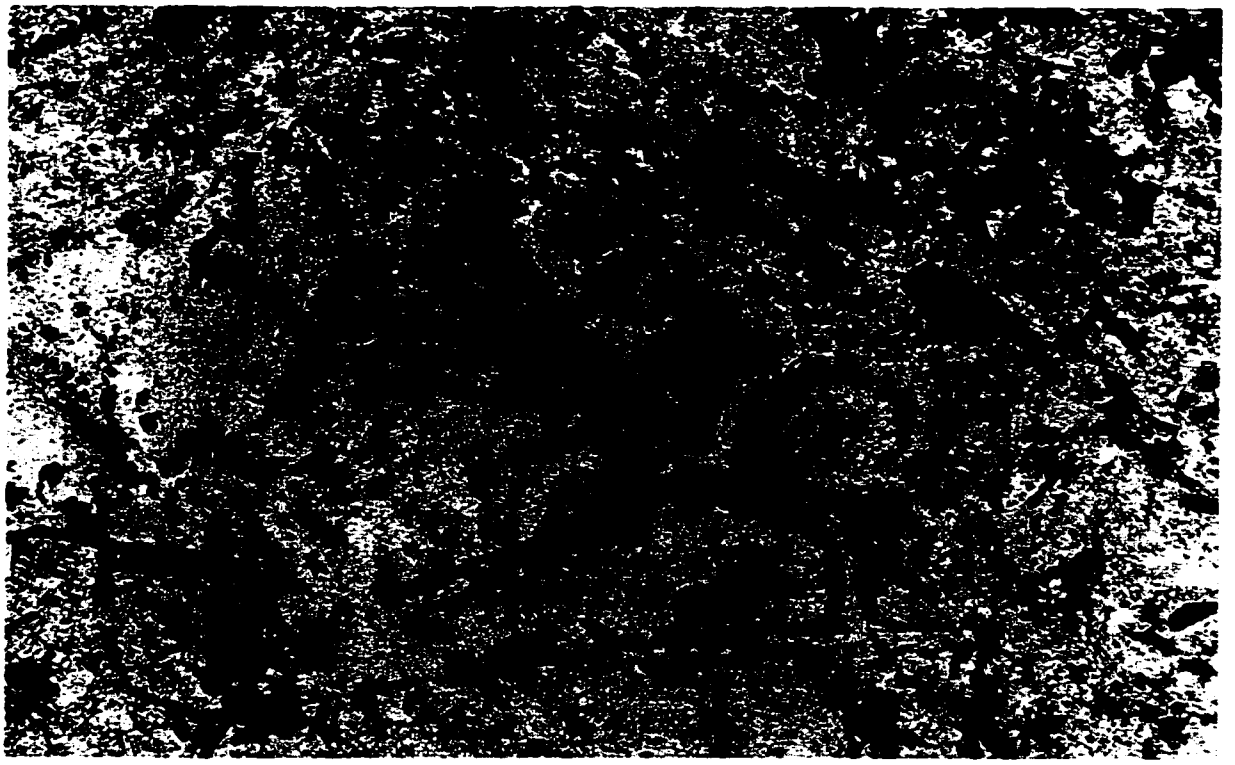

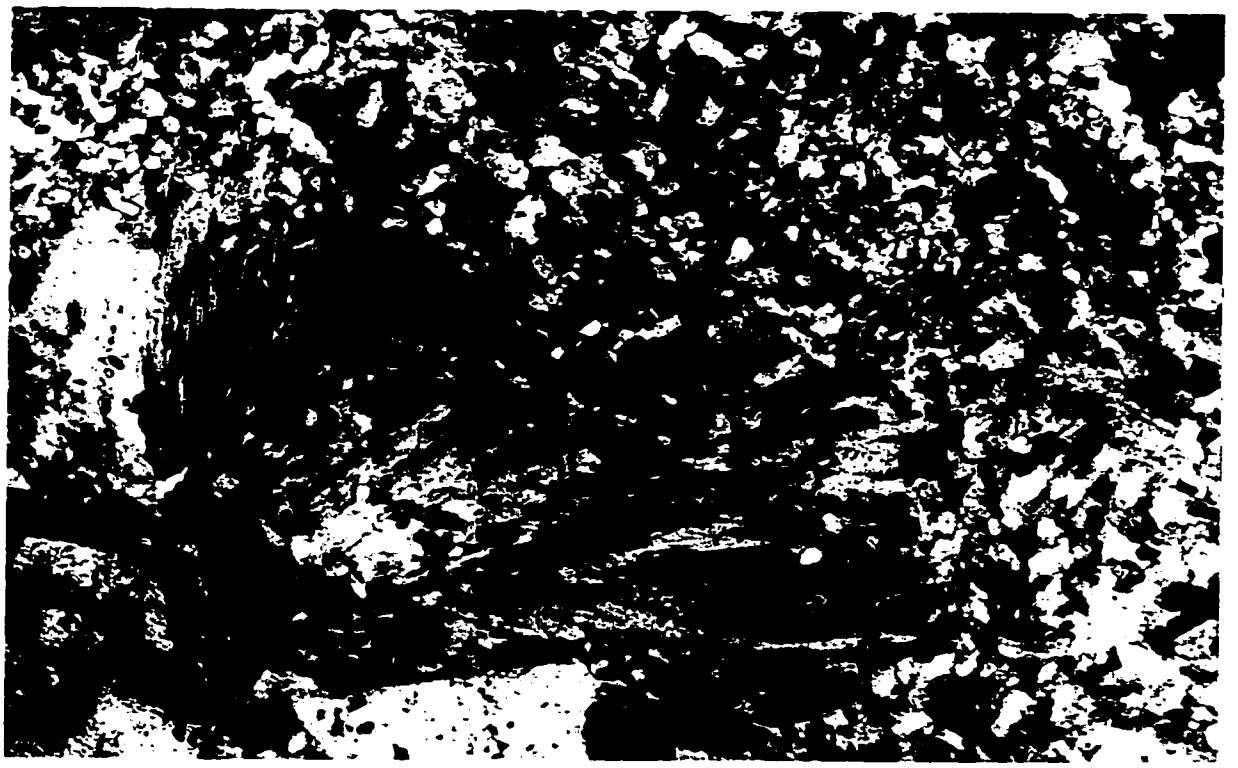

2.3.2 SERICITE

Rocks in the sericite alteration zone are yellow to yellow-green or buff in colour (plate 10). Sericite alteration increases in intensity adjacent to the albitized core of the hydrothermal system. In places, sericite alteration cuts the quartz-albite alteration zone; where it does not cut it is always found with moderate to strong carbonate alteration. All facies of the Host Iron-Tholeiitic meta-volcanic rocks host sericite alteration including massive and pillowed flows and variolitic ±hyaloclastite rocks. Sericite is dominantly in veins, but may appear as such due to subsequent deformation, *e.g.* rocks of the sericite alteration zone commonly have a strong foliation due to its perfect cleavage. In the komatiitic footwall, sericite alteration is expressed as fuchsite.

2.3.3 CARBONATE

Carbonate alteration is pervasively developed throughout the mine sequence. Meta-volcanic rocks of this zone are medium to dark green in colour developing a rusty weathering colour upon exposure to the atmosphere. The rusty coloration is due to the oxidation of the dominant carbonate mineral, ankerite. Several episodes of alteration are responsible for the emplacement of the carbonate alteration zone as evidenced by cross-cutting veins. The texturally destructive nature of carbonate alteration is shown by the flooding of fine-grained carbonate minerals which are predominantly ankerite.

2.3.4 HEMATITE

Hematite alteration occurs as patchy domains throughout the mine. Hematized rocks are typically dark mauve to dark gray, but appear quite red in rocks that contain significantly more quartz and plagioclase. Where found, the hematite alteration is pervasive, but in some instances it occurs in open-space fillings as large acicular crystals. The two forms of hematite alteration represent different episodes. Early hematization is illustrated in plate 12

Plate 10: Photograph of typical sericite alteration. This sample was collected from the 430 metre level of the west mine workings and is buff yellow in colour due to strong sericite alteration. Later quartz-albite veins are shown to crosscut the sericite alteration.

Plate 11: Photomicrograph of sericite alteration overprinting quartz-albite alteration. Sample 485-105, CPL, field of view = 2 mm. Sericite alteration is shown filling the fractures of a silicified-albitized variolitic meta-volcanic rock. This is evidence that pervasive sericite alteration (see the bottom left corner of the photomicrograph) overprints an earlier quartz-albite alteration event.

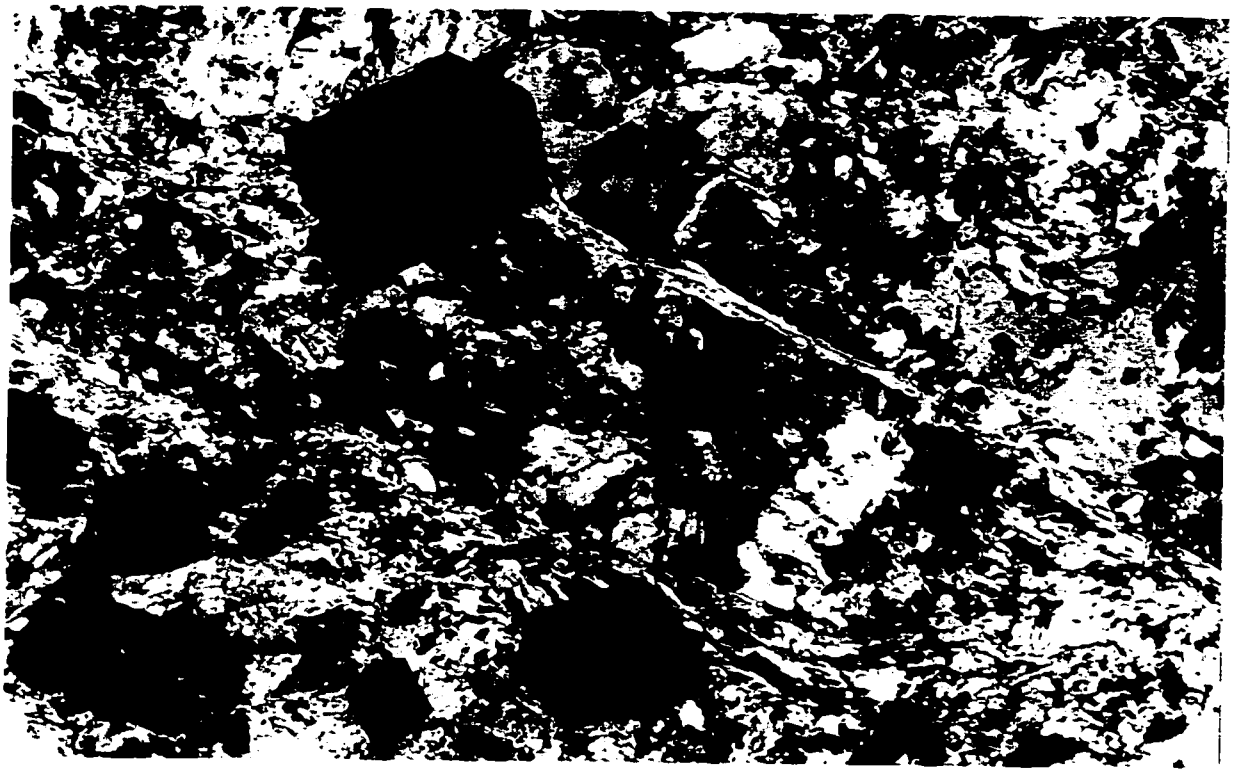

Plate 12: Photomicrograph of early hematite alteration. Sample 550-101, PPL, field of view = 2 mm. Pervasive hematite alteration occurs with early quartz-albite alteration and is crosscut by later quartz-albite veins.

Plate 13: Photomicrograph of late hematite alteration. Sample 505-106, PPL, field of view = 2 mm. Late hematization illustrates the delicate acicular texture of hematite that occurs in open space filling. Hematite of this form occurs with coarse-grained carbonate minerals in environments of open space filling.

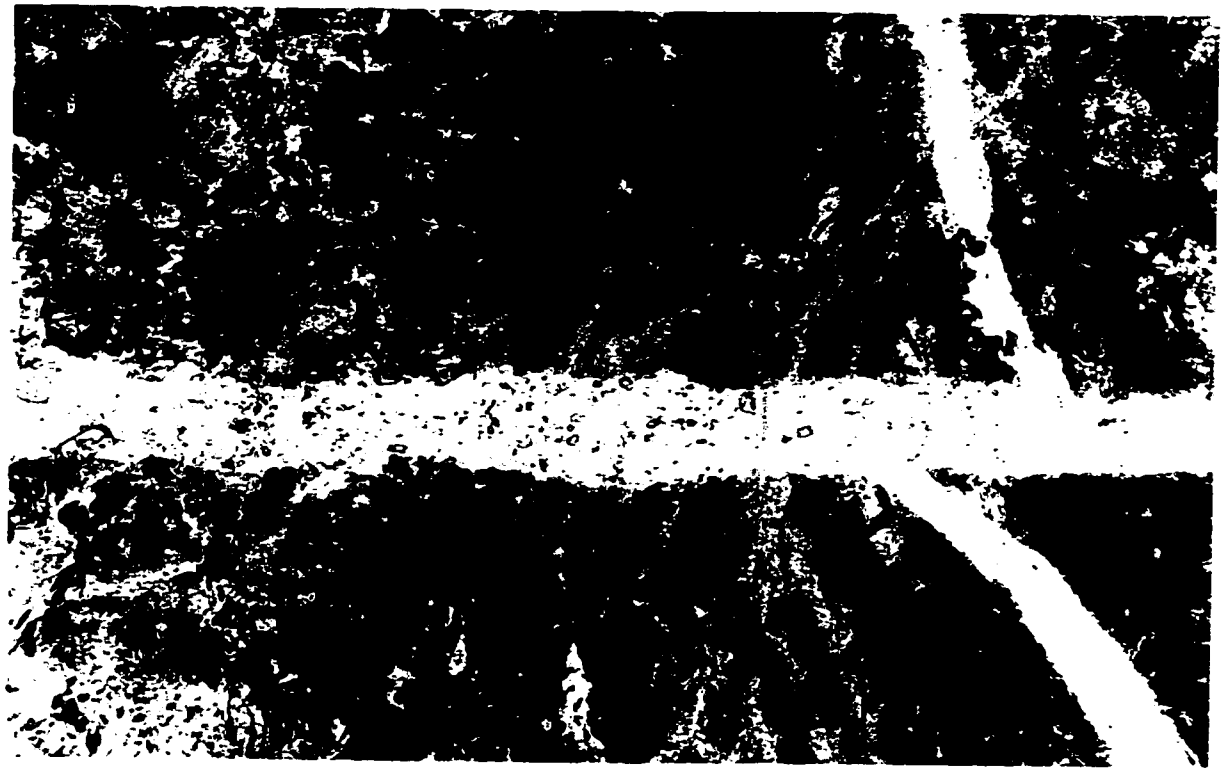

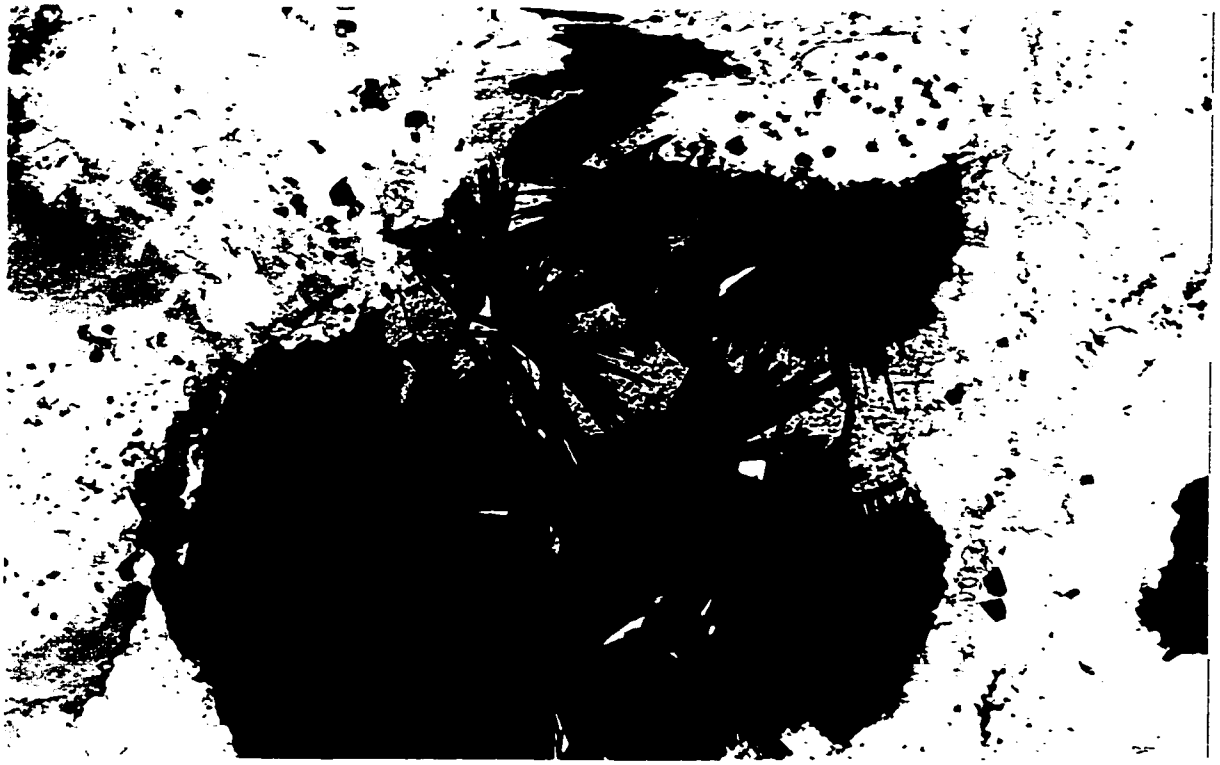

where hematite and early silicic-albite alteration co-exist such that it appears the two are nearly synchronous. Hematization occurred later than the early silicification-albitization event as illustrated by the hematization of a cross-cutting dyke and the ore zone in some areas. Where hematite alteration is pervasive and dominant, gold grades are below economic concentrations. Late-stage hematite alteration form delicate acicular masses that have not been destroyed by deformational events. Plate 13 shows the nature of late-stage hematite alteration with carbonate in open-space filling.

2.4 MINERALIZATION

Within the underground workings, the ore zones are divided into a west zone and an east zone. Two episodes of gold mineralization have occurred at the Holloway deposit. The west zone hosts early Lightning Zone mineralization (plate 1). The east zone hosts Lightning Zone and later vein-type mineralization (plate 14).

Lightning Zone mineralization is hosted by variolites, hyaloclastites, and other flow top facies of meta-volcanic rocks. The mineralization is characterized by alteration assemblages of quartz, albite and/or sericite. The Lightning Zone is located at the base of the Host Iron-Tholeiitic meta-volcanic rocks (unit V of DPC) just above the footwall contact with meta-komatiitic rocks (unit VI of DPC). Variolites that host Lightning Zone mineralization appear to be favourable horizons for gold deposition (figure 2.3).

Lightning Zone mineralization was developed prior to 2672 Ma, the age of an intermineral dyke (plate 16; section 2.5). An intermineral dyke crosscuts stratigraphy, but is not mineralized (table 2). In the west ore zone, the Lightning Zone is surrounded by large alteration envelopes of sericite and carbonate. These large alteration envelopes are missing from the east ore zone, instead, vein-type mineralization occurs above the Lightning Zone, where overlapping veins sometimes give the appearance of pervasive sericite alteration.

Plate 14: Photograph of vein-type mineralization. This sample was collected from the 505 metre level of the east mine workings. Quartz-albite and pyrite occupy the core of the veins that crosscut massive mafic meta-volcanic rocks. Sericite alteration forms a halo around the vein, and in places where many veins overlap, sericite alteration becomes pervasive.

Plate 15: Photomicrograph of vein-type mineralization. Sample 520-101, CPL, field of view = 2 mm. Sericite forms an alteration halo surrounding this Au-bearing arsenopyrite stringer vein. Also, pervasive carbonate alteration is apparent throughout the thin section, displaying its textually destructive nature.

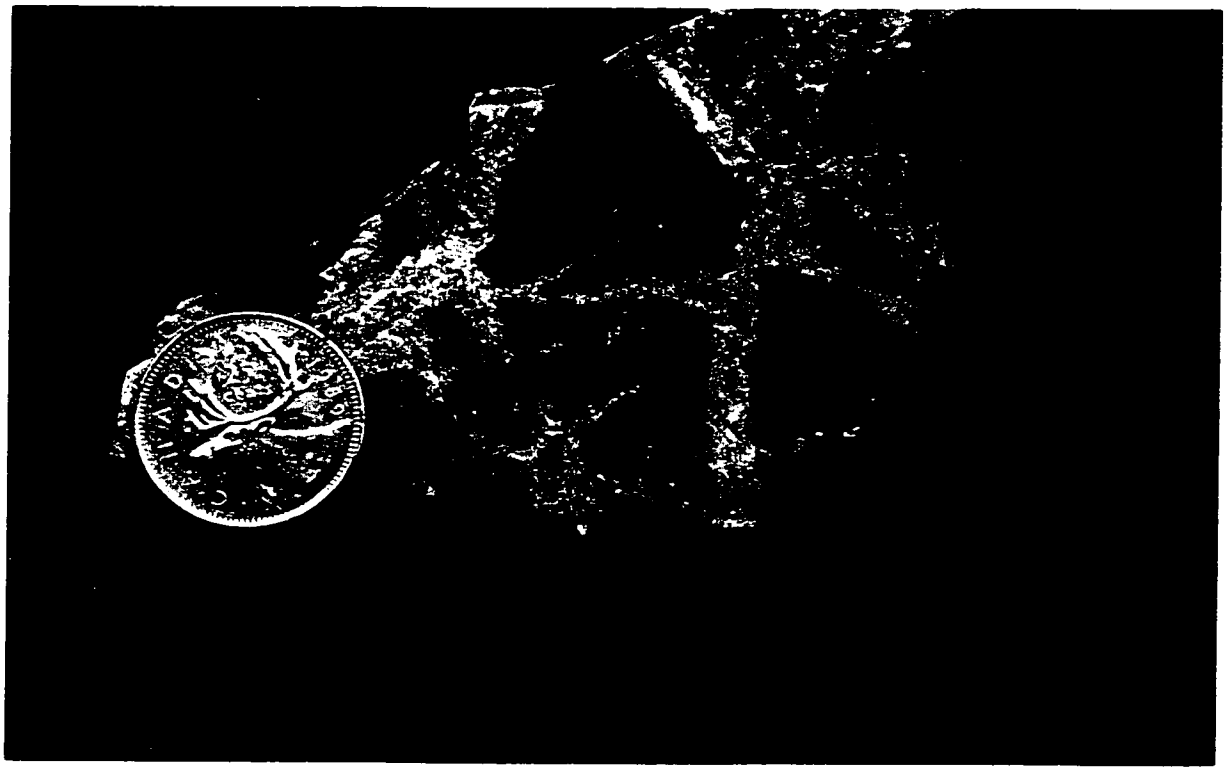

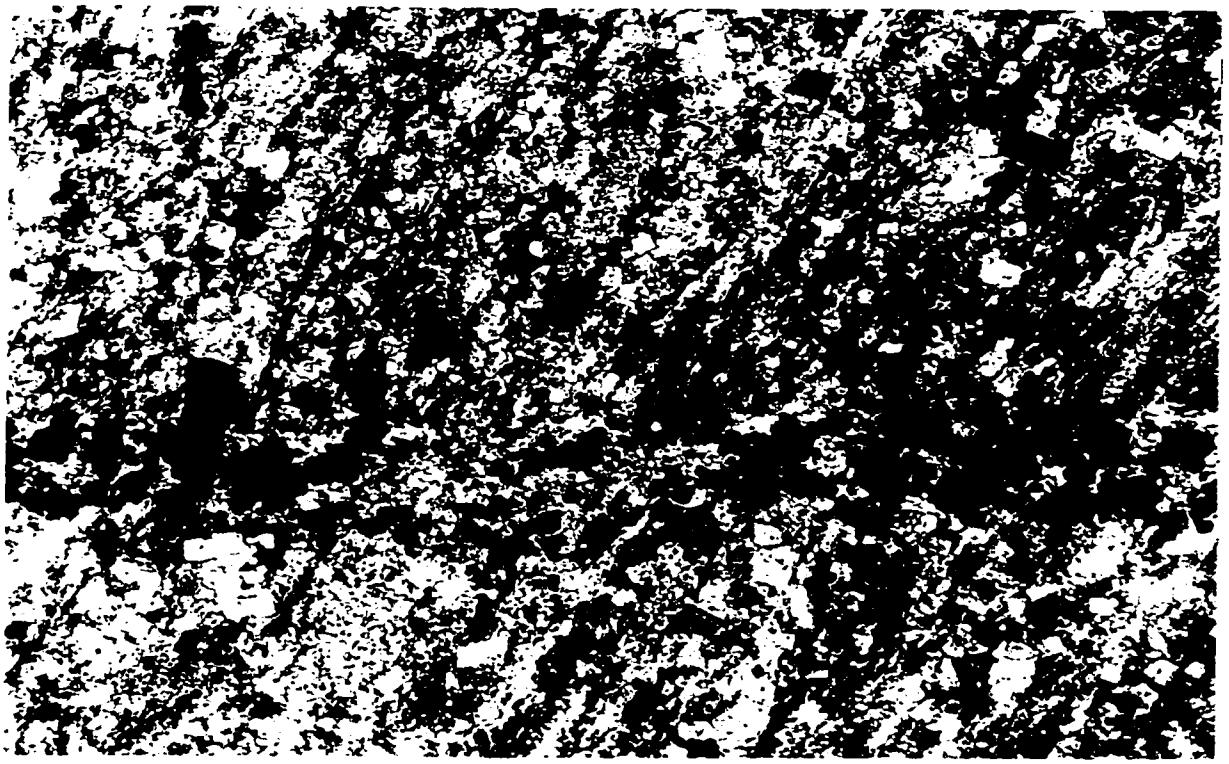

Plate 16: Photograph of the intermineral dyke. This photograph was taken from the 505 metre level of the east mine workings (west wall). The intermineral dyke crosscuts stratigraphy, and in this photograph it is shown cutting the variolitic meta-volcanic rocks which host Lightning Zone mineralization. The dyke is not mineralized, but has been subjected to hematite and sericite alteration. Late quartz-albite veins crosscut the dyke.

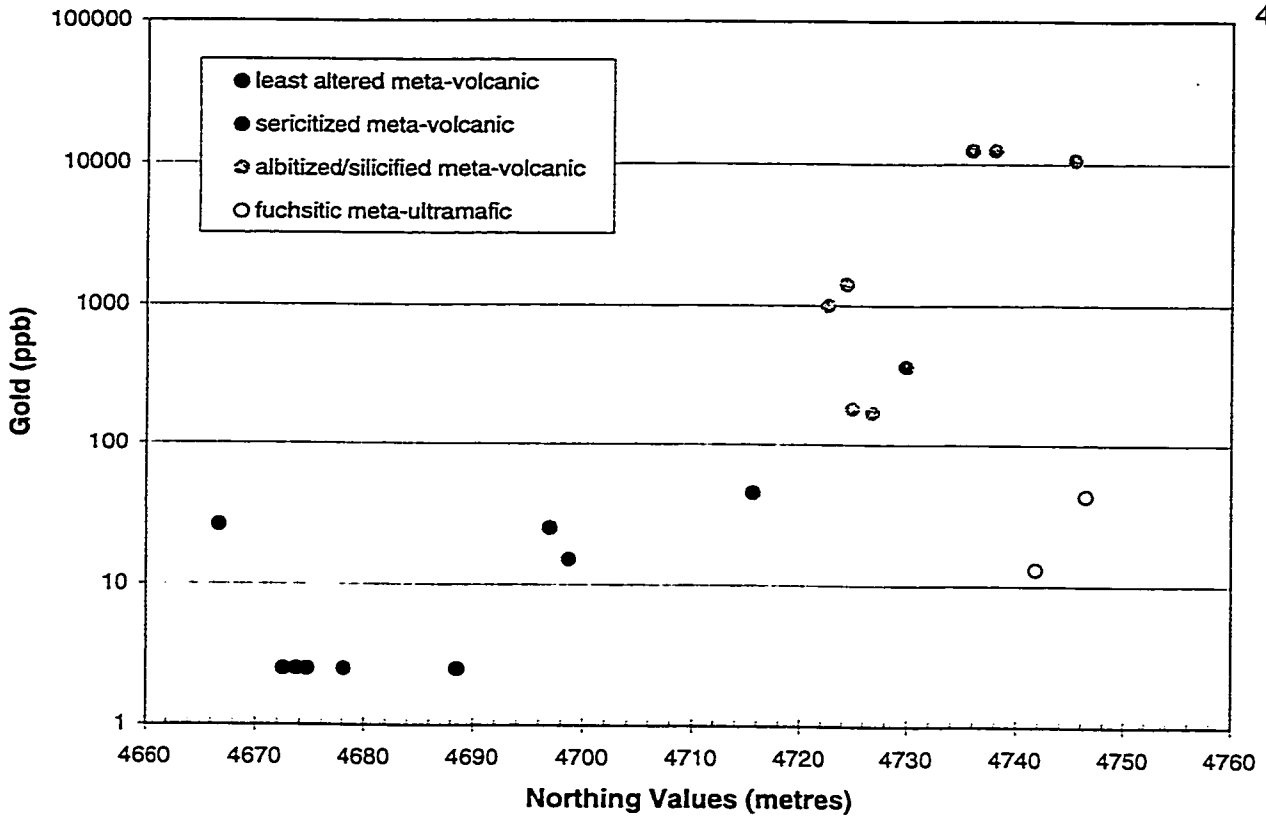

Figure 2.3: North-south cross section of the west ore zone on the 415 level showing the relationship between lithology and gold concentration.

Table 2: Au concentrations for the Lightning Zone and intermineral dyke.

Lithology	465E Au (ppb)	485E Au (ppb)	505E Au (ppb)
Lightning Zone	122	1870	4210
intermineral dyke	<5	<5	<5

In its current orientation, Lightning Zone mineralization is overlain by massive mafic meta-volcanic rocks that exhibit vein-controlled alteration, termed vein-type mineralization. Vein-type mineralization is characterized by stringer arsenopyrite±pyrite, surrounded by bleached haloes of albite plus sericite. The host lithology is typically green massive basalt that has undergone various degrees of sericitization. Vein-type mineralization stratigraphically overlies the Lightning Zone and sometimes overlaps it, particularly in the east zone of the mine.

According to Mueller and Groves (1991) classification scheme, the Holloway deposit belongs to the sericite-ankerite-albite alteration deposit class. Ore deposition for this class occurs at temperatures of 250-350 °C and pressures between 1-2 kb (depth of 3-7 km). The principle gangue minerals in the ore zone include ankerite, dolomite, quartz, sericite, and albite, and the sulphides present consist of pyrite, arsenical pyrite and arsenopyrite.

Figures 2.4 and 2.5 illustrate the differences in geology between the west and east mine workings.

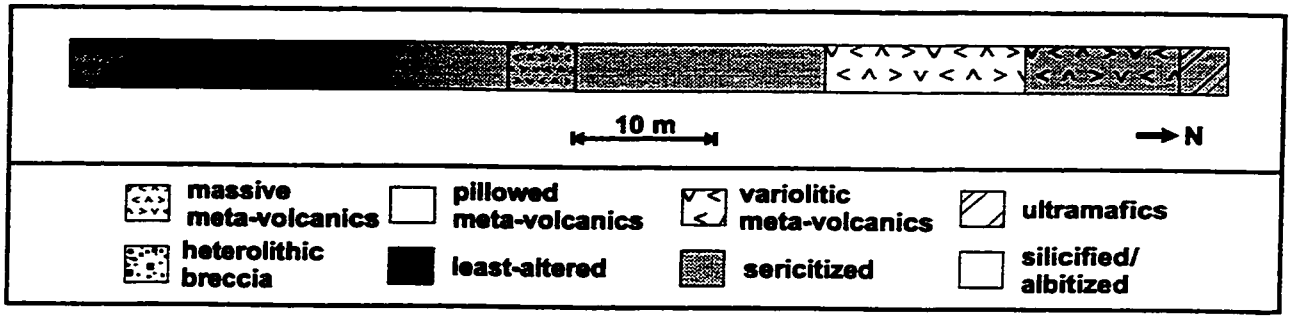

Figure 2.4: South to north cross section through the west mine workings at the 430 metre level. Least altered (*i.e.* carbonatized) mafic meta-volcanic rocks in the south, consisting of pillowed and massive flows, grade into the sericite alteration halo. The sericite halo overprints massive, pillowed, and variolitic hyaloclastite rocks. The Lightning Zone, hosted by variolitic hyaloclastites, has a gradational boundary to the south with the mafic meta-volcanic rocks, and a fault boundary with the meta-komatiitic rocks to the north.

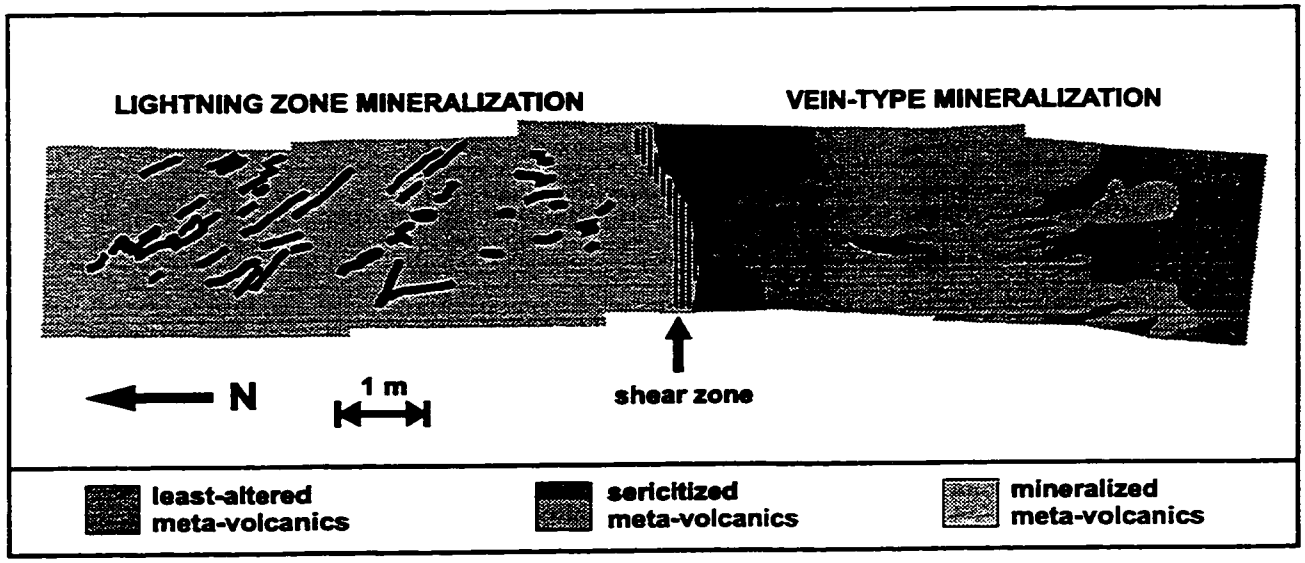

Figure 2.5: North to south cross section through the east mine workings at the 505 metre level (drawpoint 05). Mafic meta-volcanic rocks in the east zone are dominated by massive flows, although pillowed flows are sometimes present. Least altered mafic meta-volcanic flows finger into sericite-altered rocks. The sericitized alteration halo in the east hosts vein-type mineralization and contains patches of least altered green meta-volcanic rocks. The Lightning Zone is bounded by a shear zone between the mafic meta-volcanic rocks and the hosting variolitic hyaloclastites. The Lightning Zone contains south-dipping quartz-albite veins. Similar to the west zone, a fault boundary exists between the Lightning Zone and the meta-komatiites to the north.

2.5 RADIOMETRIC AGES

Radiometric ages were determined by U-Pb zircon geochronology for three samples from the Holloway mine area: a conglomerate (unit III of the DPC), the 3D-CG heterolithic breccia (unit V of the DPC), and an intermineral dyke (refer to figure 2.2 for stratigraphy).

The conglomerate (unit III) is a matrix-supported polylithic conglomerate. Clast types include ultramafic and mafic meta-volcanic rocks, larger-sized quartz-feldspar porphyry, and rare sulphide-bearing and meta-sedimentary rock clasts. The interbedded sandstone sample was collected from an unconformably-bounded conglomerate unit that is stratigraphically younger than the Seagers Hill meta-volcanic rocks (unit II of the DPC). The conglomerate unit displays a well-defined foliation (080°) and crenulation cleavage (040°). Three populations of detrital zircons were separated from the rock yielding U-Pb ages of 2724.1 ±2, 2695.9 ±1.8, and 2684.3 ±1.3 Ma. The 2684 Ma age represents the maximum age of sedimentation for the sample. Corfu (1993) places the Timiskaming period between 2681 and 2676 Ma. Regarding the conglomerate, 2724 and 2696 Ma rocks are not present in immediate map area in Ontario, however they correlate with the Deloro and Blake River assemblages respectively in Quebec (Ayer *et al.*, 1999). 2684 Ma rocks can be correlated with some syenite intrusions in the area, although local intrusions are ~2678 Ma (e.g. Garrison Stock). Locally, the Kidd-Munro assemblage is dated at 2716 Ma by a calc-alkaline tuff breccia northeast of Holloway Mine (Berger & Amelin, 1999). Also in the Holloway mine area, the Kinojevis assemblage is dated at 2701 Ma by a flow banded rhyolite in southern Harker Township (Berger & Amelin, 1999). The lack of radiometric ages corresponding to local assemblages suggests that there was no local input of sediments. The conglomerate is correlative with the age of Timiskaming sedimentation (Corfu, 1993).

A sample of the 3D-CG heterolithic breccia was collected from near the base of the unit, structurally above (*i.e.* south of) the Lightning Zone on the 550 metre level in the east mine workings. The 3D-CG heterolithic breccia is hosted within the Host Iron-Tholeiitic meta-

volcanic rocks (*i.e.* unit V of the DPC). Two populations of zircons were separated from the rock. Four zircons from the main population gave ages of 2717.2 ±2.4, 2694.1 ±4.4, 2694.7 ±2.0, and 2686.8 ±1.8 Ma. A small sub-population of larger and slightly rounded zircons were not analyzed and may represent crustal contamination (Kamo & Kwok, 1999). The 2687 Ma age represents the maximum age for sedimentation of this unit which indicates a Timiskaming age for this unit.

A dyke crosscuts stratigraphy in the east mine workings and can be traced from the 465 to 505 metre levels. The dyke is a pale green to yellow, fine-grained, strongly sericitized intermediate dyke that contains some millimetre-sized fuchsite grains. Foliation is not well developed in this dyke, and its emplacement is presumably pre-D_1. The sample was collected from the east wall of drawpoint 4 on the 465 metre level. Three zircon grains overlapped within their error estimates and gave a mean age of 2671.7 ±1.9 Ma for crystallization of zircon and emplacement of the dyke. This age is close to same age as 2673 Ma albitite dykes (Corfu *et al.*, 1989) at the McIntyre mine in Timmins with which gold mineralization is genetically associated (Melnik-Proud, 1992). The 2672 Ma age date for the intermineral dyke confines the timing of the first mineralizing event. The dyke is not mineralized but crosscuts stratigraphy that is gold-bearing, therefore the first mineralizing event occurred prior to 2672 Ma.

2.6 PARAGENESIS

Mueller and Groves (1991) describe the sequence of low temperature progressive carbonatization facies of basalt in a typical Archean terrane whereby:

amphibole + epidote (unaltered basalt) ➡ calcite-chlorite assemblage (outer zone)

chlorite ➡ ankerite (or ferro-dolomite) + alumina & iron (proximal to fluid conduit)

alumina & iron + introduced alkalis & sulphur ➡ sericite

Silicification and/or albitization involving decarbonization is common in the innermost zones of most intense alteration (Mueller & Groves, 1991). This alteration sequence is observed at the Holloway deposit, where early albite alteration is overprinted by sericite and carbonate alteration. Figure 2.6 identifies the relative timing of alteration and mineralization events that occurred at the Holloway deposit.

Quartz-albite alteration was the earliest event to occur at the Holloway deposit. It is overprinted by sericite and hematite alteration. Pyrite and gold mineralization are closely associated with the early quartz-albite event. A non-mineralized intermineral dyke crosscuts stratigraphy and is dated at 2672 Ma. The dyke is subsequently hematized and sericitized. Many episodes of carbonate alteration overlap, therefore carbonate alteration is pervasive throughout the deposit and covers the widest range of time. A later gold mineralizing event is associated with pyrite, arsenopyrite, and later quartz-albite and sericite alteration. Lastly there is a late hematite event whose delicate acicular textures are preserved in cavities with carbonate minerals. Also, late chlorite veins crosscut everything and are not related to any mineralizing events.

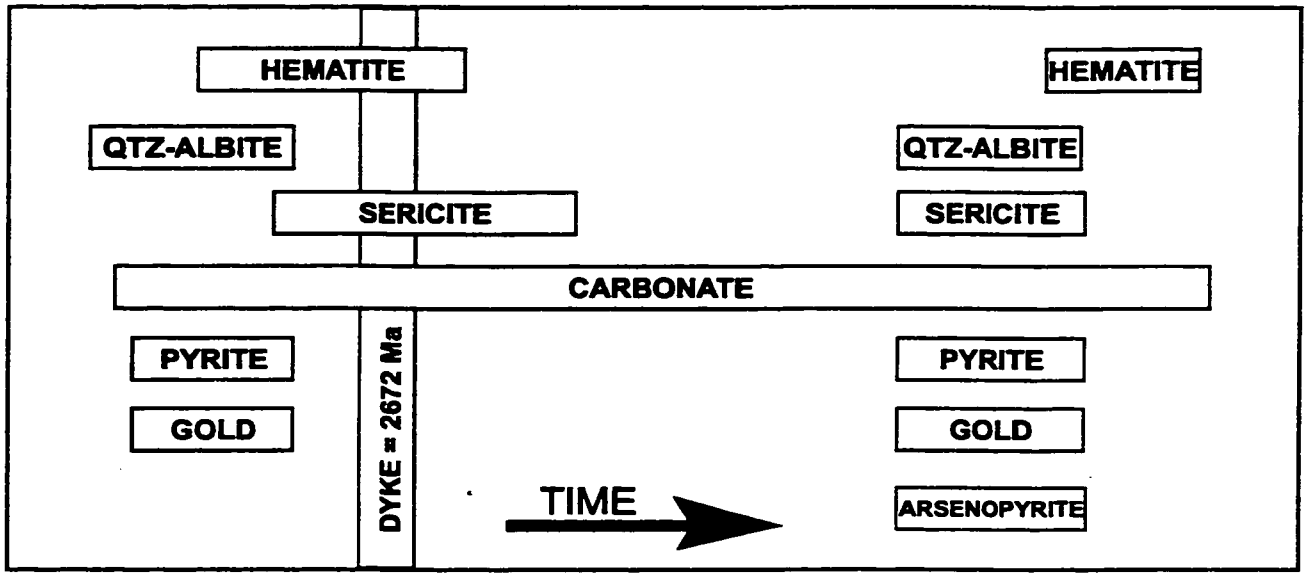

Figure 2.6 Relative timing of alteration and mineralizing events at the Holloway deposit.

2.7 CHAPTER SUMMARY

Rocks from the Holloway deposit represent a sequence of meta-komatiite to tholeiitic meta-volcanic rocks with associated hyaloclastite and variolitic-rich meta-volcanic rcks, mafic and felsic dykes and meta-sediments. Rock units at Holloway strike east-west and dip steeply to the south. The mine footwall is comprised mainly of meta-ultramafic flows with some mixed tholeiitic meta-volcanic flows and clastic meta-sedimentary rocks that are in fault contact with a hanging wall sequence of tholeiitic meta-volcanic flows. The fault contact delineates a structural discontinuity that acted as a fluid conduit for the hydrothermal system. Ore zones within the Holloway deposit are hosted by a hanging wall sequence of tholeiitic meta-volcanic flows which are overlain by clastic sedimentary rocks. The meta-volcanic rocks are probably correlative with the Kidd-Munro assemblage, and the meta-sediments with Timiskaming Group rocks.

Holloway mine workings are divided into a west and an east zone, and at least two mineralizing events can be identified within the deposit. The west zone hosts early Lightning Zone mineralization and large alteration haloes, whereas the east zone hosts both Lightning Zone and later vein-type mineralization. The Lightning Zone is characterized by disseminated pyrite that is hosted by albitized hyaloclastite and variolitic meta-volcanic rocks. Lightning Zone mineralization occurred prior to 2672 Ma as defined by the radiometric age date for a non-mineralized crosscutting dyke. Vein-type mineralization is characterized by stringer pyrite plus arsenopyrite hosted by sericitized massive meta-volcanic rocks.

Large alteration haloes are present in the west mine workings of the Holloway deposit. The silicified-albitized core of the hydrothermal system structurally lies just above the fault contact between the meta-komatiite footwall and the hanging wall tholeiitic meta-volcanic rocks. Sericite alteration occurs adjacent to the silicified-albitized core and is manifested as fuchsite within the footwall meta-komatiite rocks. Carbonate alteration is pervasive

throughout the Holloway deposit as a result of multiple overlapping hydrothermal systems. In the east mine workings, such a large sericite alteration halo is not observed. Instead, the Lightning Zone is sharply bounded by massive meta-volcanic rocks that have variable sericite alteration, often containing patches of less-altered green massive meta-volcanic rocks.

Three radiometric age dates have been acquired for the Holloway mine area. A conglomerate unit south of the mine, stratigraphically younger than the host meta-volcanic rocks, has a maximum age for sedimentation of 2684 Ma. A heterolithic breccia unit that lies within the host meta-volcanic rocks has a maximum age for sedimentation of 2687 Ma. Lastly, a radiometric age of 2672 Ma for a cross-cutting dyke confines the upper age for the first period of gold mineralization at the Holloway deposit.

CHAPTER THREE: ANALYTICAL TECHNIQUES

Samples from the Holloway mine area were collected during the 1997 and 1998 summer field seasons. The objective during sampling was to collect a suite of least to most altered specimens from the meta-volcanic rocks across mineralized zones. The Lightning Zone and later vein-type mineralization are represented by samples collected underground at the Holloway mine.

All samples were halved; one half was kept for hand specimen reference, and the other half was prepared for thin sectioning and geochemical analysis. Large veins and weathered surfaces were removed from the prepared sample before it was processed through a steel jaw crusher. Next, the sample was split into a ~60 gram portion, pulverized in a steel ring mill shatterbox, and stored in glass vials. Whole rock, trace element and gold analysis were done at Activation Laboratories Limited (ACTLABS) in Ancaster, Ontario. Carbon, sulphur, and water analysis were done at the GSC in Ottawa, Ontario. Ferrous iron determinations were done at the University of Ottawa, Ontario. Table 3 presents the precision error for each element where n is the number of times one sample analysis was repeated and N is the number of duplicate determinations of numerous samples. The precision error (Kretz, 1985) was determined according to the equation

$$\pm\frac{t}{\sqrt{n}} * s$$

t = student's t

n = # of measurements

s = standard deviation

The value used for the student's t depends on the number of measurements and the desired confidence level. For the purpose of this alteration study, a confidence level of 80% was chosen due to errors associated with the analytical methods. At an 80% confidence level the student's t = 1.886 for n = 3, and student's t = 1.476 for n = 6. Since the standard deviations for H_2O, CO_2, S, and FeO are well known, the z-distribution was used (instead of the

student's t) to calculate precision error (Kretz, 1985). For a confidence level of 80%, z = 1.282 and the precision error = z*s.

Table 3: Precision error for elements depending on their associated method of analysis

Element	n	Precision Error	Method
SiO_2	3	0.26	ICP-AES
TiO_2	3	0.03	ICP-AES
Al_2O_3	3	0.16	ICP-AES
Fe_2O_3	3	0.41	ICP-AES
MnO	3	0.00	ICP-AES
MgO	3	0.23	ICP-AES
CaO	3	0.11	ICP-AES
Na_2O	3	0.05	ICP-AES
K_2O	3	0.06	ICP-AES
P_2O_5	3	0.02	ICP-AES
LOI	3	0.05	ICP-AES
CO_2	N=11	0.12	LECO®
S	N=11	0.03	LECO®
H_2O	N=7	0.21	LECO®
FeO	N=84	0.20	titration
As	6	1.36	ICP-MS
As	6	3.75	INAA
Au	6	3.13	INAA
Ba	6	10.17	ICP-MS
Ba	3	3.50	ICP
Ba	6	44.18	INAA
Be	3	0.00	ICP
Ca	6	0.38	INAA
Co	6	1.57	ICP-MS
Co	6	2.84	INAA
Cr	6	1.54	ICP-MS
Cr	6	5.92	INAA
Cs	6	0.07	ICP-MS
Cs	6	0.80	INAA
Cu	6	7.94	ICP-MS
Fe	6	0.39	INAA
Ga	6	0.45	ICP-MS
Ge	6	0.20	ICP-MS
Hf	6	0.02	ICP-MS
Hf	6	0.25	INAA
Mo	6	0.07	ICP-MS
Mo	6	2.21	INAA
Na	6	0.01	INAA
Nb	6	0.09	ICP-MS
Ni	6	4.42	ICP-MS
Rb	6	0.89	ICP-MS
Rb	6	5.30	INAA
Sb	6	0.45	ICP-MS
Sb	6	0.16	INAA
Sc	3	2.18	ICP
Sc	6	2.27	INAA
Sn	6	0.38	ICP-MS
Sr	6	2.59	ICP-MS
Sr	3	8.03	ICP
Ta	6	0.01	ICP-MS
Tl	6	0.03	ICP-MS
V	6	3.73	ICP-MS
V	3	41.98	ICP
W	6	0.19	ICP-MS
W	6	1.48	INAA
Y	6	0.50	ICP-MS
Y	3	1.89	ICP
Zn	6	11.41	ICP-MS
Zn	6	15.27	INAA
Zr	6	1.04	ICP-MS
Zr	3	1.09	ICP
La	6	0.12	ICP-MS
La	6	0.00	INAA
Ce	6	0.26	ICP-MS
Ce	6	1.01	INAA
Pr	6	0.04	ICP-MS
Nd	6	0.17	ICP-MS
Nd	6	2.52	INAA
Sm	6	0.08	ICP-MS
Sm	6	0.10	INAA

Element	n	Precision Error	Method
Eu	6	0.01	ICP-MS
Eu	6	0.05	INAA
Gd	6	0.10	ICP-MS
Tb	6	0.02	ICP-MS
Tb	6	0.30	INAA
Dy	6	0.11	ICP-MS
Ho	6	0.02	ICP-MS
Er	6	0.05	ICP-MS
Tm	6	0.01	ICP-MS
Yb	6	0.06	ICP-MS
Yb	6	0.19	INAA
Lu	6	0.01	ICP-MS
Lu	6	0.06	INAA
U	6	0.00	ICP-MS
U	6	0.44	INAA
Th	6	0.01	ICP-MS

3.1 X-RAY FLUORESCENCE (XRF)

The original intention was to analyze samples from the Holloway deposit by XRF at the University of Ottawa. Several difficulties were encountered with the procedure and XRF analysis were abandoned for ICP analysis instead. The presence of abundant pyrite and other sulphides in mineralized Holloway samples caused the first major problem. High sulphur concentrations eroded platinum crucibles during the preparation of fused glass discs. This problem was overcome by roasting the samples in a muffle furnace prior to fusion. The second problem persisted after the roasting procedure was implemented. Many samples yielded totals that were unacceptably low (72-98%). Upon closer investigation, it was determined that the problem was inherent to the XRF matrix calculations at the University of Ottawa, which are designed for rocks having low sulphide contents.

During the XRF technique, samples are excited by x-ray radiation (10-100 kV) causing ionization of discrete orbital electrons (Potts, 1987). When the electrons return to the ground

state, fluorescent x-rays of energy are emitted as characteristic spectra for each element. Fluorescent x-ray counts are not directly proportional to atomic concentrations, therefore matrix correction programs are required to do the conversion. X-ray spectra can overlap and cause interference effects when measuring some elements.

The presence of arsenopyrite in samples indicated that arsenic concentrations may be significant. At the University of Ottawa, the XRF spectrometer was not calibrated for arsenic. Arsenic x-ray spectra overlap with lead and caused errors in the matrix correction program since arsenic was identified as lead. Re-calibrating the matrix correction program to include arsenic would have been a formidable task, beyond the scope of this thesis, so analysis by ICP was selected.

3.2 Inductively Coupled Plasma (ICP)

ACTLABS utilize a lithium metaborate ($LiBO_2$) and tetraborate ($Li_2B_4O_7$) fusion for their whole rock and trace element analytical packages. Lithium metaborate and tetraborate are non-oxidizing fluxes that readily decompose most refractory minerals (Chao & Sanzolone, 1992). The fusion process involves digesting the molten fusion bead in a weak nitric acid solution. Although lithium tetra/metaborate fusions are proclaimed to be exceptionally effective for the rapid decomposition and dissolution of silicate rocks, some minerals remain partly decomposed including zircon, some metal oxides, some rare-earth phosphates, fluorcerite and many sulphides (Cremer & Schlocker, 1976). Some of the relevant data from Cremer and Schlocker's experiments on lithium borate decomposition are presented in table 4.

Potts (1987) expresses doubt about the effectiveness of lithium tetra/metaborate fusions in systematically dissolving all minor and trace element phases. More recently, Chao and Sanzolone (1992) state that additional treatments, such as roasting samples, should be considered for samples containing significant amounts of resistant minerals such as

sulphides. Cremer and Schlocker's (1976) results presented in table 4 indicate that several Fe-bearing minerals are only partly decomposed. Since one of the thesis objectives is to characterize hematite alteration in the Holloway deposit, accurate determinations of iron are important. This topic is further addressed in section 3.5. ACTLABS (1999) claim that the quality of lithium tetra/metaborate fusion-ICP whole rock data meets or exceeds the quality of data by fusion-XRF.

Table 4: Percent undecomposed and characteristics of residue from mineral fusions (Cremer & Schlocker, 1976)

Mineral	Formula	% residue after fusion in 2:1 lithium tetra/metaborate
albite	$NaAlSi_3O_8$	<0.5
ankerite	$Ca(Mg, Fe^{2+}, Mn)(CO_3)_2$	<0.5
quartz	SiO_2	<0.5
ilmenite	$FeTiO_3$	0.7
magnetite	$FeFe_2O_4$	<0.5
pyrite	FeS_2	25.6
chalcopyrite	$CuFeS_2$	44.3

Once the sample has been decomposed (lithium tetra/metaborate fusion) it is ready for analysis by inductively coupled plasma (ICP) atomic emission spectrometry (AES). ICP-AES is a technique in which a sample solution is aspirated into a radio frequency excited argon plasma and thermally ionized at ~8000 °K (Potts, 1987). Each element produces a characteristic spectrum and the intensity of the spectral line is proportional to the concentration of element present. Rock samples produce many spectral lines and overlap interferences may be troublesome. The advantage of ICP-AES is that multiple elements can be analyzed simultaneously.

The procedure is slightly different for ICP-MS, such that ions are removed from the argon plasma through an orifice into a pumped vacuum system and into a mass spectrometer (Potts, 1987). Matrix interferences are avoided using this technique.

Holloway samples were analyzed by ICP-AES for major oxides plus Sc and Be; trace elements were analyzed by ICP-MS. The data is presented in Appendix A. Note that data acquired for mineralized samples is semi-quantitative for the chalcophile elements Ag, As, Bi, Co, Cu, Mo, Ni, Pb, Sb, Sn, W, and Zn (ACTLABS, 1999).

3.3 Instrumental Neutron Activation Analysis (INAA)

INAA measures primary gamma radiation emitted by radioactive isotopes produced when samples are irradiated by a known neutron flux in a nuclear reactor (Rollinson, 1993). INAA determines elements non-destructively, meaning there is no concern with respect to whether the element is in solution. ACTLABS (1999) report a detection limit of 5 ppb for gold analyzed by INAA. Gold values are presented in Appendix A.

3.4 CO_2, S, & H_2O

Carbon, sulphur and water were determined in the Analytical Chemistry Laboratory of the Geological Survey of Canada, Mineral Resources Division. Carbon and sulphur were determined simultaneously by LECO® SC-444DR. The sample is combusted in a concentric tube and carbon and sulphur are measured by infrared detection cells. Accuracy is reported at $\pm 0.1 + 3\%$ of concentration for carbon and $\pm 0.1 + 5\%$ of concentration for water. CO_2 and S values are presented in Appendix A.

H_2O was analyzed by LECO® RMC-100 rapid moisture determinator. The RMC-100 rapid moisture determinator first heats the weighed sample to a low temperature (~110°C) to drive off the free moisture. Next the furnace is ramped up to a temperature (~1000 °C) high

enough to drive off the water locked up in the mineral structures. The weight percent water is determined by an infrared detection cell which is not sensitive to other volatiles or gases. Accuracy is reported at ±0.02 + 5% of concentration of water. The reported H_2O value (essential water) was determined at a higher temperature (1050 °C) after the free moisture (non-essential water) was driven off. H_2O values are presented in Appendix A.

3.5 Ferrous Iron Determination

Chao and Sanzolone (1992) warn that no single decompositional technique exists for dissolving all minerals in all types of geological samples. Because of this I tried to develop a technique to account for undissolved iron-bearing phases during hydrofluoric (HF) decomposition. Accurate determination of ferrous iron is imperative to characterize hematite altered zones and to describe the tholeiitic meta-volcanic rocks which host Holloway's ore zones.

Ferrous iron determinations by wet chemical methods produce results that are considered unreliable due to errors associated with the technique (Johnson & Maxwell, 1981):

- refractory iron-bearing minerals (*e.g.* pyrite) do not decompose,
- introduction of "tramp" iron during crushing and grinding,
- aerial oxidation during acid decomposition,
- presence of sulphide minerals (*i.e.* if decomposable, S^{2-} will reduce some Fe^{3+} especially in a closed system),
- presence of organic carbon (*i.e.* oxidized during titration; gives high result for Fe^{2+}),
- presence of trivalent vanadium (*i.e.* oxidized during titration; gives high result for Fe^{2+})

Some of these errors are overcome by taking the following precautions: conduct acid decomposition in the presence of an oxidant, and conduct acid decomposition in an open system to decrease error by the presence of S^{2-}.

Ferrous iron was determined by the modified Wilson cold acid technique (Wilson, 1960; Whipple, 1974). Ammonium metavanadate is added to the samples to oxidize all of the Fe^{2+}. Hydrofluoric (HF) acid is added to the solution, and samples are left to dissolve for 24 hours. HF is a weak non-oxidizing inorganic acid that utilizes the complexing ability of F^- to decompose geological samples by destroying the silicate lattice (Chao & Sanzolone, 1992). Fluorides of As, B, Ti, Nb, Ta, Ge, Sb, and Si are partially or completely lost due to volatilization (Chao & Sanzolone, 1992). A sulphuric/phosphoric acid mixture is added to the solution and then the solution is brought up to 100 mL with distilled-deionized water. 2 mL of the solution are transferred for ICP-AES analysis of total iron under the assumption that Fe_2O_3T - FeT_{ICP} = pyrite. A known amount of ferrous ammonium sulphate is added to the solution to consume the remaining vanadate. The known amount of ferrous iron added is determined by running a blank. The excess ferrous iron is determined by redox titration with potassium dichromate using barium diphenylamine p-sulphonic acid as an indicator.

Total iron from the titrated solution was measured by ICP and converted to represent weight percent of the sample. The calculated value of total iron for the titrated solution (dissolved by HF digestion) was subtracted from the total iron for the sample (dissolved by lithium metaborate fusion) to yield the percent of pyrite from the titration according to the equation

$$\%pyrite_{(titration)} = (\%Fe_2O_3T - (\%Fe_{soln} * \frac{159.6922}{2*55.847})) * \frac{2*119.979}{159.6922}$$

where the molecular weights of Fe_2O_3 = 159.6922, Fe = 55.847, and FeS_2 = 119.979. The percent of insoluble iron is assumed to represent the mineral pyrite and is plotted on the x-axis of figure 3.1. If a sample contains pyrite as the only sulphur-bearing mineral, a correction can be applied to the determined ferrous and ferric values. The correction for pyrite appears on the y-axis of figure 3.1 and is calculated as

$$\%pyrite_{(sulphur)} = \frac{\%sulphur}{32.066} * 0.5 * 119.979$$

where the molecular weights of S = 32.066 and FeS_2 = 119.979. When %pyrite (calculated from sulphur) values are compared to %pyrite (calculated from iron titration), it is common that %pyrite values from titration are higher than those predicted by the sulphur value (figure 3.1). This indicates that iron is present in undissolved mineral species other than pyrite.

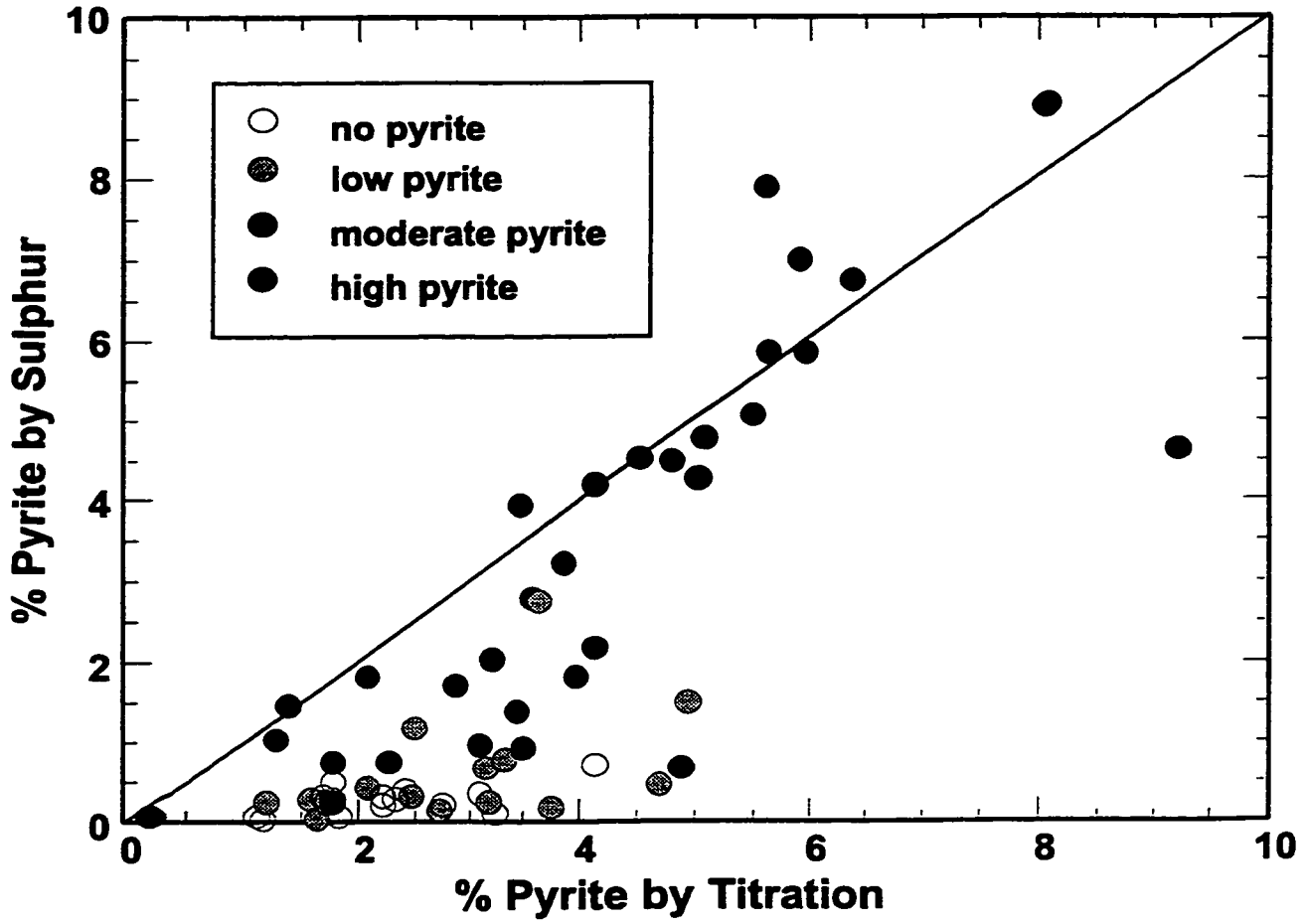

Figure 3.1: Percent pyrite calculated from sulphur concentrations versus percent pyrite determined by HF decomposition. Samples with zero, low (0-2%), and moderate (2-5%) amounts of pyrite have calculated pyrite values by titration that are higher than expected from sulphur concentrations. This indicates that Fe-bearing mineral species other than pyrite are present in the sample. Samples that contain a high (>5%) amount of pyrite have calculated pyrite values that are comparable using both techniques.

Similar discrepancies between calculated pyrite values were determined for the international standard MRG-1. The petrology of MRG-1 is reported by Perrault *et al.* (1973) as 51.2% augite, 9.2% olivine, 14.0% plagioclase, 10.1% opaques (magnetite and ilmenite), and 1.3% accessory minerals. According to CIPW norm calculations, pyrite is present at 0.14% (Perrault *et al.*, 1973). The accepted international standard values for MRG-1 are: Fe_2O_3T = 17.94%, Fe_2O_3 = 8.36%, FeO = 8.66%, S = 0.061%. Table 5 below presents ferrous iron data based on 3 repeat analysis of MRG-1 and calculated pyrite percentages.

Table 5: Ferrous iron determinations and calculated pyrite percentages for MRG-1

	accepted Intl. standard values	**Ropchan's values**
FeO (MRG-1)	8.66	8.58 ±0.12 (n=3)
% Pyrite	0.11% (sulphur = 0.061%)	7.3% (Fe_{soln} = 9.15%)

Calculation of the percent of pyrite from the accepted international sulphur value gives a value of 0.11%, close to that determined by Perrault *et al.*'s (1973) preliminary CIPW normative calculation of 0.14%. The calculated pyrite percentage based on the titration calculation is much higher at 7.3% and represents other Fe-bearing phases such as magnetite and ilmenite.

The titration technique for determining the percent of insoluble Fe-bearing phases is unable to distinguish between minerals, but does remind us that ferrous iron determinations only represent soluble Fe-bearing phases. As a result, ferrous iron values were used without applying adjustments for insoluble Fe-bearing phases and are not an accurate representation of the Fe^{2+}/Fe^{3+} composition of the rock, particularly the igneous composition.

3.6 DENSITY MEASUREMENTS

Density measurements were required for mass balance calculations. The Beckman Model 930 Air Comparison Pyconometer was used to measure the volume of powdered rock samples. The volume measurement along with the mass of the sample allow for determination of the density of the sample.

CHAPTER FOUR: GEOCHEMISTRY OF THE HOLLOWAY DEPOSIT

4.1 PRELUDE

Following the thesis objective to determine the nature of the rocks prior to mineralization, geochemical data from the Holloway deposit were closely examined. Prior to this detailed study of the Host-Iron Tholeiitic meta-volcanic rocks, Guy (1996) determined that pillowed and massive flow facies had uniform basaltic chemical compositions and represent the same Fe-tholeiitic magma. Macroscopic inspection of hand specimens eludes only differences in alteration. Through examination of geochemical data, particularly TiO_2 versus Zr plots (figure 4.17) and REE plots (figure 4.3), it was revealed that the rocks comprise a tholeiitic suite of rocks which can be divided into three groups: type I tholeiitic meta-basaltic rocks, type II Fe-tholeiitic meta-volcanic rocks, and type III variolitic meta-volcanic rocks. A Jensen plot (figure 4.10) illustrates a bimodal tholeiitic sequence where type I is distinct and separate from types II and III which appear to belong to another group comprising a continuous tholeiitic trend. The distribution of the types of meta-volcanic rocks is shown in figure 4.1 where the general geology is presented for the west and east mine workings.

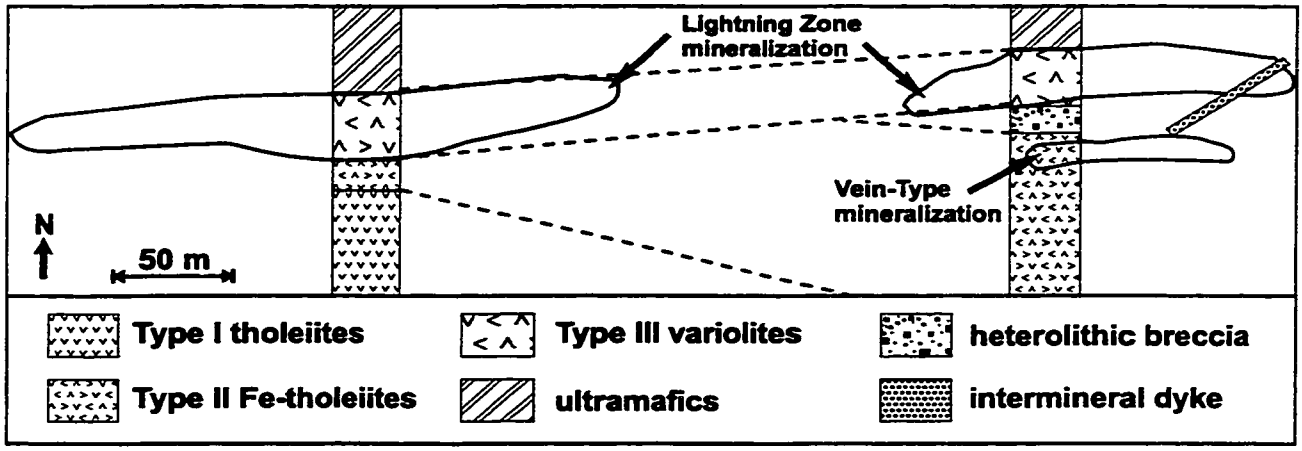

Figure 4.1: Generalized level plan of the mine workings for the Holloway deposit. Type I tholeiitic meta-basaltic rocks are present in the west mine workings, but not in the east. The east mine workings host Lightning Zone mineralization and later vein-type mineralization.

The widespread presence of pillowed texture demonstrates that the tholeiitic meta-volcanic rocks of the Holloway deposit were deposited in a submarine environment. Consequently the rock assemblage would have immediately undergone low-grade alteration by circulating seawater. Spilites are formed by sea floor metasomatism of mid-oceanic basalts, through the introduction of Na and H_2O into the rock converting the primary mineral assemblage to albite, chlorite, actinolite, titanite and calcite +/- epidote, prehnite, and laumonite (Staudigel & Hart, 1983).

Staudigel and Hart (1983) report the mobility of various elements subject to seawater alteration of basaltic glass. Seawater alteration involves two processes; decomposition of primary volcanic phases such as basaltic glass, plagioclase and olivine, and deposition of secondary mineral phases such as palagonite, zeolites and carbonates in vein and vug fillings (Staudigel & Hart, 1983). Glass alteration results in a significant loss of most elements, except for Ti and Fe which are immobile during seawater alteration, and K, Rb, Cs, H_2O and CO_2 which are enriched (Staudigel & Hart, 1983). Most elements are redeposited in veins and vugs (Staudigel & Hart, 1983). Several authors (Michard, 1989; Staudigel & Hart, 1983) conclude it is unlikely that seawater alteration significantly affects REE patterns because REE concentrations in seawater are 10^{-6} those of MORB, and under typical water/rock ratios the release of MORB REE will dominate the signature of circulating seawater. Bau (1991) states that water/rock ratios would have to be greater that 10^3 to change a whole-rock REE patterns. Therefore the process of seawater alteration is not a major concern for this comparative study, at least for the less mobile elements such as the REE and HFSE.

McCuaig and Kerrich (1994) summarize the results of previous hydrothermal alteration studies (Kerrich, 1983; Lesher *et al.*, 1986) which show that for various intensities of alteration, high-field-strength elements (HFSE: Th, Nb, Ta, Zr, Ti, Y, P, Al, Ga), rare-earth elements (REE: La-Lu), and compatible trace elements (Sc, V, Cr, Ni) are alteration insensitive or isochemical. Alternatively, lode gold deposits typically show enrichments of precious metal (Au, Ag), associated trace elements (As, Sb, Se, Te, Bi, W, B), large-ion-

lithophile elements (LILE: K, Rb, Ba, Li, Cs, Tl), and volatiles (McCuaig and Kerrich, 1994). Base metals (Cu, Zn, Pb) will usually have low abundances due to the chemistry of the transporting fluid. Chondrite-normalized REE patterns for hydrothermal fluids are LREE-enriched and have a large positive europium anomaly (Klinkhammer *et al.*, 1994; Michard, 1989). In order to transport REE in hydrothermal fluids for any significant distance, the formation of complexes with F^-, Cl^-, CO_3^{2-}, and PO_4^{3-} is required (Henderson, 1984). However, gold and associated elements are usually solubilized in hydrothermal solutions by sulphur complexes, whereas base metals form chlorine complexes (Seward, 1973). Thus, during gold mineralization the REE are not expected to be mobilized.

4.2 REE Plots

REE plots are commonly used as empirical evidence to discriminate the tectonic regime under which igneous rocks formed. Geochemical patterns cannot solve tectonic problems, however the use of geochemical trends can be used to make correlations with modern day rock suites of known tectonic settings. For example, oceanic island basalts (OIB) have LREE-enriched profiles, whereas tholeiitic mid-oceanic ridge basalts (MORB) have flat-lying REE profiles (Sun & McDonough, 1989). When studying Archean volcanic rocks, it is important to keep in mind that modern tectonic models may not be applicable, and that REE patterns cannot be simply correlated to modern environments. However, REE abundance patterns can be very useful for studying potential tectonic affinities, and for modeling processes that control rock composition such as differentiation.

There is evidence that the REE abundances of rocks in this study have not been modified by hydrothermal fluid signatures such that REE profiles reflect the primary geochemical signature of rocks despite varying intensities of alteration. Figure 4.2 shows average REE abundance patterns for modern OIB and MORB. REE abundance patterns for samples from the Holloway deposit are plotted in figure 4.3 and display REE profiles that have not been affected by extreme alteration. Also, in section 4.7.1, quantitative analysis of the meta-

volcanic rocks is done to evaluate elemental gains and losses during alteration. This analysis demonstrates that the REE remained relatively immobile during alteration. Additional support for this assumption is provided by the flat-lying REE profiles characteristic of Holloway's meta-volcanic rocks (figure 4.3). Since the concentration of REE in hydrothermal fluids is 5 X 10^2 to 10^6 less than the surrounding rocks, a very high water/rock ratio is required to modify the REE signature of the host rocks (Michard, 1989). If the rocks had taken on a hydrothermal fluid signature, the REE profile would be LREE-enriched and display a positive Eu anomaly.

Several distinct populations of samples from the Holloway deposit can be observed in figure 4.3. Meta-komatiite rocks from the Holloway deposit have relatively flat-lying REE profiles with concentrations 1-7 times chondrite. A suite of flat-lying tholeiitic meta-volcanic rock REE profiles range from ten to one hundred times chondrite. In contrast to the meta-volcanic rocks, meta-sedimentary and coarse-grained heterolithic breccia units within Holloway have steep slopes (figure 4.3) with LREE equal to 200-300 times chondrite and HREE equal to 2-3 times chondrite. LREE-enriched patterns are common for sedimentary rocks. LREE are preferentially mobilized during weathering under acidic conditions and accumulate in sedimentary rocks (Fleet, 1984).

The flat-lying Host Iron-Tholeiitic meta-volcanic rocks are divided into three groups on the basis of their REE profiles. Type I tholeiitic meta-basaltic rocks have flat REE profiles with concentrations approximately equal to ten times chondrite. Type II have flat profiles with chondrite-normalized concentrations near fifty. Type III has flat patterns with chondrite-normalized REE concentrations around one hundred and small negative Eu anomalies. The discovery of three types of tholeiitic meta-volcanic rocks is a significant advancement because Lightning Zone mineralization is only associated with type III variolitic meta-volcanic rocks.

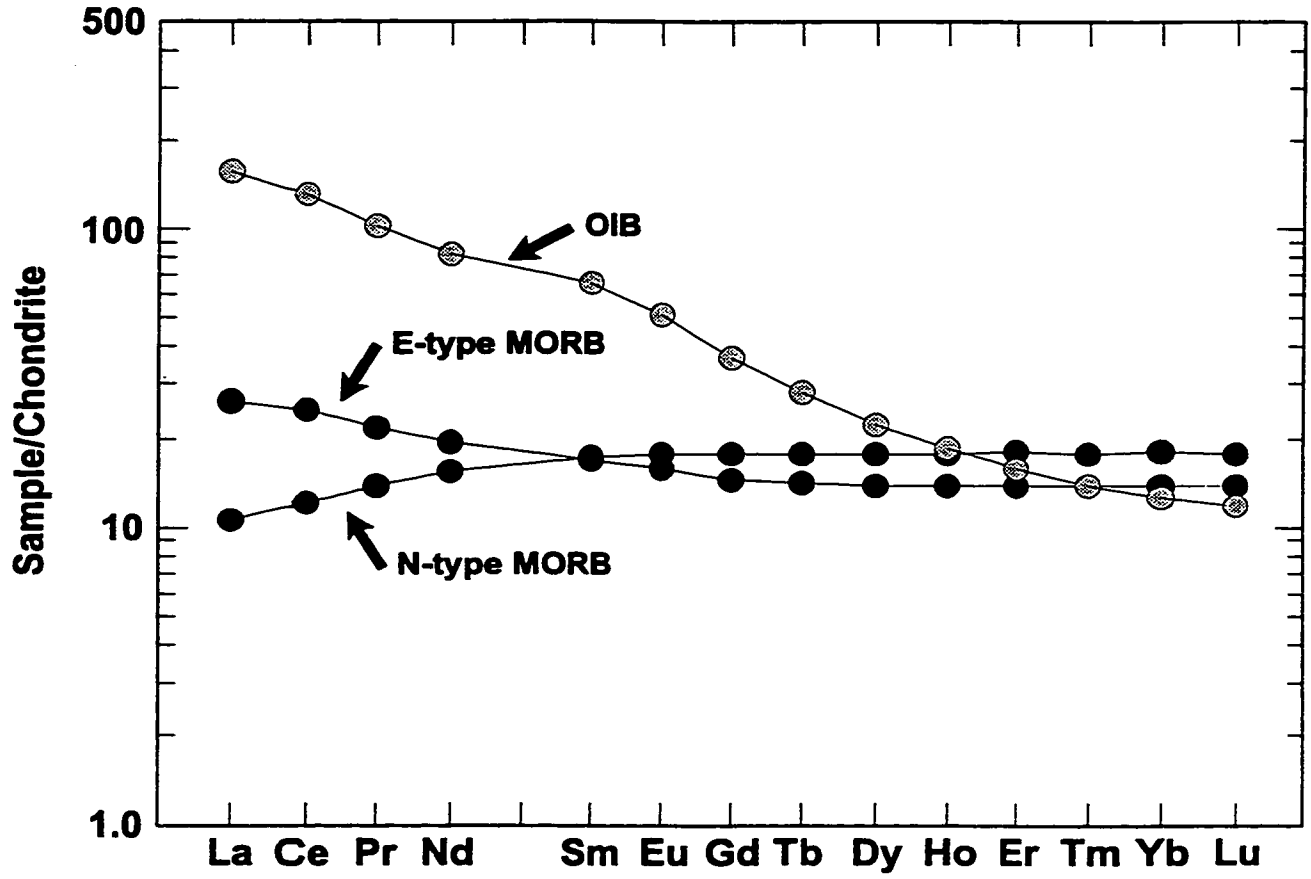

Figure 4.2: Chondrite-normalized REE abundance pattens for average modern MORB and OIB (Sun & McDonough, 1989).

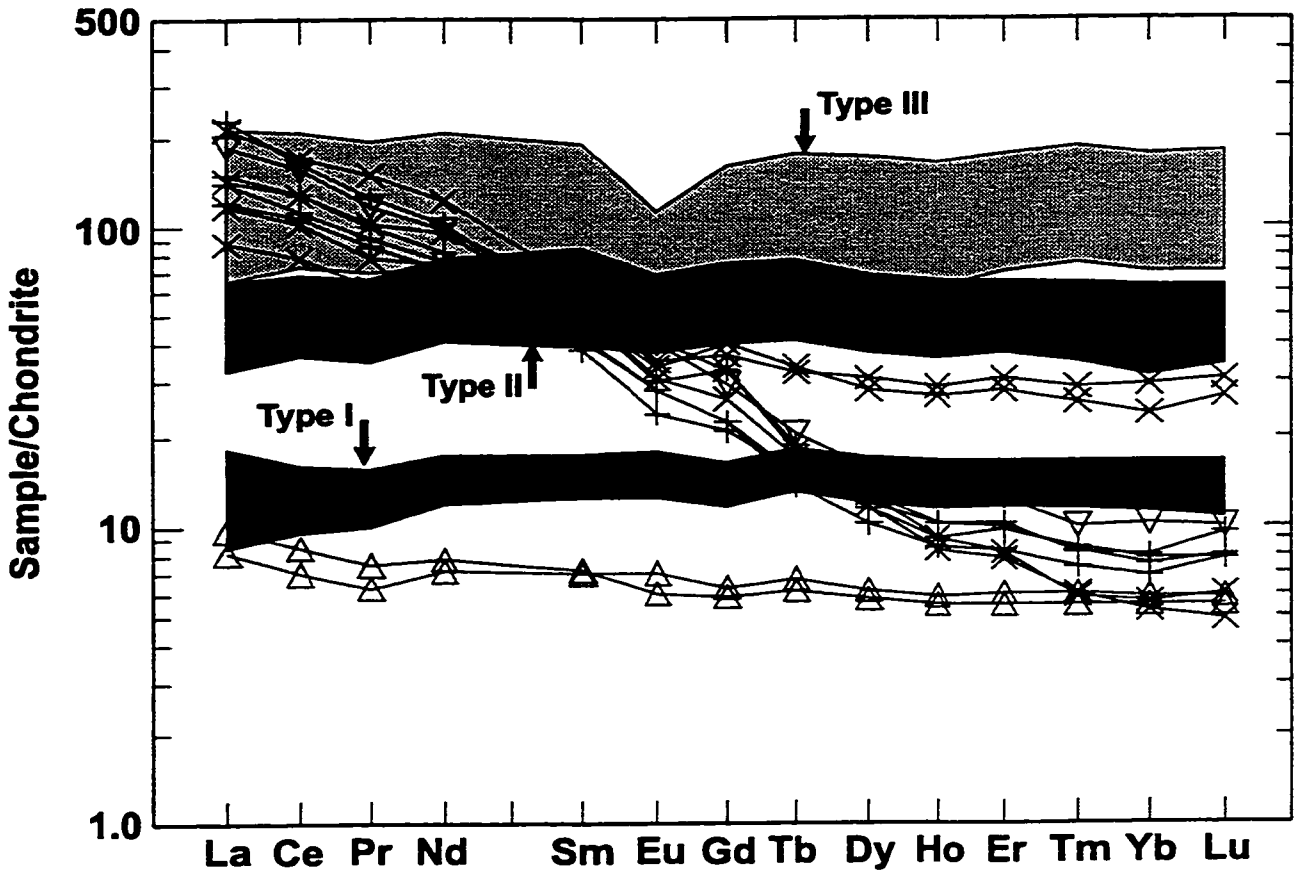

Figure 4.3: Chondrite-normalized REE abundance patterns for samples from the Holloway deposit. Squares, type I tholeiitic meta-basaltic rocks; diamonds, type II Fe-tholeiitic meta-volcanic rocks; circles, type III variolitic meta-volcanic rocks; triangles, meta-komatiite rocks; inverted triangles, meta-sediments; asterisks, west 3D-CG heterolithic breccia; crosses, east 3D-CG heterolithic breccia; plus signs, intermineral dyke.

The REE patterns for meta-volcanic rocks from the Holloway deposit are similar to Fowler and Jensen's unaltered (1988) tholeiitic Kinojevis suite of rocks (figure 4.4). Figure 4.4 shows flat lying patterns with REE concentrations from ten to one hundred times chondrite and small negative Eu anomalies in evolved rocks for basalt to rhyolite suites of tholeiitic rocks. Evolution of the tholeiitic suite was dominated by fractional crystallization of olivine, pyroxene, plagioclase and Fe-Ti oxides, such that at least 90% crystallization was required to form the most evolved REE signatures (Fowler & Jensen, 1988). Fowler and Jensen (1988) conjectured that this occurred in a high-level magma chamber.

Lesher *et al.*'s (1986) study of massive sulphide ore-associated and barren felsic meta-volcanic rocks allowed them to classify Archean felsic meta-volcanic rocks into three major groups based on trace-element geochemistry. FIIIb-type felsic meta-volcanic rocks have flat-lying REE profile around one hundred times chondrite with pronounced negative europium anomalies (figure 4.5). This rock type is inferred to originate from high-level magma chambers which are required for the generation of hydrothermal fluids associated with massive base-metal sulphide deposits. The similarity of Holloway's type III variolitic meta-volcanic rocks to Lesher *et al.*'s (1986) FIIIb-type, indicate rocks with this REE profile have economic importance for gold deposits as well as massive sulphide deposits.

It has always been assumed that volcanic rocks at the Holloway deposit originally had similar chemical signatures because the rocks were thought to be undifferentiated meta-basalts (*e.g.* Broughton *et al.*, 1991; Guy, 1996). The recognition of three groups of tholeiitic meta-volcanic rocks within the Holloway deposit was a crucial step to make before an accurate alteration study could be undertaken. Least altered specimens need to be carefully chosen for each type of meta-volcanic rock to represent the original chemistry. Under the original assumption that all the meta-volcanic rocks at the Holloway deposit had similar chemistry, some patterns may have been misidentified as products of alteration instead of differentiation.

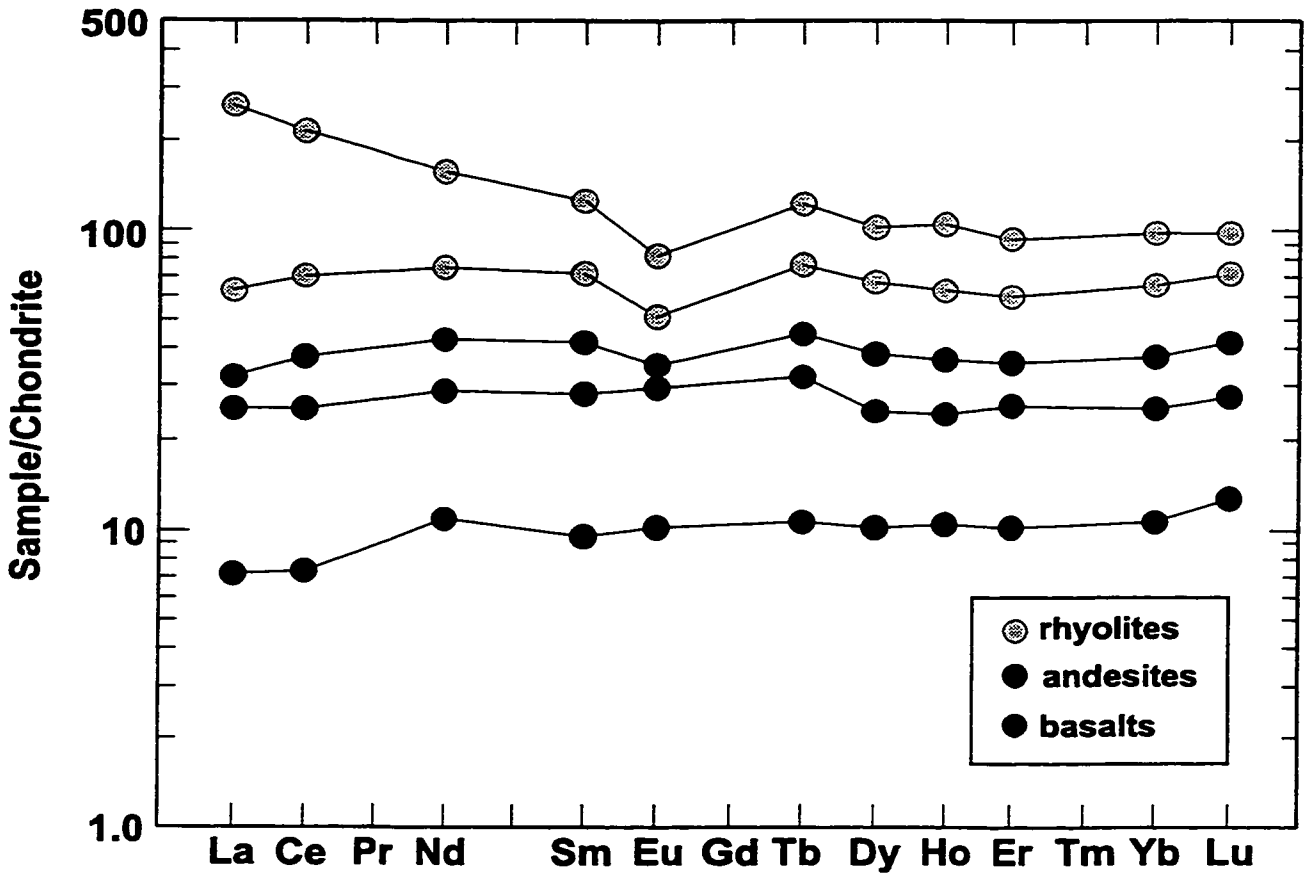

Figure 4.4: Chondrite-normalized REE abundance patterns for the Kinojevis suite (after Fowler & Jensen, 1988). The differentiated pattens were produced by fractional crystallization.

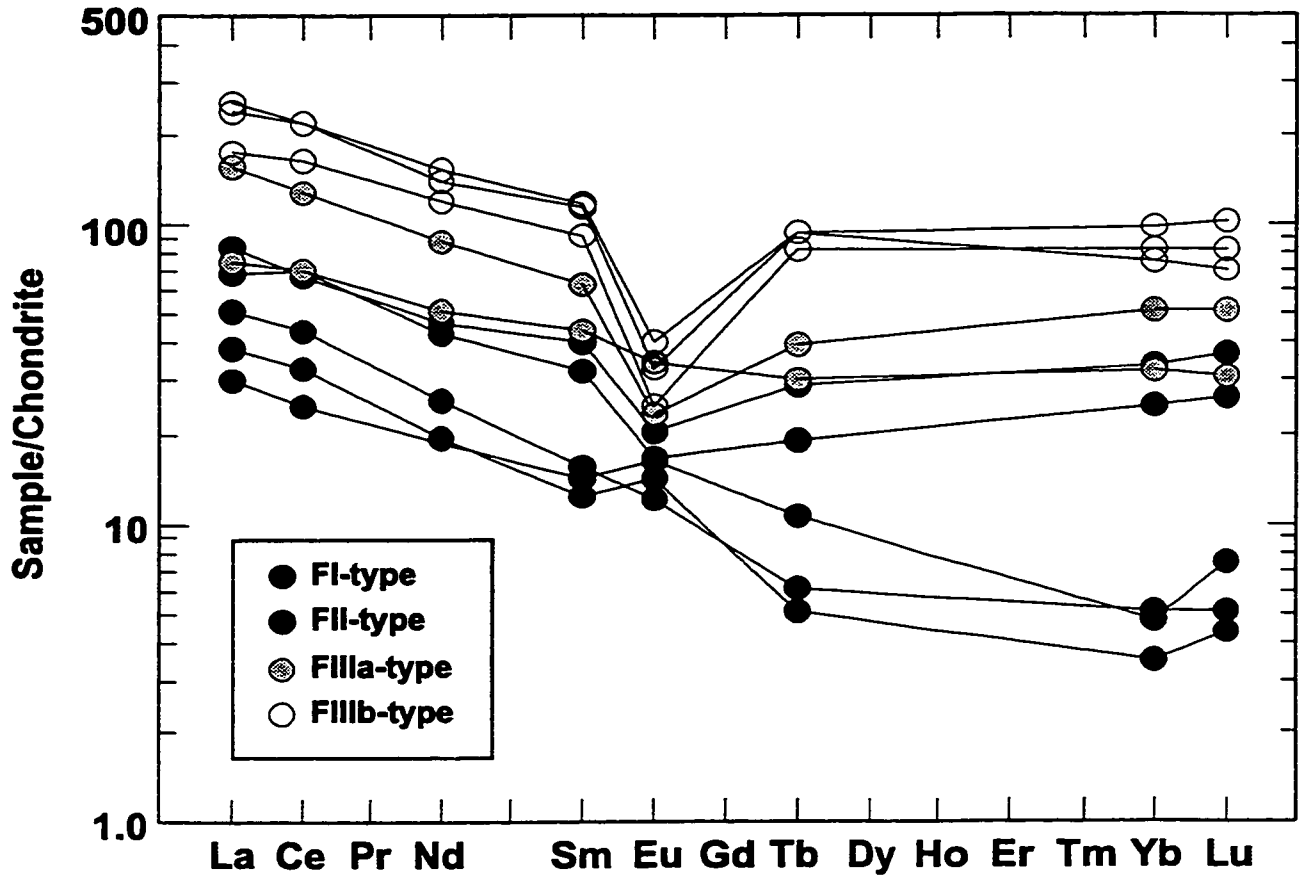

Figure 4.5: Chondrite-normalized REE abundance patterns for Lesher *et al*'s (1986) rhyolites. FIIIb-type felsic meta-volcanic rocks have flat-lying REE profile around one hundred times chondrite with pronounced negative europium anomalies.

4.3 SPIDER DIAGRAMS

Spider diagrams is a colloquial term used to describe mantle-, chondrite-, or MORB-normalized multi-element diagrams. Commonly, two types of information can be gleaned from spider diagrams: comparison of rock chemistry with a 'mantle' source, and comparison of rock chemistry to the most abundant rock type, MORB (Rollinson, 1993). Chondrite-normalizing values are preferred over mantle-normalizing values to represent a 'mantle' source, since they are directly measured. Primitive mantle normalizing values represent the composition of the mantle prior to the formation of continental crust and are merely estimations (Rollinson, 1993). Figure 4.6 presents chondrite-normalized spider diagrams for the three types of meta-volcanic rocks from the Holloway deposit. The chondrite-normalizing values used are those of Thompson (1982).

Chondrite-normalized spider diagrams provide a means for comparing the chemistry of rocks to that of a 'mantle' source. All of the meta-volcanic rocks from the Holloway deposit have a fairly flat pattern for immobile elements and variably enriched LILE concentrations. These results are likely a function of alteration by seawater or hydrothermal fluids as LILE are highly mobile. Type I immobile elements have a flat lying pattern approximately ten times chondrite concentrations, with P_2O_5, Zr and Hf displaying weak negative anomalies. Type II meta-volcanic rocks also have flat lying immobile element patterns with a strong negative Sr anomaly, a weak positive P_2O_5 anomaly, and a weak negative TiO_2 anomaly. Type III meta-volcanic rocks have the most evolved immobile patterns with strong negative Sr, P_2O_5 and TiO_2 anomalies.

Spider diagrams are a useful way to depict basalt chemistry and therefore are often presented as MORB-normalized diagrams. Figure 4.7 presents MORB-normalized spider diagrams for the meta-volcanic rocks of the Holloway deposit. The MORB-normalizing values used are those of Pearce (1983).

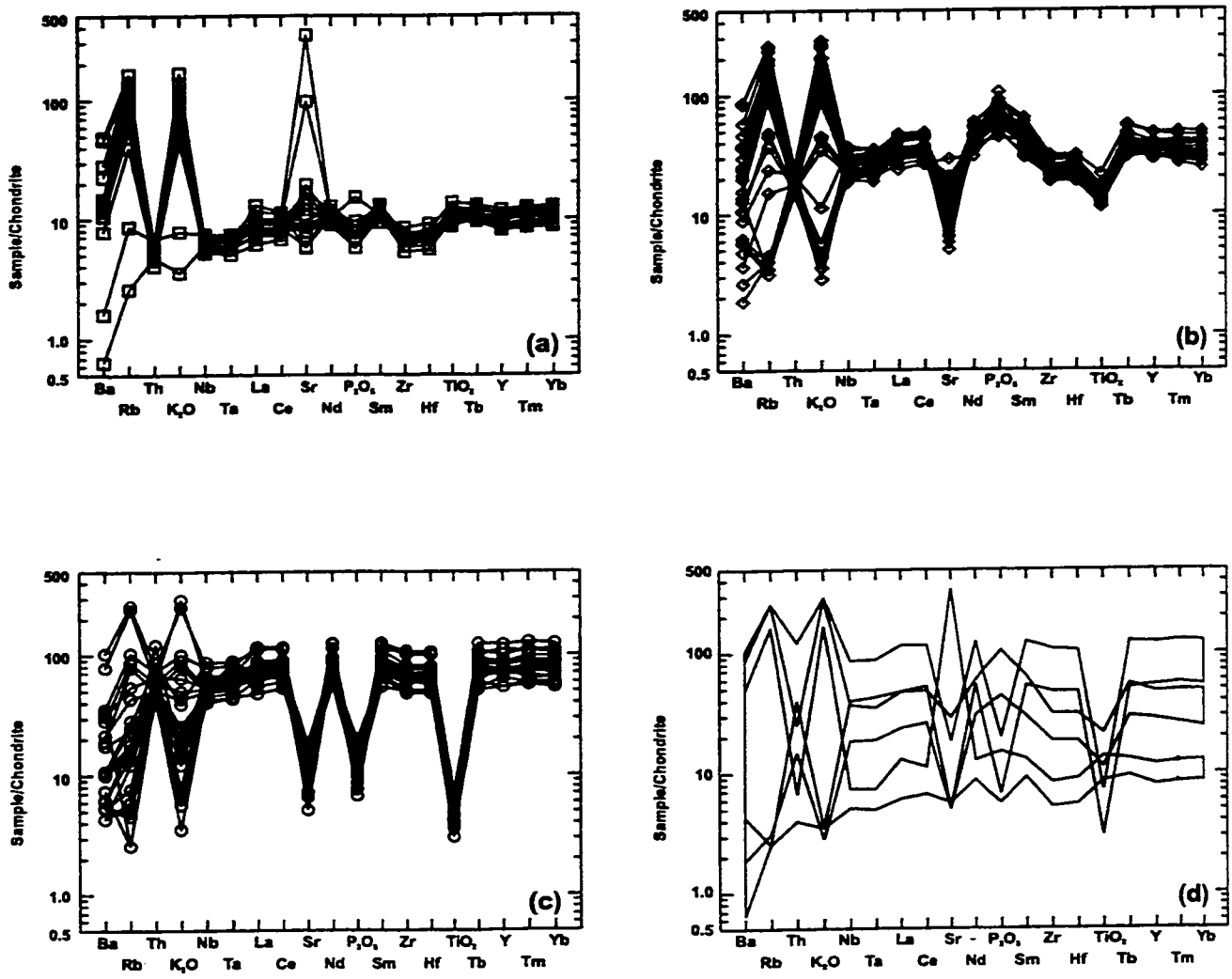

Figure 4.6: Chondrite-normalized spider diagrams for meta-volcanic rocks from the Holloway deposit. (a) Type I tholeiitic meta-volcanic rocks. (b) Type II Fe-tholeiitic meta-volcanic rocks. (c) Type III variolitic meta-volcanic rocks. (d) Group distributions demonstrating variable LILE concentrations due to alteration and progressive enrichment of incompatible elements from type I to type III.

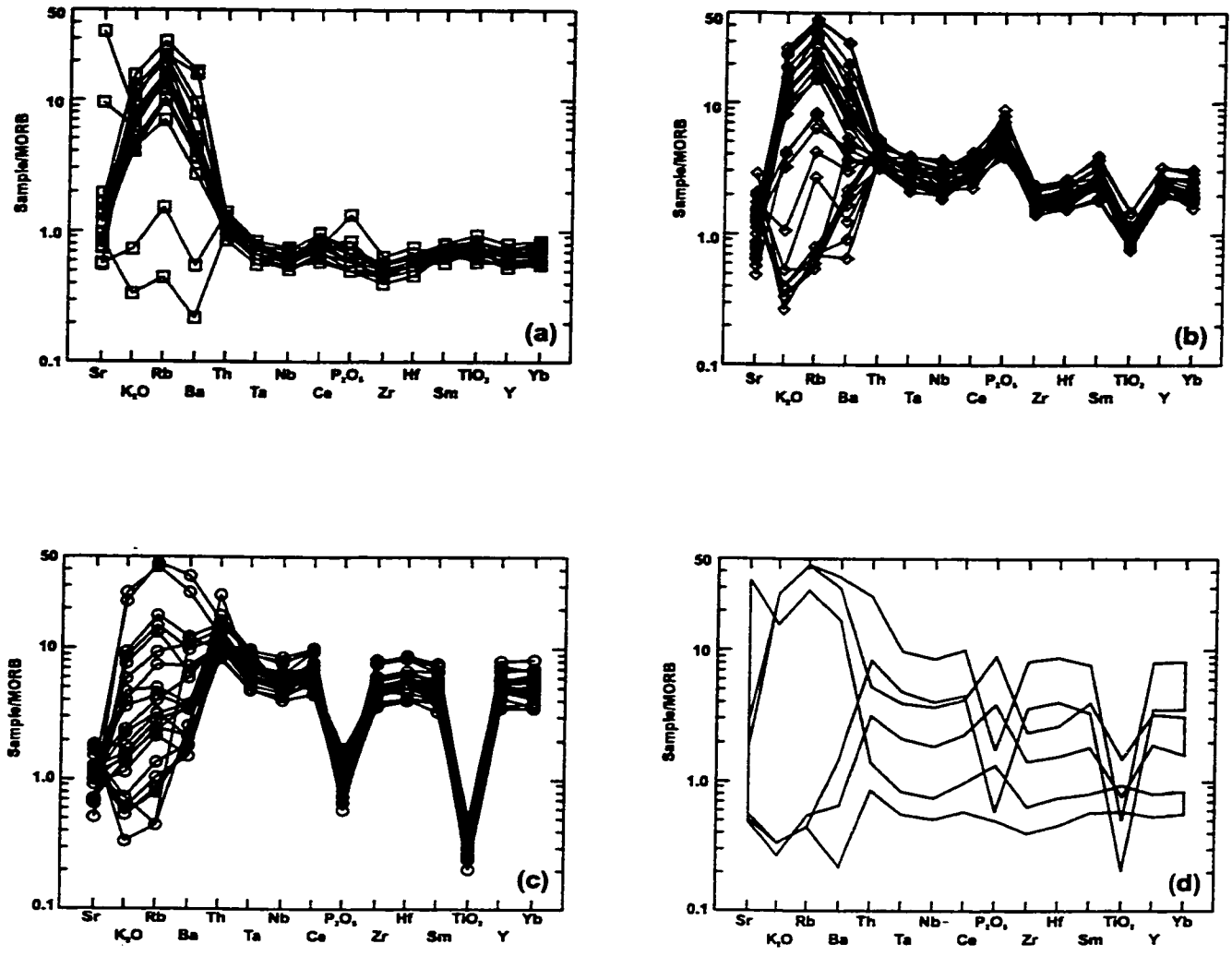

Figure 4.7: MORB-normalized spider diagrams for meta-volcanic rocks from the Holloway deposit. (a) Type I tholeiitic meta-volcanic rocks. (b) Type II Fe-tholeiitic meta-volcanic rocks. (c) Type III variolitic meta-volcanic rocks. (d) Group distributions demonstrating variable LILE concentrations due to alteration and progressive enrichment of incompatible elements from type I to type III.

Immobile elements for type I tholeiitic meta-volcanic rocks (figure 4.7a) plot as a nearly horizontal line slightly below one times MORB. The LILE demonstrate a high degree of mobility with values 7 to 35 times MORB. Two of the least altered specimens have LILE concentrations closer to one. Type II Fe-tholeiitic meta-volcanic rocks (figure 4.7b) maintain relatively flat patterns that are more evolved than MORB and display positive P_2O_5 and negative TiO_2 anomalies. Again the LILE demonstrate a high degree of mobility with variable concentrations. Type III variolitic meta-volcanic rocks (figure 4.7c) have immobile element concentrations 35 to 90 times MORB-normalizing values and display prominent negative P_2O_5 and TiO_2 concentrations.

The spider diagram results indicate that types II and III were derived from a magma source similar to type I tholeiitic meta-volcanic rocks. For example, TiO_2 is a compatible element that shows progressively stronger depletion in more evolved rocks. The positive P_2O_5 anomaly in type II meta-volcanic rocks has an unknown origin (*i.e.* does not show an abundance of apatite in thin sections) and may provide interesting information on the petrogenesis of the rock suite.

4.4 Basalt Determination & Jensen Diagrams

Meschede (1986) developed a ternary diagram to discriminate between different types of basalts. Meta-volcanic rocks from the Holloway deposit are plotted on a Zr-Nb-Y diagram in figure 4.8 and cluster within the N-type MORB field.

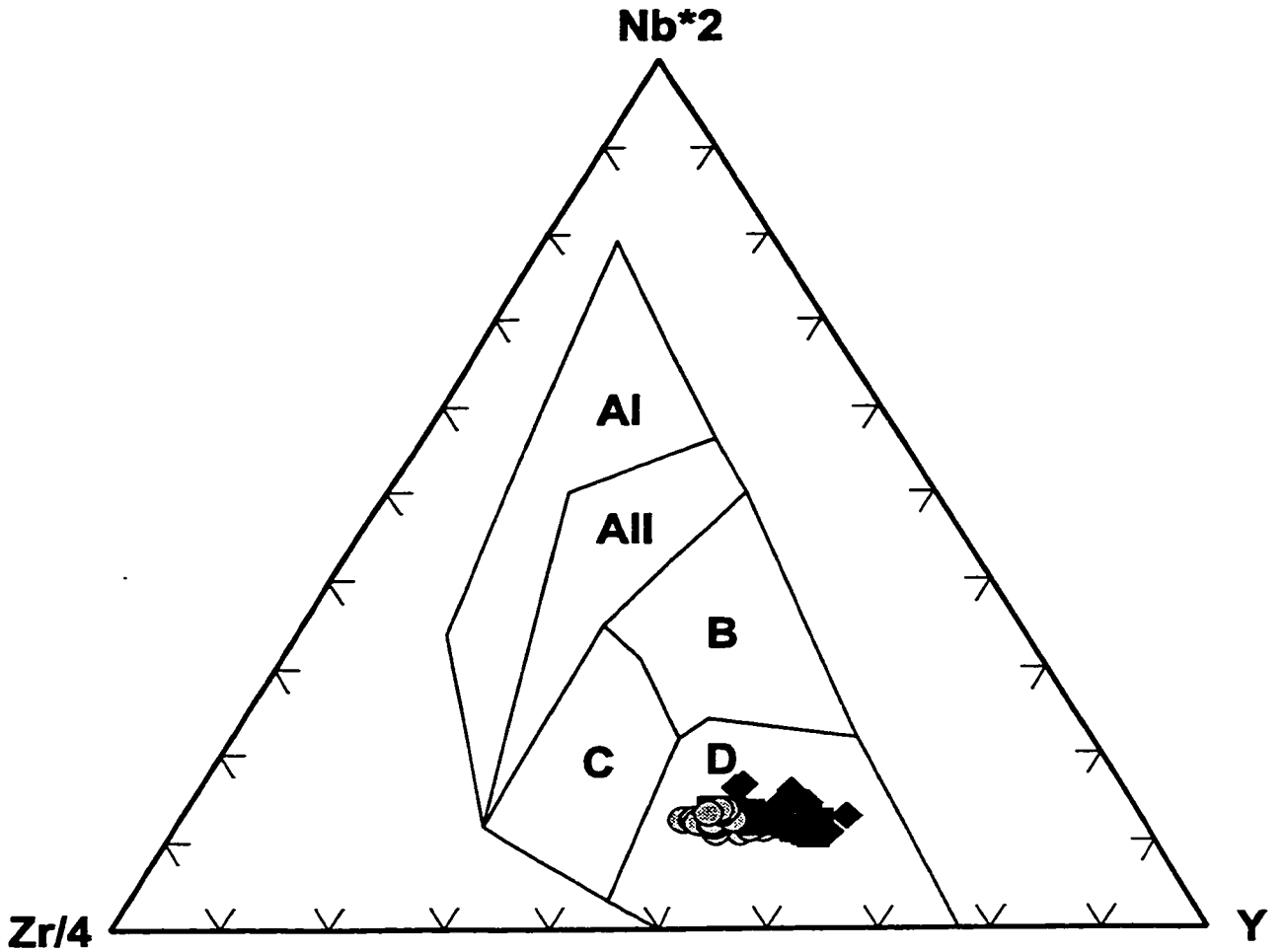

Figure 4.8: Zr-Nb-Y discrimination diagram for meta-volcanic rocks from the Holloway deposit. Squares, type I tholeiitic rocks; diamonds, type II Fe-tholeiitic rocks; circles, type III variolitic rocks. The fields are defined as: AI, within-plate alkali basalts; AII, within-plate alkali basalts and within-plate tholeiites; B, E-type MORB; C, within-plate tholeiites and volcanic-arc basalts; D, N-type MORB and volcanic-arc basalts (after Meschede, 1986).

Irvine & Baragar (1971) developed a chemical classification scheme for common volcanic rocks. Their classification scheme consisted of a ternary (AFM) diagram where the apices represented $A = Na_2O + K_2O$, $F = FeO + 0.8998*Fe_2O_3$, and $M = MgO$, all in weight percent. Jensen (1976) identified potential problems associated with the AFM diagram and made appropriate adjustments to the diagram to compensate for the mobility of the alkali elements (Na_2O and K_2O). The resulting ternary diagram is known as the Jensen plot with the apices defined by oxides (cation percent) of Al_2O_3, $FeO + Fe_2O_3 + TiO_2$, and MgO (Jensen, 1976). Jensen (1976) chose these oxides because they are less mobile than K, Na, Ca and Si, they have a relationship to rock colour as observed on outcrop, and they have nearly equal percentage ranges within the spectrum of subalkalic volcanic rocks. Jensen diagrams discriminate bewteen Fe- and Mg-rich tholeiitic basalts. Grunsky *et al.* (1992) warn that the Jensen diagram was created based on Superior Province Archean greenstone belts and may not be relevant to subalkalic volcanic rocks outside of this environment.

Chemical analyses of tholeiitic meta-volcanic rock samples collected from the Holloway deposit are plotted on a Jensen subalkalic volcanic rock discrimination diagram (figure 4.10). Two clusters of samples are recognizable: (1) least-evolved type I tholeiitic meta-basalts consisting of carbonatized and sericitized massive and pillowed mafic meta-volcanic rocks and, (2) a tholeiitic trend of high Fe-tholeiitic basalt (type II) to rhyolite (type III) consisting of carbonatized and sericitized massive and pillowed meta-basalts plus silicified and albitized hyaloclastite and variolitic meta-volcanic rocks. Type III tholeiitic meta-volcanic rocks generally have the highest concentration of pyrite, therefore they sometimes plot too high on the $FeOt+TiO_2$ axis.

Type I tholeiitic meta-basaltic rocks plot as a cluster near the boundary between Mg- and Fe-rich tholeiitic rocks. The second cluster of samples on the Jensen plot represent types II and III meta-volcanic rocks whose fields overlap. Both clusters plot along the tholeiitic trend and the gap between type I and type II tholeiitic meta-volcanic rocks may indicate that the rocks erupted from different sources, that volcanism stopped for a period of time for sufficient

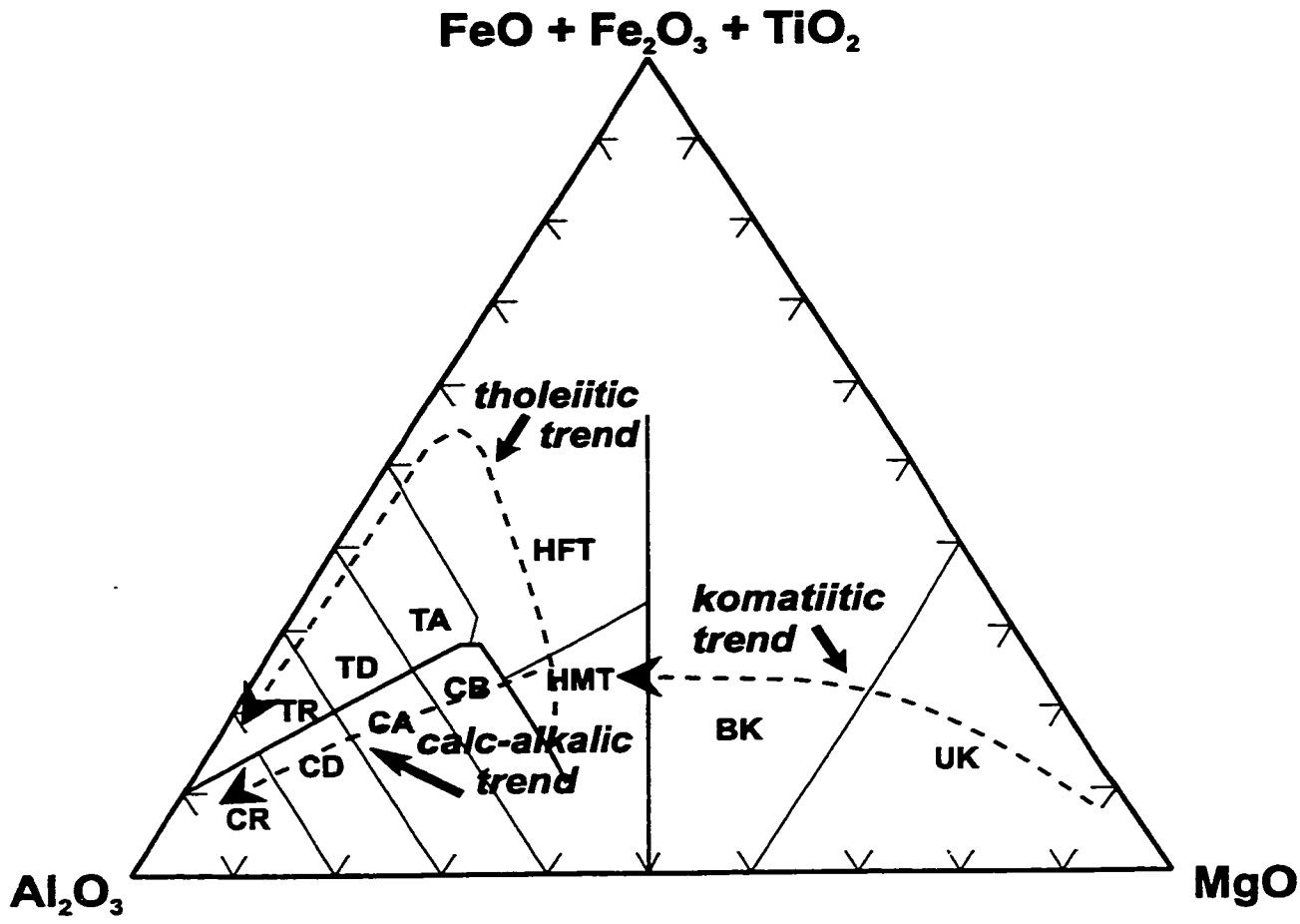

Figure 4.9: Schematic Jensen plot showing field descriptors and the Fe-enrichment trend for tholeiitic rocks (after Jensen, 1976). Dashed lines represent enrichment trends for tholeiitic, calc-alkalic and komatiitic rocks. UK, ultramafic komatiite; BK, basaltic komatiite; HMT, high Mg-tholeiite; HFT, high Fe-tholeiite; TA, tholeiitic andesite; TD, tholeiitic dacite; TR, tholeiitic rhyolite; CB, calc-alkalic basalt; CA, calc-alkalic andesite; CD, calc-alkalic dacite; CR, calc-alkalic rhyolite.

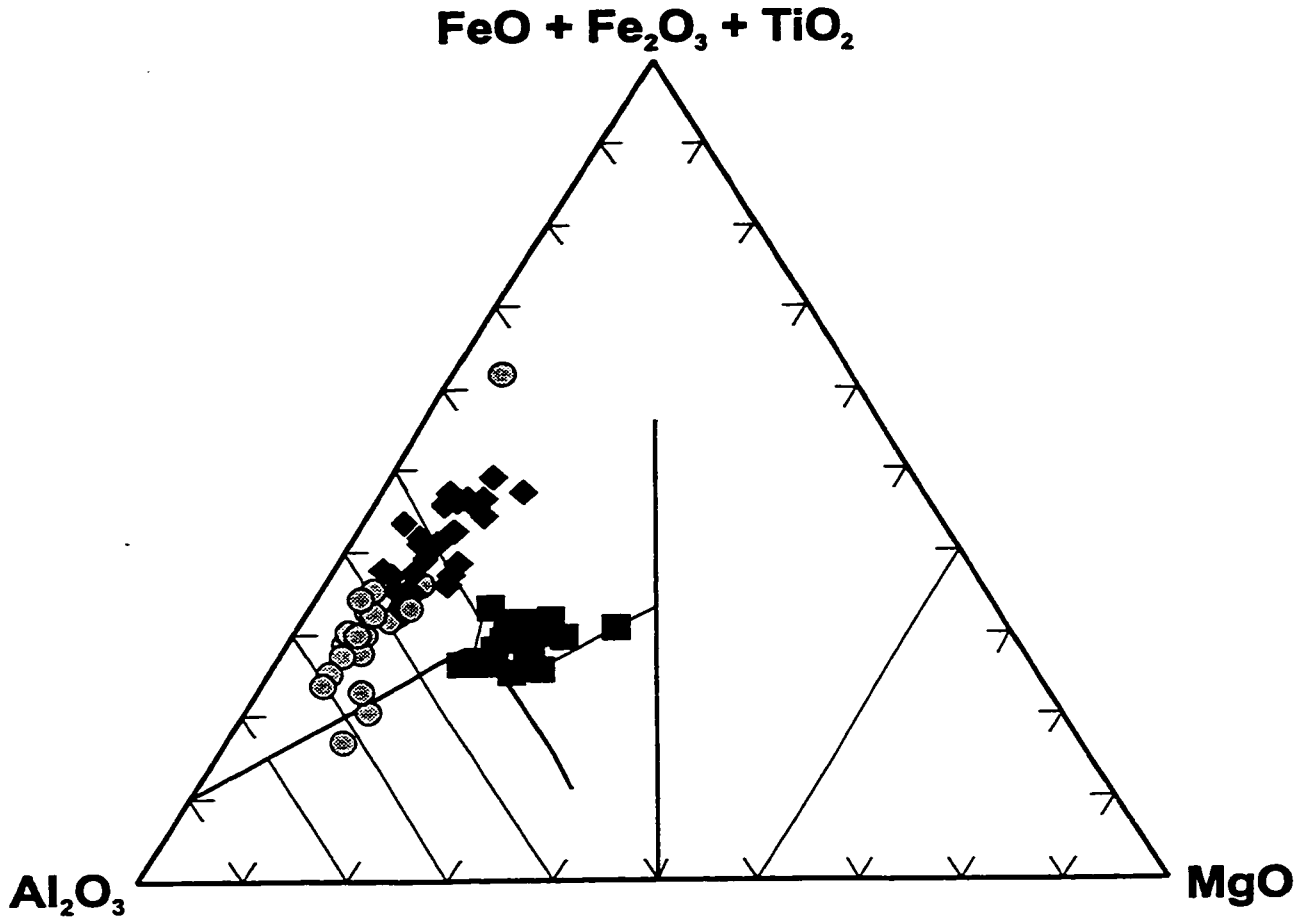

Figure 4.10: Jensen plot of meta-volcanic rocks from the Holloway deposit. Squares, type I tholeiitic meta-volcanic rocks; diamonds, type II Fe-tholeiitic meta-volcanic rocks; circles, type III variolitic meta-volcanic rocks. Types I to III illustrate a Fe-enrichment trend for the tholeiitic meta-volcanic rocks at the Holloway deposit.

differentiation to occur, or least likely incomplete sampling. If differentiation is the case, then it is possible that the volcanic stratigraphy in the mine is opposite to the regional south-younging direction. That is to say that the Host Iron-Tholeiitic meta-volcanic rocks are more evolved, thus younger, to the north. But, if differentiation occurred in the magma chamber, the most evolved magmas would be at the top the first to be erupted, followed by the undifferentiated basalts (*i.e.* tops to the south).

4.5 GEOLOGICAL PROCESSES

Several petrogenetic processes can influence the elemental composition of volcanic rocks as the magma is transported from its source region to its present day location. Petrogenetic processes which may account for differentiated suites of rocks consist of liquid immiscibility, partial melting, and fractional crystallization. Further processes that affect the primary composition of a melt include magma mixing, assimilation, or a combination of these. Other modifications to elemental chemistry occur during and post-eruption and include outgassing, hydrothermal alteration, weathering and metamorphism. It is amazing that geologists can glean any useful information from Archean volcanic rocks that have been subjected to several geological processes.

Watson (1976) rejects immiscible liquids as a differentiation process for typical basalt-rhyolite associations. Experiments by Ryerson & Hess (1978) and Watson (1976) found that for immiscible liquids, mafic melts are enriched in P_2O_5, REE, Ta, Ca, Cr, Ti, Mn, Zr, Mg, Sr, Ba, and Fe and felsic melts are enriched in alkalis (Cs, Rb, K). The results of those experiments is opposite to what is found in the field, therefore typical basalt-rhyolite associations are probably not generated by 2-liquid phase separation (Watson, 1976).

Other processes such as magma mixing and assimilation are not likely for differentiation of meta-volcanic rocks at the Holloway deposit. Significant magma mixing is unlikely in mafic systems because effusion is direct from the source and residence time in shallow chambers is

low. Also, the chemistry of magma at spreading centers is mostly basaltic, hence mixing would not likely cause significant contamination, unlike calc-alkalic systems where the crust is thick and considerable variation in magma composition is known to occur in magma chambers. Holloway's meta-volcanic rocks are normalized to primitive mantle values (Hofmann, 1988) and plotted on a Th-Nb-La ternary diagram in figure 4.11. All but one of the meta-volcanic rocks plot within or near the MORB field. Jochum *et al.* (1991) state that the diagram does not serve as a discrimination diagram, rather a way to illustrate chemical differences between mafic-ultramafic rocks. Figure 4.11 demonstrates that crustal contamination is not valid for meta-volcanic rocks from the Holloway deposit since they do not follow the crustal contamination trend. Moreover, to the author's knowledge there is no field evidence for assimilation because xenoliths and enclaves are not represented within the flows.

Only partial melting and fractional crystallization remain as likely candidates for the differentiation of meta-volcanic rocks from the Holloway deposit. The continuum of REE profile evolution for the meta-volcanic rocks suggests that fractional crystallization of olivine, pyroxene, plagioclase, and Fe-Ti oxides is responsible for differentiation. Also, the first melts (*e.g.* type III) derived by partial melting should exhibit LREE-enriched abundance patterns, and consequently one would expect the later melts (*e.g.* type I) to have LREE-depleted patterns, neither of which is the case for Holloway's meta-volcanic rocks. The Treuil method (Maaløe, 1985) was applied to Holloway's meta-volcanic rocks because it can test which process is responsible for differentiation. But first, it must be shown that the meta-volcanic rocks are derived from the same magma source.

Magma source characteristics can be identified from ratio-ratio plots of highly incompatible elements such as Th, Ta, and Tb (Rollinson, 1993). Incompatible elements minimize the effects of differentiation and can be used to determine magma source characteristics (Rollinson 1993). The ratio plot (figure 4.12) for types I, II, and III are relatively similar, indicating that Holloway's meta-volcanic rocks were derived from the same magma source.

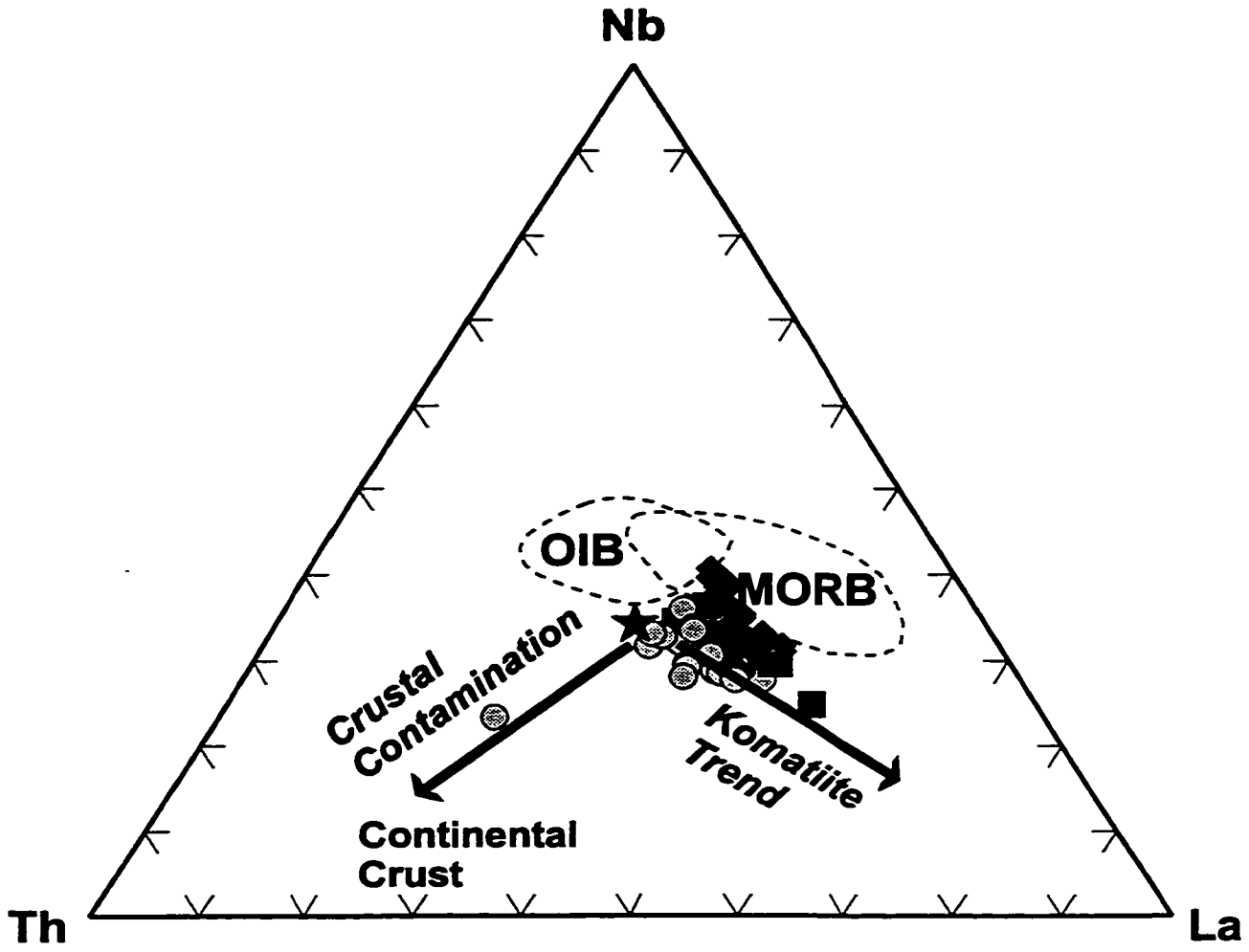

Figure 4.11: Th-Nb-La diagram for illustrating chemical differences associated with crustal contamination (after Jochum *et al.*, 1991). Meta-volcanic rocks from the Holloway deposit were normalized to primitive mantle values of Th = 0.0813, Nb = 0.6175, and La = 0.6139 (Hofmann, 1988) and plotted as: squares, type I tholeiitic rocks; diamonds, type II Fe-tholeiitic rocks; circles, type III variolitic rocks. The star indicates the composition of primitive mantle, and the arrows define the crustal contamination and komatiite trends. Holloway's meta-volcanic rocks plot near the MORB field.

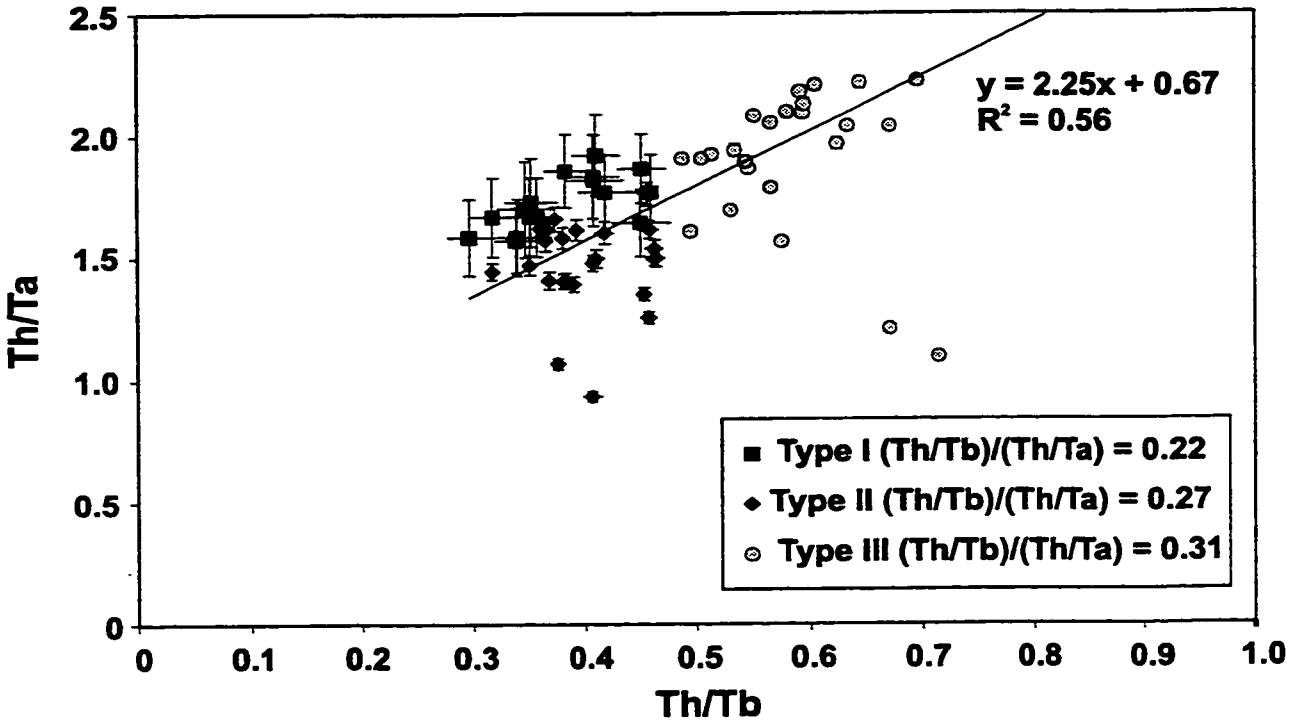

Figure 4.12: Bivariate ratio plot of Th/Ta versus Th/Tb of meta-volcanic rocks from the Holloway deposit. The (Th/Tb)/(Th/Ta) ratios for types I, II, and III are 0.22, 0.27, and 0.31 respectively, indicating that it is reasonable to assume the meta-volcanic rocks were derived from the same magma source.

Partial melting and fractional crystallization are geochemical processes that can be modeled mathematically. First, the Nernst distribution (or partition) coefficient

$$K_d = C_i^{mineral}/C_i^{melt}$$

describes the distribution of trace elements between phases, where C is the concentration of trace element "i" (Rollinson, 1993). When the mineral/melt distribution coefficient is equal to one, the element it describes is equally distributed between the mineral and melt phases. A distribution coefficient greater than one indicates that the trace element has a preference for the mineral phase and is considered a compatible element. An incompatible element has a distribution coefficient that is less than one, indicating a preference for the melt phase.

For a rock system, a bulk distribution coefficient (D) is defined by weighting the distribution coefficient of constituent minerals according to their mass proportions. The bulk distribution coefficient is

$$D_i = x_1Kd_1 + x_2Kd_2 + x_nKd_n \ldots$$

where x is the proportion of mineral n, and Kd is the distribution coefficient for mineral n (Rollinson, 1993). Allègre *et al.* (1977) provide an alternative method for determining bulk distribution coefficients based on inversion techniques. They determined that the slope of a log-log plot of a highly incompatible trace element (*e.g.* Ta) against any other trace element is proportional to the bulk distribution co-efficient. For compatible elements (D>1) the slope is equal to (D-1), and moderately incompatible elements (D<1) the slope is equal to (1-D). Examples from Holloway's meta-volcanic rocks are presented in figure 4.13. Vanadium was chosen as a representative of Fe-Ti oxides, and since it is a compatible element its concentration will be higher in less evolved rocks. Europium was chosen to represent plagioclase crystallization. Although Eu is susceptible to mobilization during alteration, it is less mobile than alternative elements that represent plagioclase such as Sr. The results of

determining bulk distribution co-efficients by both techniques are presented in table 6.

Table 6: **Bulk distribution co-efficients calculated** for selected elements using the bulk distribution equation and inversion techniques.

Element	$D_{calculated}$	$D_{inversion}$
Tb	0.42	0.16
V	3.6	2.3
Sc	1.3	1.5
Ni	6.4	1.5
Eu	0.5	0.4

It is shown that although the bulk distribution co-efficients determined by the inversion technique are bimodal and sometimes trimodal, for the most part are relatively close to those determined using mineral/melt partition co-efficients and mineral proportions. The trimodal distribution of samples using the inversion technique reflects the chemistry of types I to III meta-volcanic rocks due to differentiation. If samples existed with compositions that were intermediate to the different types, they would likely smooth the gaps between clusters on the log-log inversion diagrams.

$D_{calculated}$ values were calculated assuming mineral proportions of 45% clinopyroxene, 40% plagioclase, 10% magnetite, and 5% quartz as per Jensen and Langford's (1985) average composition of Fe-tholeiitic meta-basalts in the area. Mineral/melt partition co-efficients used for the calculation were taken from Rollinson's (1993) compilation and are presented in table 7.

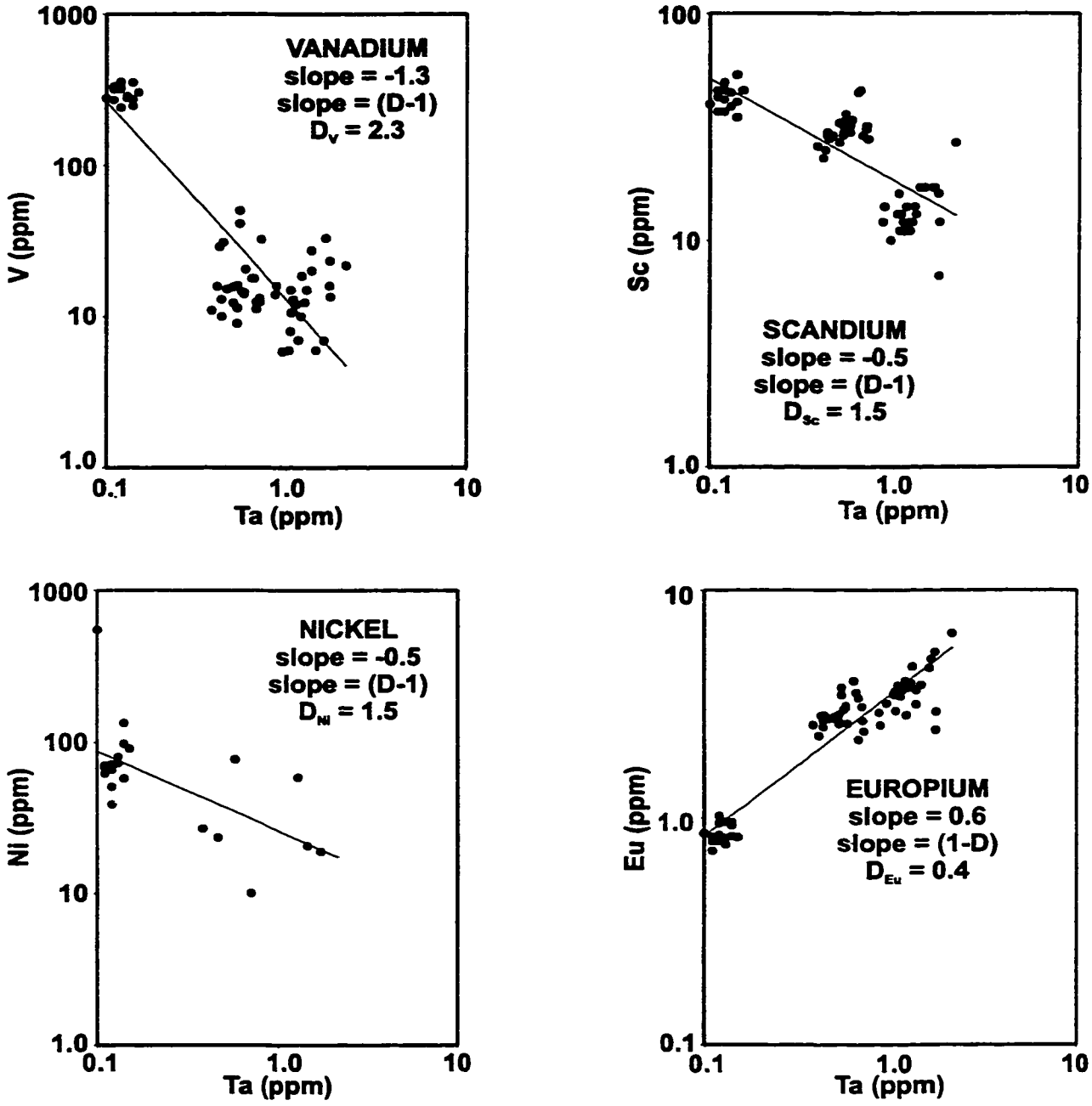

Figure 4.13: Bulk distribution co-efficients for vanadium, scandium, nickel, and europium. Bulk distribution co-efficients are calculated from the slope of log-log trace element plots. The x-axis must be a highly incompatible trace element such as Ta.

Treuil equations are derived from the well-known equations for batch melting and fractional crystallization.

$$C^l = \frac{C^{0s}}{D+F(1-D)}$$

$$C^l = C^{0l} f^{(D-1)}$$

C^l = concentration of trace element in the liquid

C^{0s} or C^{0l} = initial concentration of trace element (partial melting or fractional crystallization)

D = bulk distribution coefficient

F = weight fraction of melt produced (partial melting)

f = fraction of melt remaining (fractional crystallization)

As outlined by Maaløe (1985) the Treuil method provides equations for calculating differentiation curves. This method works on the principle that elements having small distribution co-efficients are greatly concentrated in the liquid toward the end of the crystallization process but concentrated at the start of the process for partial melting. The Treuil method plots the variation in concentration of two trace elements; C_i versus C_j. Trace element "i" is a hygromagmatophile (*i.e.* strongly incompatible) element that has a distribution coefficient near 0.01. Trace element "j" is a less incompatible element with $0.01 < D < 0.1$. The Treuil equations for partial melting are:

$$C_i^l = \frac{C_i^{0s}}{F} \qquad C_j^l = \left(\frac{C_j^{0s}}{C_i^{0s}}\right) * \frac{F}{D_j+F} * C_i^l$$

The Treuil equations for fractional crystallization are:

$$C_i^l = \frac{C_i^{0l}}{f} \qquad C_j^l = \left(\frac{C_j^{0l}}{C_i^{0l}}\right) * f^{Dj} * C_i^l$$

Treuil equations were applied to meta-volcanic rocks from the Holloway deposit and the results are presented in figures 4.14 and 4.15. Partial melting and fractional crystallization curves were modeled for i = Ta and j = Tb. The values used for the original composition (C^{0s} or C^{0l}) were estimated from the arithmetic average of the least evolved type I tholeiitic meta-basalts. Type I average elemental concentrations for Ta = 0.12 and Tb = 0.57 are in close agreement with Sun and McDonough's (1989) N-type MORB element concentrations of Ta = 0.132 and Tb = 0.670. A bulk distribution co-efficient of Ta = 0.01 was assumed according to Ferrara and Treuil (1973), and the bulk distribution co-efficient of Tb = 0.16 was determined using the inversion technique (figure 4.14 inset)

Figure 4.14 shows that Holloway's meta-volcanic rocks are best represented by the fractional crystallization model. Figure 4.15 is a close-up from which it can be determined that type II Fe-tholeiitic meta-volcanic rocks are derived from a melt that has undergone 70-80% fractional crystallization, and type III variolitic meta-volcanic rocks are derived from a melt that has undergone 85-93% fractional crystallization.

Allègre *et al.* (1977) further developed a method for determining the mean mineral assemblage involved in fractional crystallization. The method is centered around the bulk distribution coefficient. For n trace elements, n linear equations can be written in the matrix form

$$[D^i] = [D^i_{\alpha/l}] \cdot [\times_\alpha]$$

where D^i is the bulk distribution coefficient, $D^i_{\alpha/l}$ is the partition coefficient between minerals and liquids for several elements, and $\times_\alpha$ is the mean modal composition of the solid that was removed from the liquid. The trace elements used in this application must carry independent information, *e.g.* Ni representing olivine, V for Fe-Ti oxides, Sc for clinopyroxenes, and Sr for plagioclase (Allègre *et al.*, 1977). This method was tested on Holloway's tholeiitic meta-volcanic rocks using the calculated bulk distribution coefficients for V, Sc, Ni, and Eu and

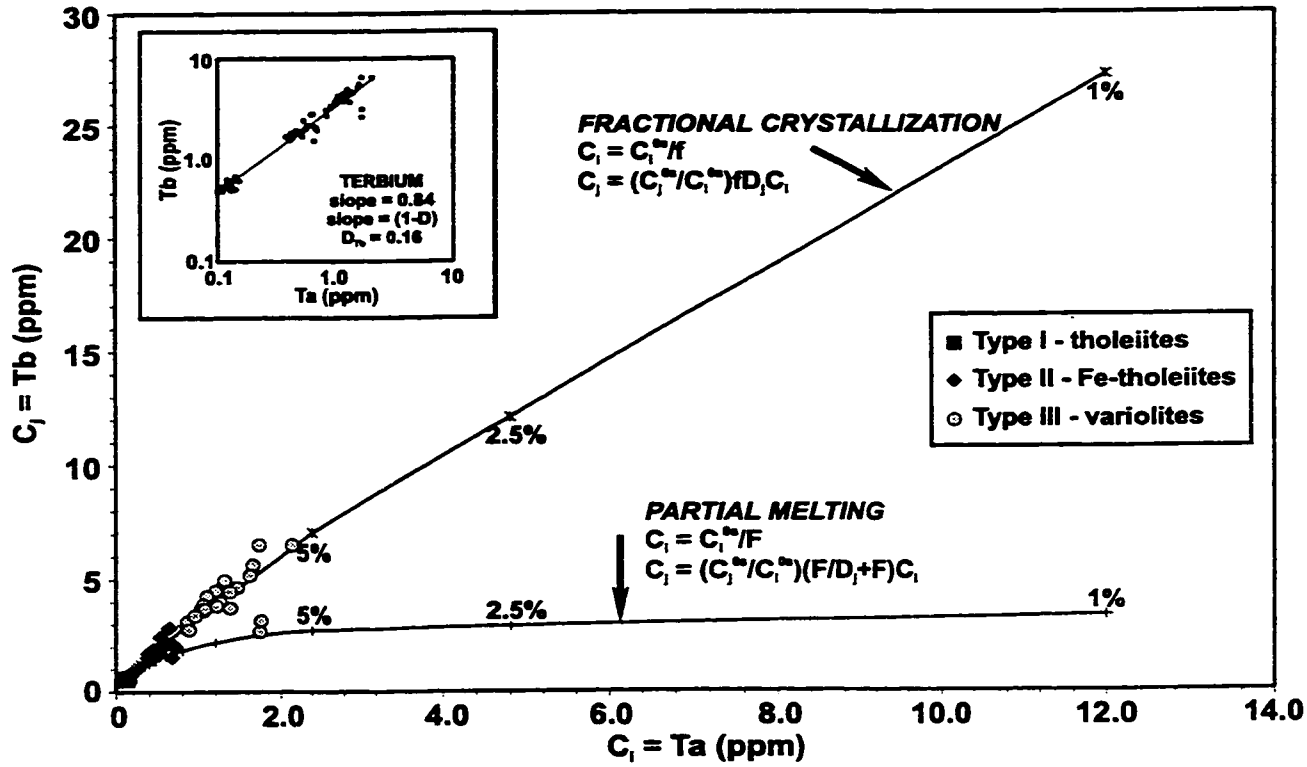

Figure 4.14: Variation of trace element concentration by different degrees of partial melting and fractional crystallization (after Ferrara & Treuil, 1973). The initial concentration of Ta is 0.12 ppm and Tb is 0.57 ppm. The distribution co-efficient for Ta is assumed 0.01 and the distribution co-efficient for Tb is 0.16 as determined by the inversion technique (see inset). Meta-volcanic rocks from the Holloway deposit are represented by the fractional crystallization model. Percent values refer to the percent of liquid remaining in the system.

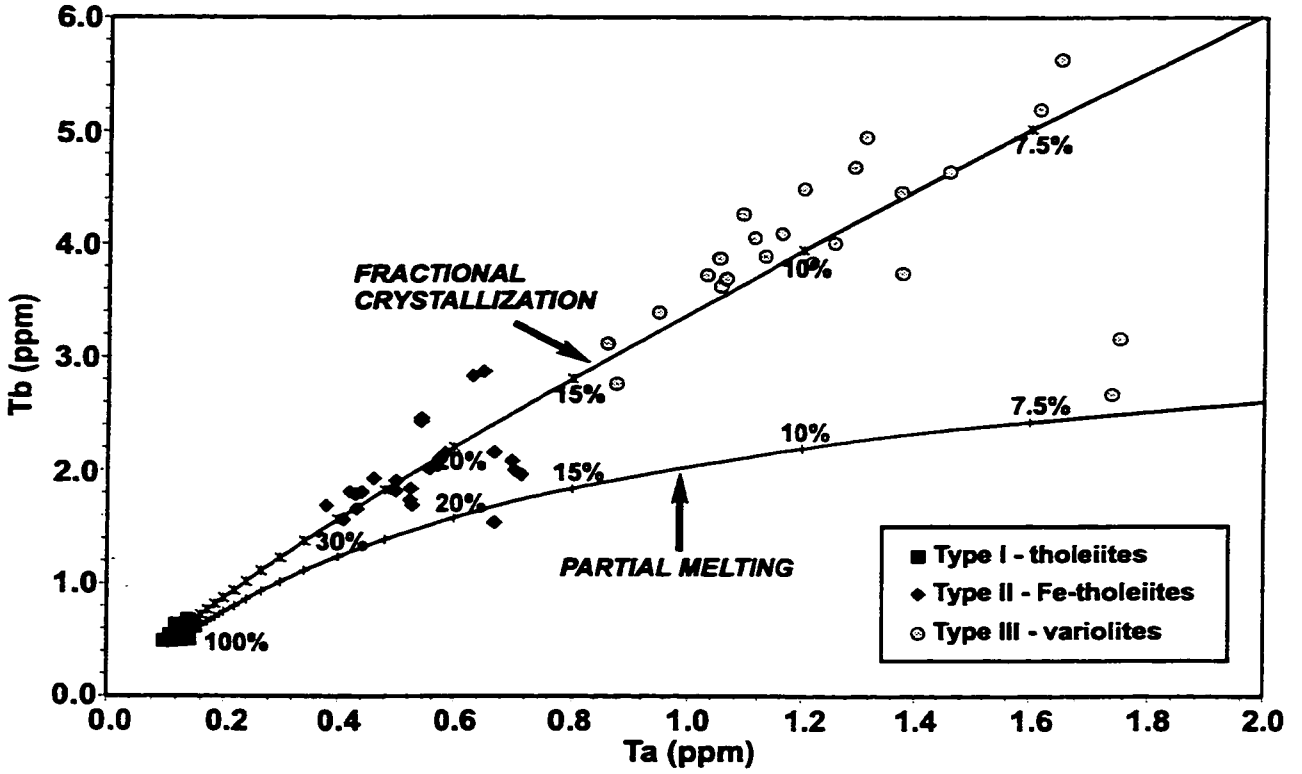

Figure 4.15: Close-up of figure 4.14. Type II Fe-tholeiitic meta-volcanic rocks are derived from 70-80% fractional crystallization of a N-MORB source, and type III variolitic meta-volcanic rocks are derived from 85-93% fractional crystallization.

mineral/melt partition coefficients summarized by Rollinson (1993) for basaltic liquids. Where mineral/melt partition coefficients were not available for basaltic liquids, andesitic liquids were substituted and are indicated by an asterisk in table 7. Values indicated by parenthesis were used and represent the median for partition coefficients having a range of values.

Table 7: Bulk distribution and partition coefficients used to determine the mean modal composition of solids produced during fractional crystallization of Holloway's meta-volcanic rocks.

Trace Element	$D_{calculated}$	Partition Coefficient for OL	Partition Coefficient for CPX	Partition Coefficient for PLAG	Partition Coefficient for MAG	Mean Modal Composition of Solid
V	3.6	0.06	1.35	0.01*	26.0	Olivine -0.02
Sc	1.3	0.17	1.7-3.2 (2.45)	0.01*	2.0*	CPX 0.44
Ni	6.4	5.9-29 (17.45)	1.5- 14 (7.75)	0.01*	29.0	Plagioclase 0.46
Eu	0.5	0.0068	0.51	0.34	0.6-1.5 (1.05)	Magnetite 0.16
Tb	0.4		0.57	0.03	1.0-2.0 (1.5)	

The results of the matrix calculation for determining the mean modal composition of the solids that were removed from the liquid are presented in table 7. The values of 44% clinopyroxene, 46% plagioclase and 16% magnetite are in close agreement with Jensen and Langford's (1985) primary mineral modes for unaltered Fe-tholeiitic meta-basalts in the area of 40-50% augite, 30-40% plagioclase, 5-10% Ti-magnetite, and 2-8% quartz. The small negative value for olivine suggests that the cumulate contains no olivine, and that this technique has several difficulties associated with it.

4.6 FRACTIONATION TRENDS

From REE abundance patterns and the Treuil method, it has been shown that meta-volcanic rocks from the Holloway deposit likely belong to a fractionally crystallized suite of tholeiitic volcanic rocks. A TiO_2 versus Zr plot is an effective way to observe fractionation trends despite varying degrees of alteration. Before analyzing a TiO_2 versus Zr plot, MacLean and Barrett (1993) stress the importance of testing HFSE for incompatibility in a rock suite. Figure 4.16 is a schematic plot of Y versus Zr that allows for the determination of magmatic affinity. Tholeiitic rocks have a Zr/Y ratio less than 5, whereas calc-alkalic rocks will range between 7 and 30 (Lesher *et al.*, 1986). Holloway's meta-volcanic rocks are plotted in figure 4.16 and show that type I and type II have a Zr/Y ratio of 2.3 and type III has a ratio of 3.1. The Zr/Y ratios for the meta-volcanic rocks are within Lesher *et al.*'s (1986) definition of tholeiitic rocks. MacLean and Barrett's (1993) experience suggests that HFSE remain highly incompatible during fractionation for basalt to rhyolite suites that have a tholeiitic affinity. Since Holloway's meta-volcanic rocks indicate a tholeiitic affinity it is safe to proceed with a TiO_2 versus Zr plot.

Ti and Zr are typically immobile elements (*i.e.* unaffected by alteration) in tholeiitic volcanic suites (MacLean & Kranidiotis, 1987). Ti is a compatible element that has a preference for the solid phase over melt/magma, whereas Zr is incompatible and serves as a monitor of igneous fractionation (MacLean, 1990). Holloway's meta-volcanic rocks are plotted on a schematic TiO_2 vs. Zr plot in figure 4.17. The tholeiitic fractionation curve was derived from Fowler and Jensen's (1989) unaltered tholeiitic Kinojevis rocks. Ideally, the fractionation curve should have been generated using unaltered meta-volcanic rock samples from the Holloway deposit, but considering the complicated stratigraphy within the DPC, it was not feasible to identify unaltered equivalents in the mine area. The fractionation curve shows a strong Ti-enrichment in the basalts (if FeO is plotted instead of TiO_2 shows strong Fe-enrichment), followed by Ti-depletion from andesite to rhyolite.

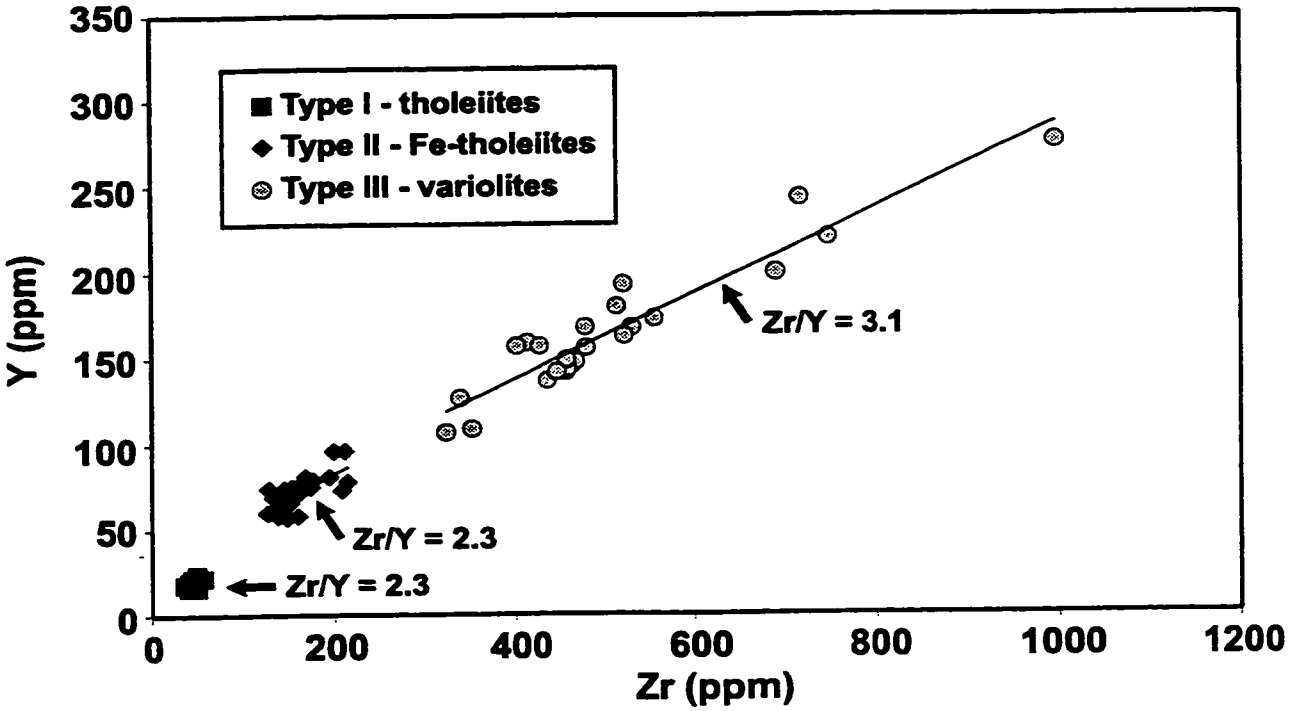

Figure 4.16: Schematic Y versus Zr plot to determine magmatic affinity. Types I and II meta-volcanic rocks have Zr/Y = 2.3, and type III = 3.1, indicating a tholeiitic magmatic affinity.

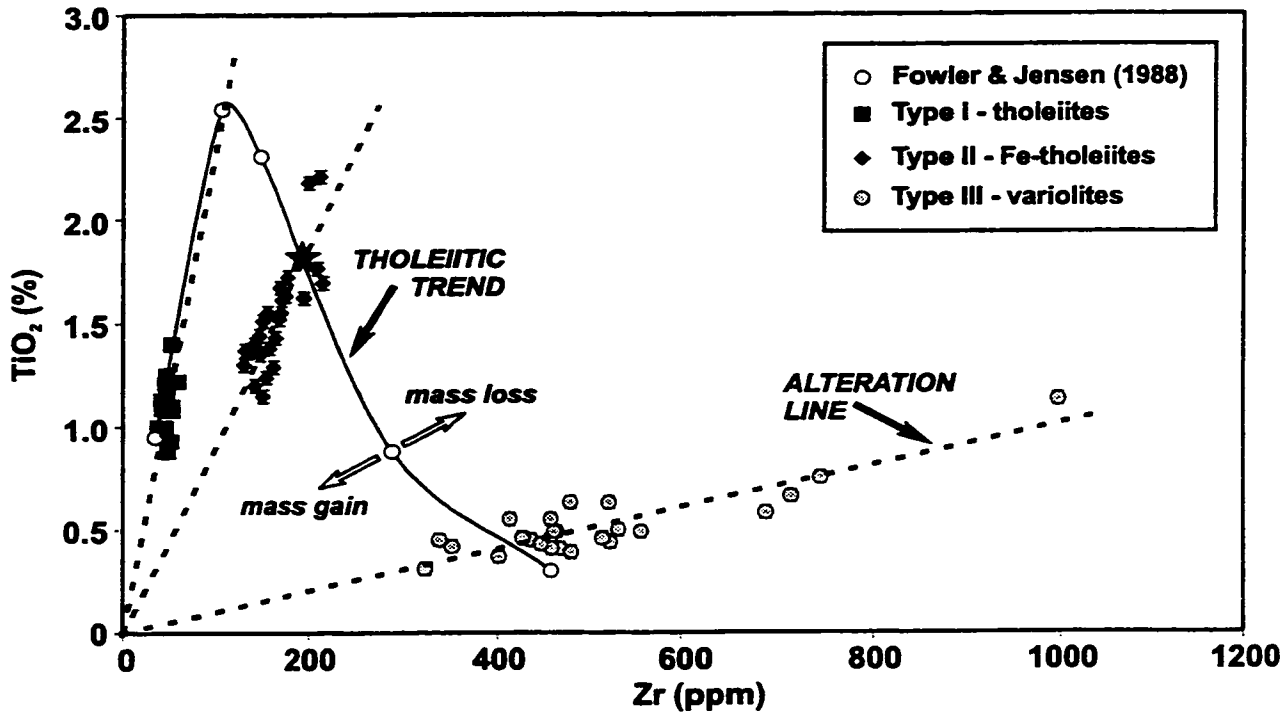

Figure 4.17: Schematic TiO_2 versus Zr plot for meta-volcanic rocks from the Holloway deposit (after MacLean & Barrett, 1993). The solid line displays a tholeiitic fractionation trend, and dashed lines represent alteration lines. Mass gain is indicated by the direction of the arrow along an alteration line having infinite dilution at the origin. The star represents the location of an unaltered sample at the intersection of an alteration line with the tholeiitic fractionation curve.

A sample may stray from the fractionation curve if it has been subjected to mobile mass change, creating a linear alteration line. Alteration lines are radial lines that pass through the origin. A sample that has undergone infinite dilution (*i.e.* infinite mass gain) will plot on the origin. The intersection of an alteration line with the fractionation curve identifies the field to which the unit belongs and the precursor composition for the unit. The alteration line defining type I tholeiitic meta-basalts intersects the fractionation curve in the basalt field. Type II samples intersect the andesite field, and type III variolitic meta-volcanic rocks are rhyolite-like in composition.

Some characteristic elemental abundances (arithmetic averages) for the different types of meta-volcanic are presented in table 8. As expected for a fractionated suite of tholeiitic rocks, Holloway's meta-volcanic rocks show that the most evolved rocks (type III variolites) are low in compatible elements (TiO_2 and Al_2O_3). Also, incompatible elements (Zr and Th) are high in the evolved type III rocks. Jones (1992) showed that varioles occur in evolved tholeiite basalt suites and correlated them with increased incompatible elements such as Zr, Y, Th, and REE as is the case for the Holloway deposit.

Table 8: Average concentrations of distinguishing elements for each type of meta-volcanic rock from the Holloway deposit.

Group	TiO_2	Al_2O_3	Zr	Th	V	Ni	Fe/Mg
Type I	1.1±0.1	12.7±1.5	46±5	0.2±0.03	312±42	73±21	2.1±0.4
Type II	1.5±0.3	11.5±1.7	164±25	0.8±0.1	18±10	n/a	8.0±2.7
Type III	0.5±0.2	10.6±2.6	506±146	2.5±0.8	14±7	n/a	8.3±4.7

The values presented in table 8 suggest that type I tholeiitic meta-volcanic rocks are extruded from a magma source that is different from the sources producing type II Fe-tholeiitic and type III variolitic meta-volcanic rocks. Type I rocks have Fe/Mg = 2 which Jensen (1976) defined as the value distinguishing between Mg- and Fe-tholeiite affinities. Types II and III

meta-volcanic rocks have Fe/Mg = 8 corresponding to Jones' (1992) finding that the Fe/Mg ratio is high (>4.0) for evolved variolitic suites. Vanadium values for types II and III rocks are similar to each other (~15 ppm) and significantly less than ~300 ppm for type I. Vanadium participates in chemical fractionation such that basaltic rocks have higher concentrations. Other elements such as Cr, Co, and Ni are found in trace amounts for type I meta-tholeiite rocks, but are below detection limits for types II and III. Based on these differences in chemistry, it is likely that type I tholeiitic meta-basalts are derived from a magma source that subsequently underwent fractional crystallization to produce types II and III. The source for types II and III fractionated over time, accounting for the decrease of compatible TiO_2 values and the increase of incompatible elements (Zr and Th) in the more evolved type III meta-volcanic rocks.

4.7 ALTERATION GEOCHEMISTRY

In this section the effects of alteration on geochemistry are determined for the three types of meta-volcanic rocks from the Holloway deposit. It was crucial to determine primary geochemical signatures within the data and to separate the samples into groups based on their chemistry. In doing so, the errors associated with comparing rocks from different magma sources were avoided. When doing alteration studies it is vital to compare altered samples against their least altered geochemical equivalents to accurately determine elemental gains and losses. This alteration study involved a multi-step process whereby immobile elements were identified and then elemental gains and losses were determined. This process was repeated for the different types of meta-volcanic rocks. Immobile elements were identified using a software package called Soma 1. Elemental gains and losses were evaluated through the use of isocon diagrams.

Gold is generally not mineralized in type I tholeiitic meta-volcanic rocks with an average content = 0.02 ±0.01 g/t (or 21 ppb). Type II Fe-tholeiitic meta-volcanic rocks have variable gold concentrations = 0.8 ±2.5 g/t (or 800 ppb) depending on the degree and type of

alteration. Lightning Zone mineralization is hosted by type III variolitic meta-volcanic rocks which have average gold concentrations = 5.0 ±9.8 g/t (or 5000 ppb). Type II rocks are not well represented in Holloway's west ore zone where gold mineralization is of the Lightning Zone style. In the east zone, where types II and III rocks are dominant, gold mineralization is comprised of both Lightning Zone and vein-type mineralization styles.

4.7.1 SOMA

Appleyard (1991) developed Soma, a package of Fortran programs, to calculate mass exchange in metasomatic and altered rocks. Soma 1 computes zero change volume factors (FV°), presenting the output as a histogram of log(FV°). FV° values are required to determine immobile elements within a group of variably altered rocks. The equation for $Fv_\eta°$ is derived from Gresens' (1967) equation for expressing the difference in composition between a fresh rock and its altered equivalent. When the volume factor (FV) is >1, replacement takes place with a volume gain and vice versa when FV <1 (Gresens, 1967).

$$FV_\eta° = \frac{\rho^\alpha * \chi_\eta^\alpha}{\rho^\beta * \chi_\eta^\beta}$$

α = parent
β = altered
η = element
ρ = density
χ = concentration

Immobile elements are identified by closely similar FV° values for each parent-altered comparison, *i.e.* immobile elements cluster together on all histogram outputs (Appleyard, 1991). The clustering of FV° values will occur at different FV values due to varying intensities of alteration (Appleyard, 1991). Element clusters show evidence of mutual immobile behaviour and is not a result of coincidence. The suite of elements identified as immobile clusters will depend on the temperature, Eh, pH, and the presence of complexing anions such as the halogens or sulphur associated with the alteration (Appleyard, 1991).

Examples of Soma 1 histogram output for types I and II meta-volcanic rocks are shown in figures 4.18 and 4.19. Soma 1 could not be used for type III meta-volcanic rocks because unaltered precursor samples were not available.

Element clusters for type I tholeiitic meta-volcanic rocks are comprised of Nb, Hf, and Th. Element clusters for type II tholeiitic meta-volcanic rocks consist of TiO_2, Al_2O_3, Hf, and Th. These elements are considered immobile (as indicated by circles in figures 4-18 & 4-19) for further applications using geochemical data from the Holloway deposit. Similarly, the REE (as indicated by squares in figures 4-18 & 4-19) are shown to cluster on log (FV°) histograms showing that they are immobile as well.

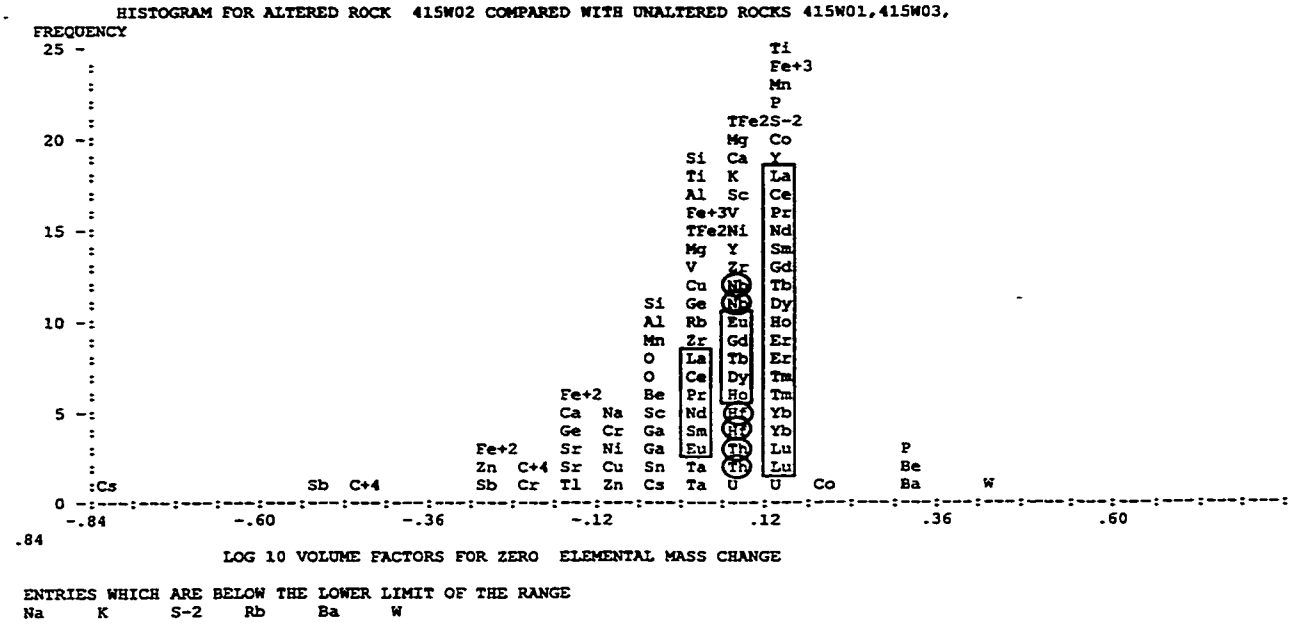

Figure 4.18a: Histogram of log (FV°) for a hematized sample (415-02) from the type I tholeiitic meta-volcanic rocks. Note the clustering of Nb, Hf, and Th. Log(FV°) values for the Nb-Hf-Th cluster occurs around +0.09 for this sample.

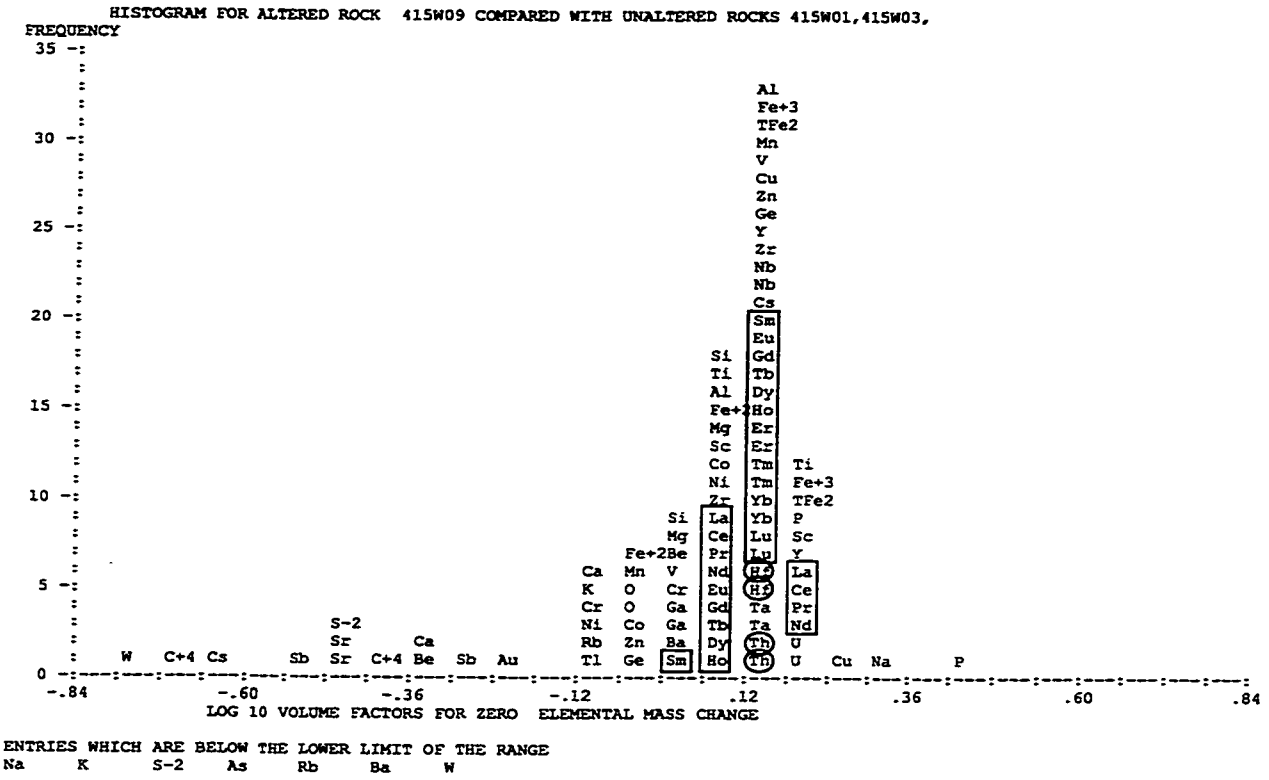

Figure 4.18b: Histogram of log (FV°) for a sericitized sample (415-09) from the type I tholeiitic meta-volcanic rocks. Log(FV°) values for the Nb-Hf-Th cluster occurs around +0.15 for this sample.

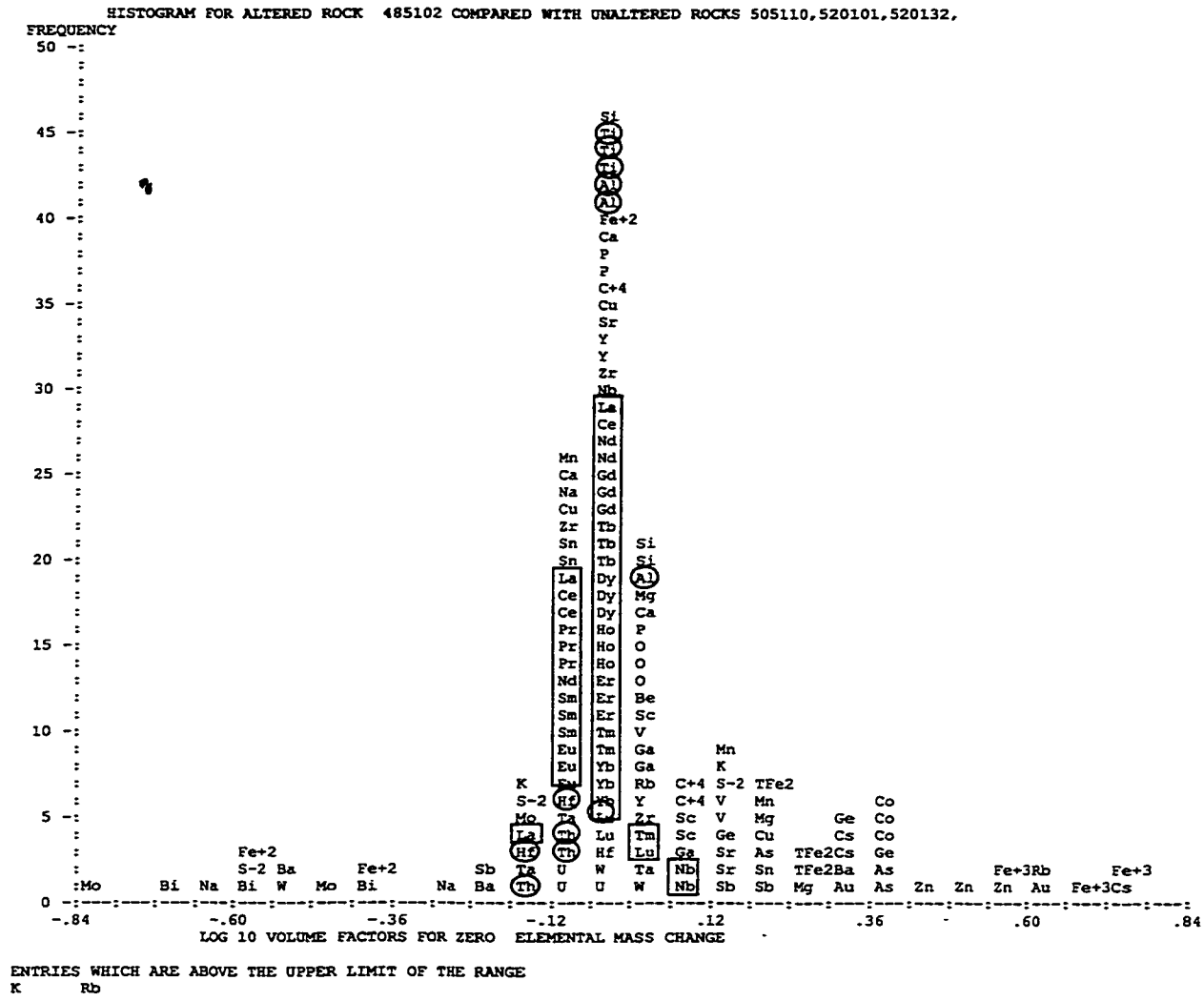

Figure 4.19a: Histogram of log (FV°) for a hematized sample (485-102) from the type II Fe-tholeiitic meta-volcanic rocks. Note there are two sets of element clusters; one cluster consists of TiO_2 and Al_2O_3, and the other consists of Hf and Th. Log(FV°) values for the TiO_2-Al_2O_3 cluster occurs at -0.03, and the Hf-Th cluster at -0.12 for this sample.

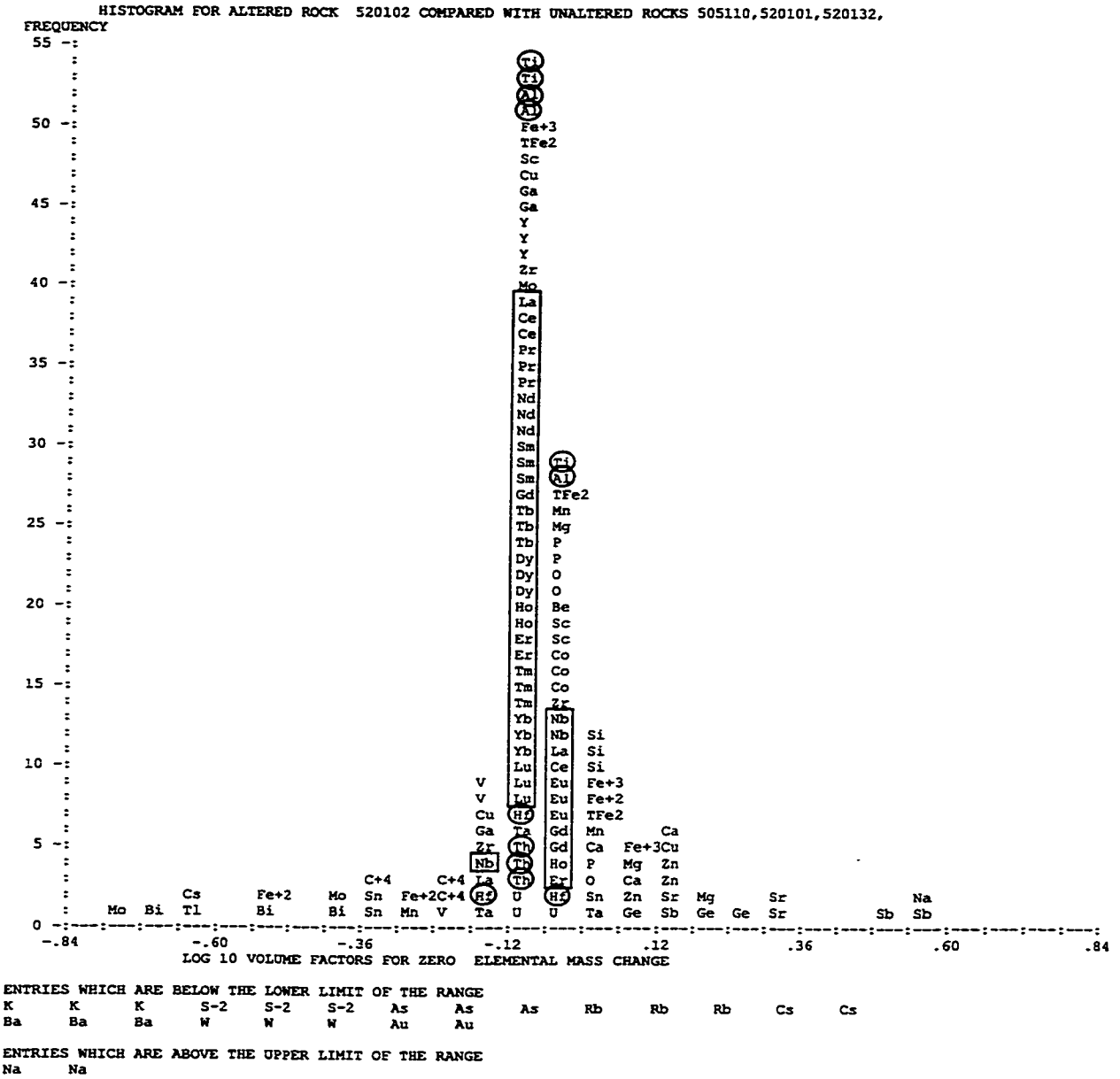

Figure 4.19b: Histogram of log (FV°) for a sericitized sample (520-102) from the type II Fe-tholeiitic meta-volcanic rocks. Log(FV°) values for the TiO_2-Al_2O_3 cluster occurs at -0.06, and the Hf-Th cluster at -0.09 for this sample.

4.7.2 ISOCON PLOTS

Grant (1986) developed isocon diagrams to plot appropriately scaled oxide abundances of an unaltered sample against its altered equivalent. Isocon diagrams shown in this thesis have been scaled by the factors shown in Table 9. Elements considered immobile define a straight line through the origin called the isocon with a slope approximately equal to one (figure 4.20). Immobile elements were determined using the Soma 1 software and are also given in Table 9. Elements having an increase in abundance plot above the isocon, whereas those lost plot below. The slope of the isocon is used to define the mass exchange associated with alteration. A slope greater than one defines a loss in volume and vice versa.

Table 9: Identification of immobile elements and scaling factors for isocon diagrams.

	Type I	Type II		Type I	Type II
SiO_2	0.5	0.5	Ni	0.05	1.0
TiO_2	10	10	Rb	0.5	0.3
K_2O	10	5	Sn	1.0	5
As	0.1	0.018	Sr	0.02	0.08
Au	0.5	0.002	Th	10	10
Ba	0.08	0.05	V	0.05	0.4
Co	0.4	1.0	W	1.0	0.4
Cr	0.15	0.8	Y	1.0	0.3
Cu	0.1	0.15	Zn	0.3	0.1
Ga	1.0	0.75	Zr	0.5	0.14
Hf	10	1.0	Immobile elements	Nb, Hf, Th	Hf, Th, TiO_2, Al_2O_3

Sericitized and hematized samples are plotted on isocon diagrams for types I and II meta-tholeiite rocks in figures 4.21 to 4.24. It was not possible to plot isocon diagrams for type III variolitic meta-volcanic rocks since an unmineralized least altered sample was not collected for comparison.

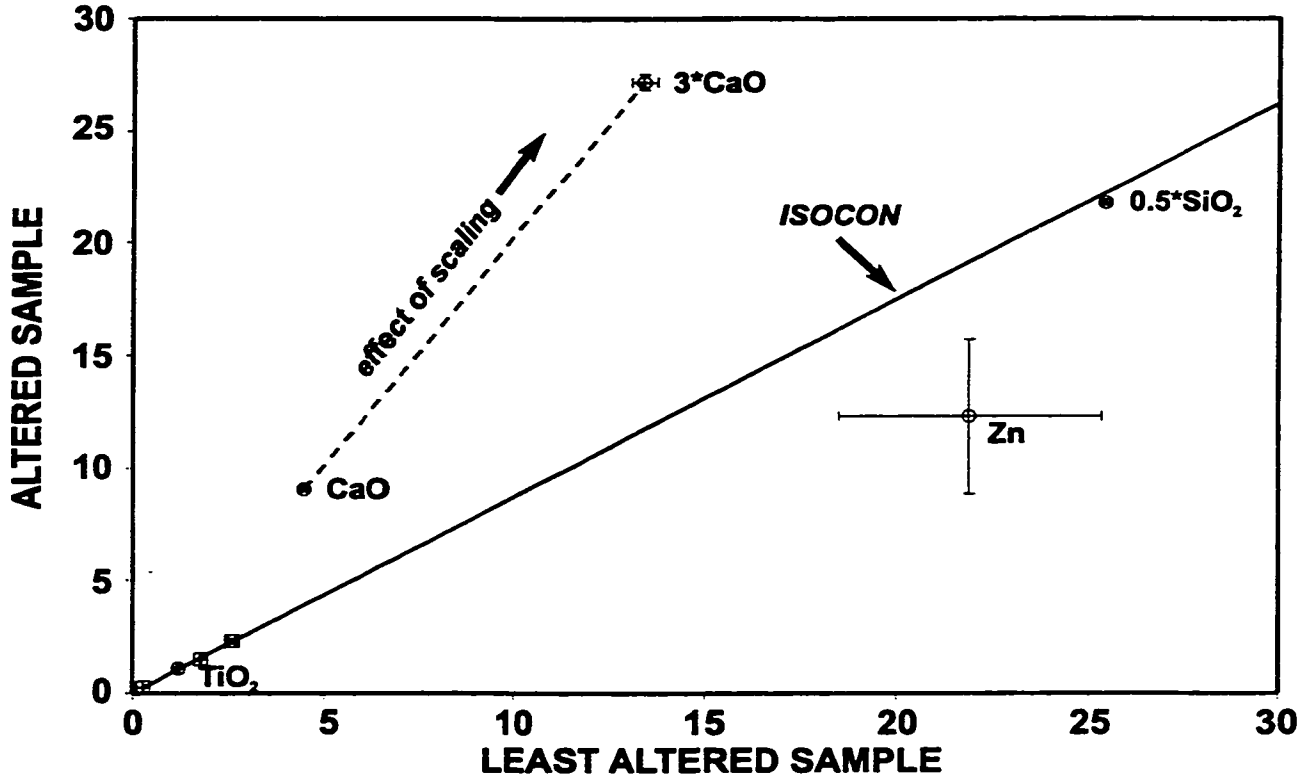

Figure 4.20: Schematic isocon plot. Precision error is indicated by error bars around the sample. The effect of scaling is illustrated by the dashed line for CaO; note that precision error bars are also scaled. The isocon is defined by Nb, Hf, and Th in this example. Elements that plot above the isocon indicate an elemental gain, and those below the isocon indicate a loss.

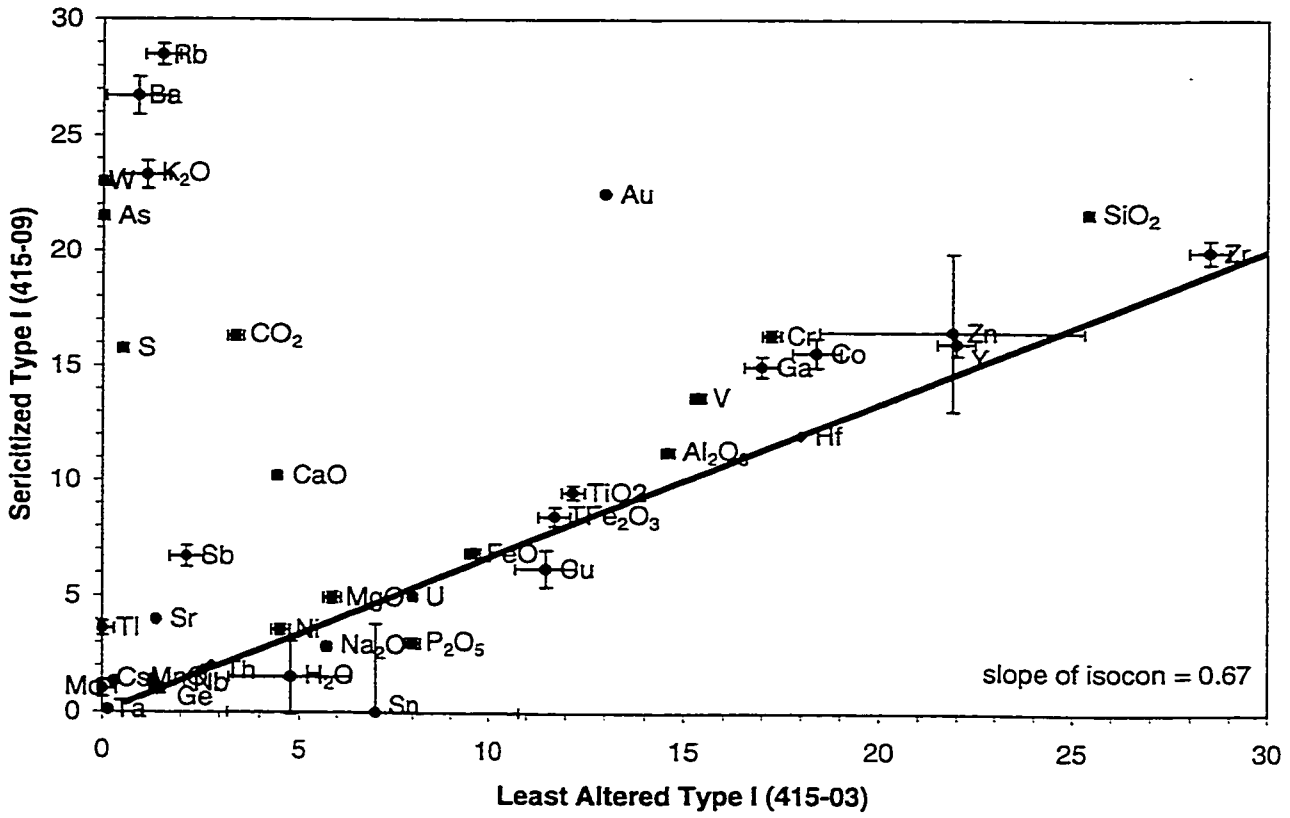

Figure 4.21: Isocon diagram for a sericitized type I tholeiitic meta-volcanic rock (415-09).

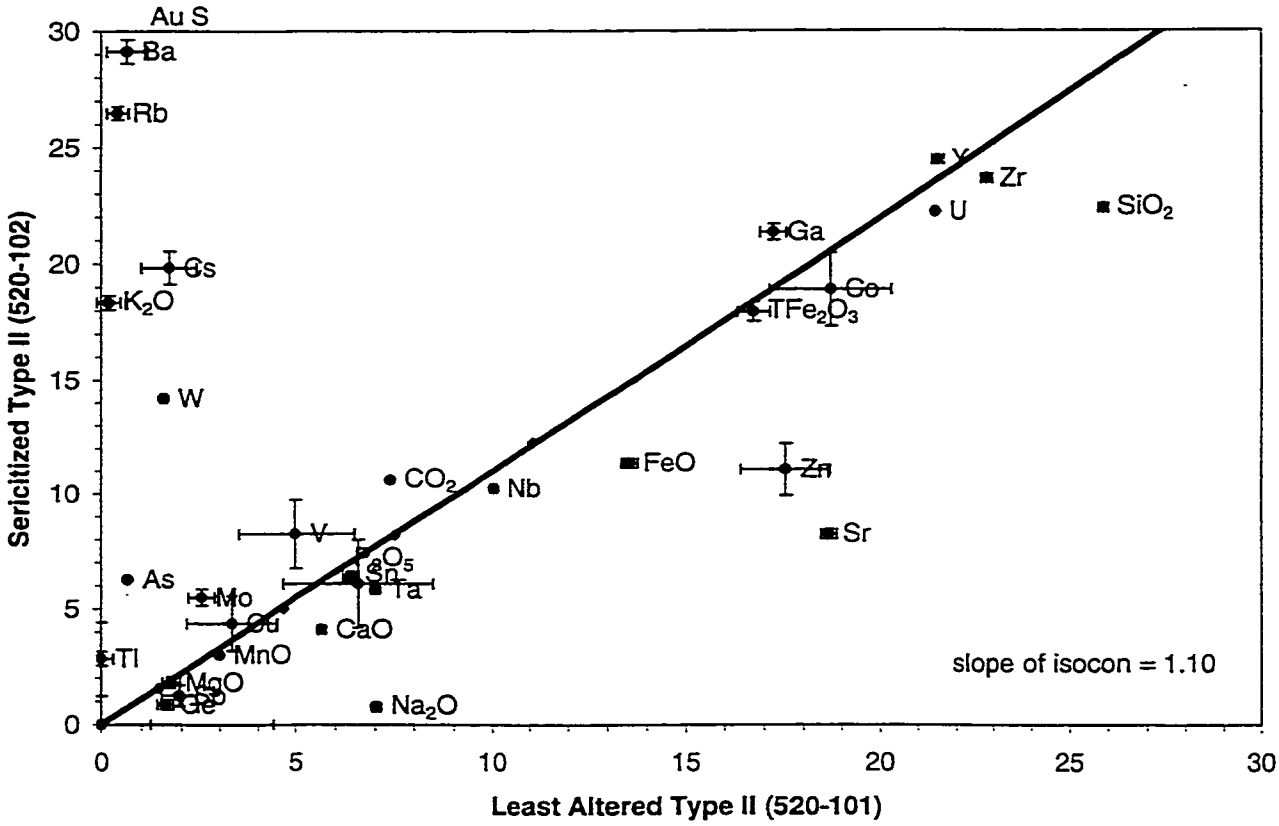

Figure 4.22: Isocon diagram for a sericitized type II Fe-tholeiitic meta-volcanic rock (520-102).

Figures 4.21 and 4.22 are representative isocon diagrams for sericitized types I and II meta-volcanic rocks respectively. These representative isocon diagrams show that sericitized samples typically have an elemental increase in CO_2, K_2O, Rb, Ba, Cs, and Sb. More importantly, gold is always shown to occur with increased S, and frequently with increased As and W together. These findings are in agreement with the general features of mesothermal lode gold deposits, *i.e.* Au, Ag (± As, Sb, Te, W, Mo, Bi) element association and the metasomatic addition of K + LILE (Rb, Ba, Cs, Tl) (McCuaig & Kerrich, 1994). The elemental increase of potassium is demonstrated mineralogically by the occurrence of sericite in samples.

Isocon diagrams for hematized samples are presented in figures 4.23 and 4.24. Only five samples were available to plot on isocon diagrams and their results are scattered. In general, it appears that FeO is typically decreased in hematized samples consistent with iron being oxidized. Elemental increases of K_2O, Rb, and Ba shown in figure 4.23 may be due to increased metasomatic activity in the west zone (where type I tholeiitic meta-volcanic rocks occur). Rocks in the west zone have larger sericitized alteration envelopes than in the east zone.

The results acquired using isocon diagrams shed some light on the nature of mineralizing fluids at the Holloway deposit. Elemental increases of CO_2, K_2O, Rb, Ba, Cs, and Sb in sericitized zones are expressed as mineral assemblage of sericite and carbonate. Where gold concentrations are elevated, S, As, and W are also increased and abundant pyrite and arsenopyrite are present. Hydrothermal fluids responsible for mineralization at the Holloway deposit were likely comprised of sulphur complexes and had high concentrations of Au, LILE, As, and W.

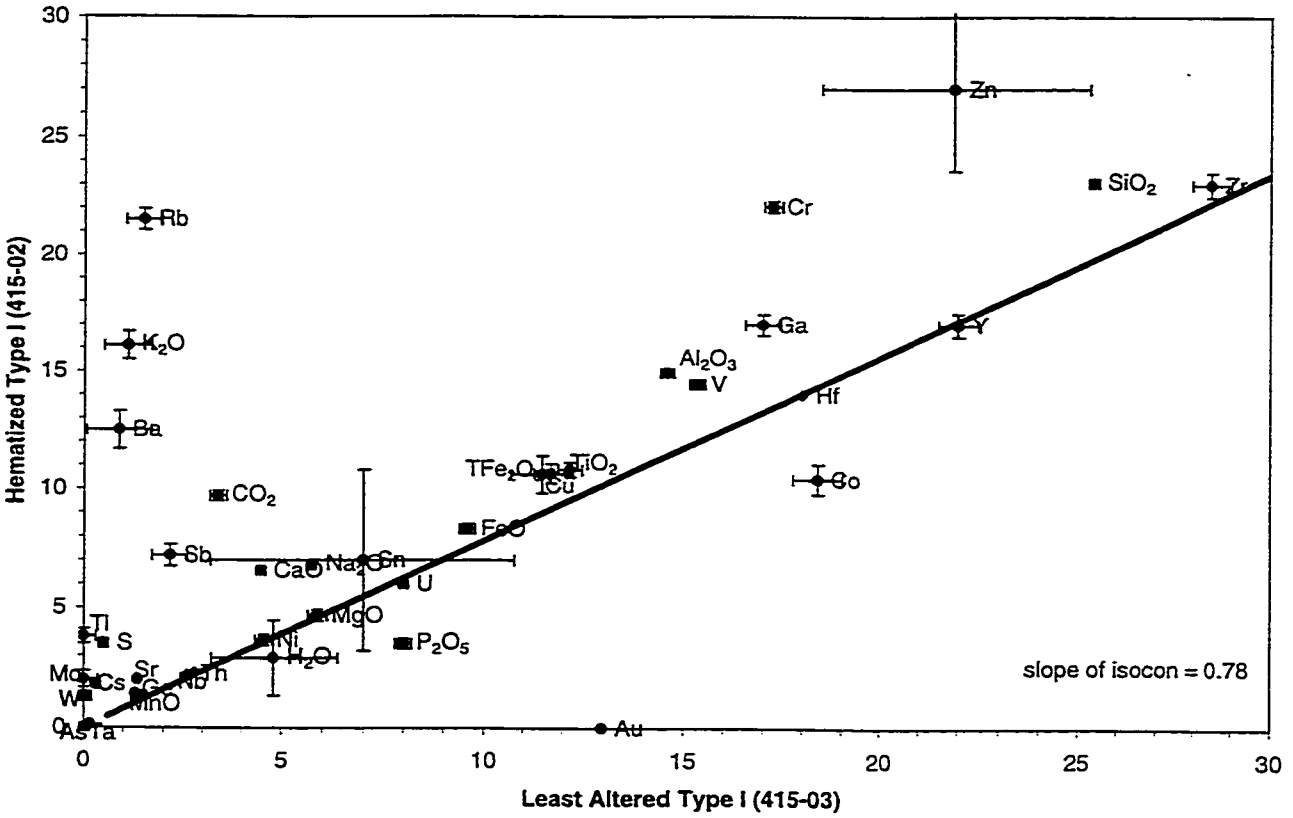

Figure 4.23: Isocon diagram for a hematized type I tholeiitic meta-volcanic rock (415-02).

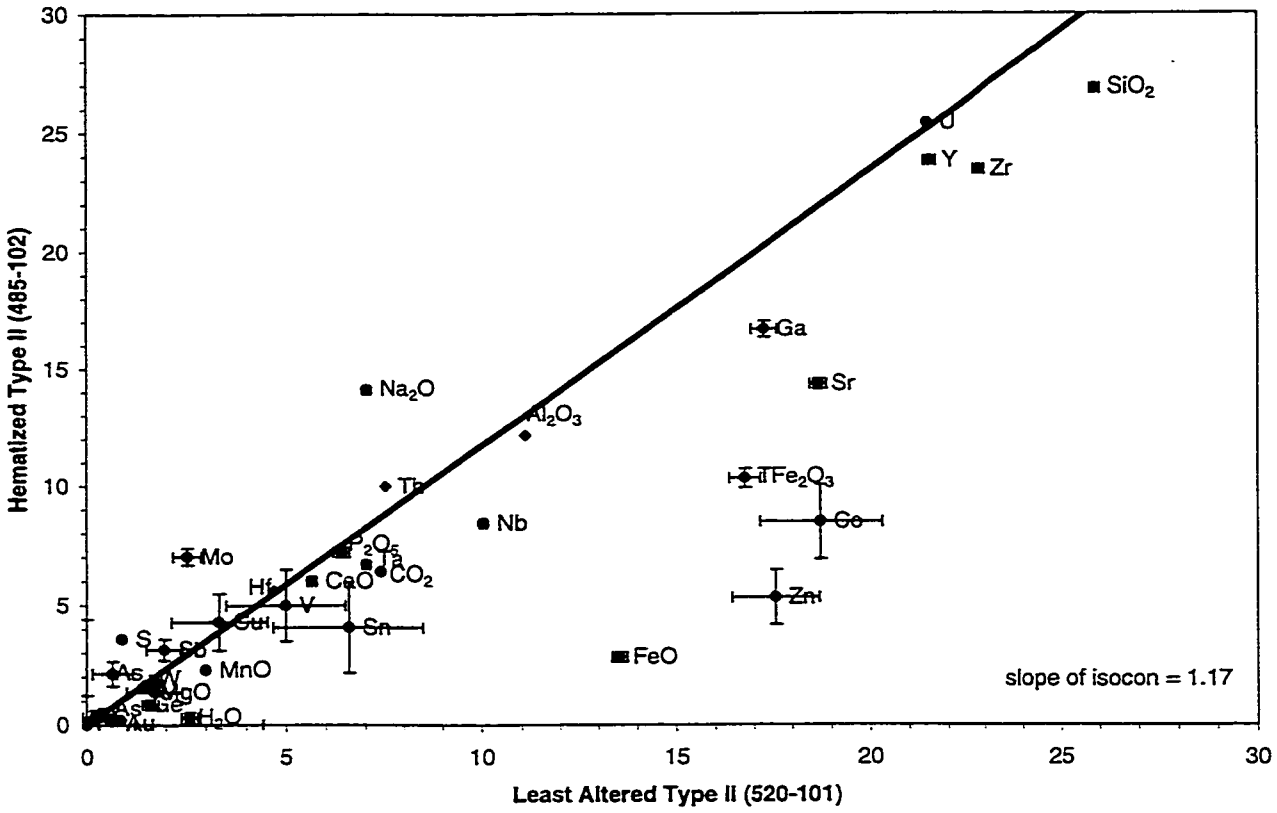

Figure 4.24: Isocon diagram for a hematized type II Fe-tholeiitic meta-volcanic rock (485-102).

4.8 FACTOR ANALYSIS

Factor analysis is a powerful tool to determine trends in variation for large multi-variate data sets, such as geochemical data. Although factor analysis alone cannot be used to make conclusions, its value lies in its ability to statistically confirm trends that the user may be suspicious of. Details of how factor analysis is conducted are too extensive and complicated to present here. For an explanation of the techniques used, the reader is referred to chapter 6 of Davis (1986). Simply speaking, factor analysis reduces the number of variables into a number of factors. A factor represents a grouping of variables that have been found to vary coherently. This technique compresses a large multi-variate data set into a small number of factors defined by the user. In choosing the number of factors, the user must carefully consider how many factors are believed to affect their data set. Typical factors in geological studies may include source input, alteration, metamorphism, weathering, and so on.

Swan and Sandilands (1995) strongly recommend that the user observes the correlation matrix and scatter diagrams (histograms) of the data set before beginning multi-variate data analysis. The goal in doing so is to ensure that the data set is normally distributed before beginning statistical techniques. Aitchinson (1986) urges geologists to apply a log-ratio transformation to their compositional data to remove the effects of a closed data set. Compositional data sets are closed and are prone to the constant sum effect which is incompatible with statistical techniques. Aitchinson (1986) explains how the log-ratio transformation can overcome the constant sum effect and defines the following equation:

$$X' = \ln(x/y)$$

When doing the log-ratio transformation, it is necessary to make sure that units of all columns are the same, *i.e.* change ppm and ppb values to percent (Swan & Sandilands, 1995). For the purposes of this study the log-ratio transformation was applied with $y = SiO_2$.

Factor analysis was performed using the software package SYSTAT 5.02. Each type of meta-volcanic rock from the Holloway deposit was run separately to avoid confusion due to difference in primary geochemistry. When performing factor analysis, different types of rotation can be applied to the correlation matrix including equamax, varimax and quartimax. Equamax rotation maximizes the variance of elements within a sample and between samples. Since the variation of elements within a sample are not a concern for this study, varimax rotation was chosen. Varimax rotation maximizes the variance of loadings within columns (*i.e.* variance of elements between samples).

Three factors were chosen for type I meta-volcanic rocks to produce the following results:
FACTOR 1 (27.8%) REE (not including La), Co, Fe^{2+}, Mn, Sc, Ti, V, Y
FACTOR 2 (17.8%) LILE (Cs, Rb, K, Ba, Sr), As, Ca, CO_2, Mo, S, Sb, Tl, W, -P
FACTOR 3 (13.3%) Hf, La, Nb, Ta, Th, U, Zr

Approximately 28% of the total variance within type I tholeiitic meta-volcanic rocks is represented by factor 1. Factor 1 characterizes the primary geochemical signature of the rocks plus or minus the effects of alteration. It is not surprising that the REE's plot together due to their similar chemical and physical properties (*e.g.* 3+ oxidation state). Factor 2 represents variation caused by the effects of hydrothermal alteration and gives an indication of the chemistry of the hydrothermal fluids affecting the rocks from the Holloway deposit. LILE's are assumed mobile under all circumstances (MacLean & Barrett, 1993), explaining their abundance in hydrothermally altered rocks. Other elements belonging to the hydrothermal factor include Ca and CO_2, representing carbonate alteration, and As, Mo, S, Sb, Tl, and W. P_2O_5 is inversely correlated with hydrothermal alteration. Identification of the elements associated with hydrothermal alteration correspond to the results determined by the isocon diagrams. Although As, W, and Au have correlation coefficients <0.75, their importance to gold mineralization becomes apparent through the use of isocon diagrams and factor analysis. Factor 3 includes Hf, Nb, Ta, Th, and Zr, representing HFSE which are generally cited as immobile elements (MacLean & Barrett, 1993). The identification of

immobile elements in factor 3 supports the results from running Soma 1.

Three factors were chosen for type II rocks producing the following results:

FACTOR 1 (49.5%) REE, Al, Ag, As, Be, Co, Cu, TFe_2O_3, Fe^{2+}, Ga, Hf, Mg, Mn, Nb, P, Sc, Sn, Ta, Ti, Th, U, Y, Zn, Zr, -Na

FACTOR 2 (10.8%) LILE, Tl

FACTOR 3 (12.1%) Au, CO_2, Cr, Mo, S, V, W

Nearly 50% of the total variance within type II Fe-tholeiitic meta-volcanic rocks is accounted for by factor 1. As for type I rocks, factor 1 represents the original chemistry of the rocks and includes the immobile elements (Ti, Al, Hf, and Th). Factors 2 and 3 would represent different hydrothermal fluids, the first composed of LILE and the later including Au-bearing fluids. The Au-bearing fluid includes CO_2, S and W. Unfortunately, factor analysis does not show the association of As with either hydrothermal fluids or Au-bearing fluids for type II rocks despite the results from isocon diagrams. Factor analysis was also performed selecting 4 factors in hopes of isolating the immobile element group as in type I, but the run was unsuccessful.

Two factors were chosen for type III rocks producing the following results:

FACTOR 1 (48.2%) REE, Al, Ag, Ba, Be, Cs, TFe_2O_3, Fe^{2+}, Ga, Hf, In, K, Mg, Nb, P, Rb, Sc, Ta, Th, Ti, Tl, U, Y, Zr,

FACTOR 2 (14.4%) Au, As, Na, S, Sr, V, W, -Ge, -Sn

Nearly 50% of the total variance within type III variolitic meta-volcanic rocks is accounted for by factor 1. Hydrothermal LILE's are included in factor 1 due to the lack of least-altered samples within this type. If unaltered samples were included it is expected that the LILE would be identified as a separate factor. As it stands, factor 1 demonstrates that all the samples had similar original chemistry and have all undergone the same degree of background alteration. Factor 2 identifies the Au-bearing fluids that have affected type III

variolitic meta-volcanic rocks. The Au-bearing fluid is composed of As, Na, S, Sr, V, and W. Again, the importance of As and W to gold mineralization at the Holloway deposit is shown by this statistically-sound technique. When factor analysis was performed choosing 3 factors, the results separated Ca, CO_2, and Mn as a third factor representing carbonate alteration.

Swan and Sandilands (1995) discuss criticisms of factor analysis which are dominated by the choices the user has to make. The user chooses the number of factors to be identified by factor analysis and will be biased due to preconceived notions of how the data set should vary. Subjectivity also influences the user's decision when controlling the rotation of the correlation matrix. At this point it is important to stress that factor analysis was merely used as a tool to support the findings of other techniques used in this alteration study.

4.9 Mineral Chemistry

Mineral chemistry was determined by electron microprobe analysis at the Ontario Geological Survey's Geoscience Laboratory. Minerals that were analyzed include chlorite, carbonate, pyrite, sericite, and albite. Samples from each of Holloway's meta-volcanic rock types were analyzed to determine how mineral chemistry varies between groups.

Figure 4.25 is a MgO versus FeO plot for carbonate and chlorite minerals. Mg and Fe^{2+} have similar chemical characteristics and commonly substitute for each other. The majority of carbonate minerals probed were identified as ankerite ($CaFe(CO_3)_2$) and the result show that carbonate minerals from types II and III tholeiite meta-volcanic rocks are Fe-enriched, while those of type I tholeiitic meta-volcanic rocks are Mg-enriched. Other carbonate varieties identified by microprobe analysis included calcite ($CaCO_3$) and siderite ($FeCO_3$). Only type I tholeiitic meta-volcanic rocks were found to contain calcite, and only types II and III Fe-tholeiitic and variolitic meta-volcanic rocks contained siderite. These results are consistent with Fe-enrichment of types II and III meta-volcanic rocks. Chlorite minerals show the same

Mg-enrichment for type I rocks and Fe-enrichment for types II and III rocks.

Pyrite group minerals typically have the formula AX_2 where X is S and A can be Fe, Ni, Ru, Pt, or Mn. The pyrite group can also be expressed as $A_4(X_2)_4$ where X can be S, As or Se. A ternary plot of As, Co, and Ni was created to observe the data for any trends in substitution. The pyrite data shows a high degree of variability, with a minor preference for Co-substitution. As-rich samples are commonly found in types II and III tholeiitic meta-volcanic rocks, but also have some occurrences in type I meta-volcanic rocks (figure 4.26).

The presence of variable amounts of arsenic in pyrite is demonstrated by zoned pyrite grains. Plate 17 displays the different pyrite morphologies present in the Holloway deposit. Commonly, the inclusion-rich pyrite grains are the ones that are zoned (plate 18). Some pyrite grains have arsenic-rich cores, while others have arsenic-rich rims. Based on a limited number of analysis, no correlation was identified.

Sericite ($KAl_2(AlSi_3O_{10})(OH)_2$) is isostructural with paragonite ($NaAl_2(AlSi_3O_{10})(OH)_2$) and so, K versus Na was plotted to determine if any trends existed between Holloway's meta-volcanic rock types. No obvious trends were observed, although some trends may be hidden due to the small sample set (5 samples).

During the probe work for the feldspar minerals, difficulty was encountered in trying to isolate grains for analysis. The challenge lay in distinguishing between feldspar and quartz grains on the back-scatter and reflected light images. Pervasive alteration has resulted in quartz-feldspar intergrowths and destruction of primary textures such as varioles that could not be discerned from the matrix. The feldspars were probed and plotted on the ternary diagram for the system orthoclase ($KAlSi_3O_8$) - albite ($NaAlSi_3O_8$) - anorthite ($CaAl_2Si_2O_8$). All of the feldspar crystals plotted in the albite field confirming that during metamorphic and hydrothermal alteration all of the primary Ca in the plagioclase has been replaced by Na.

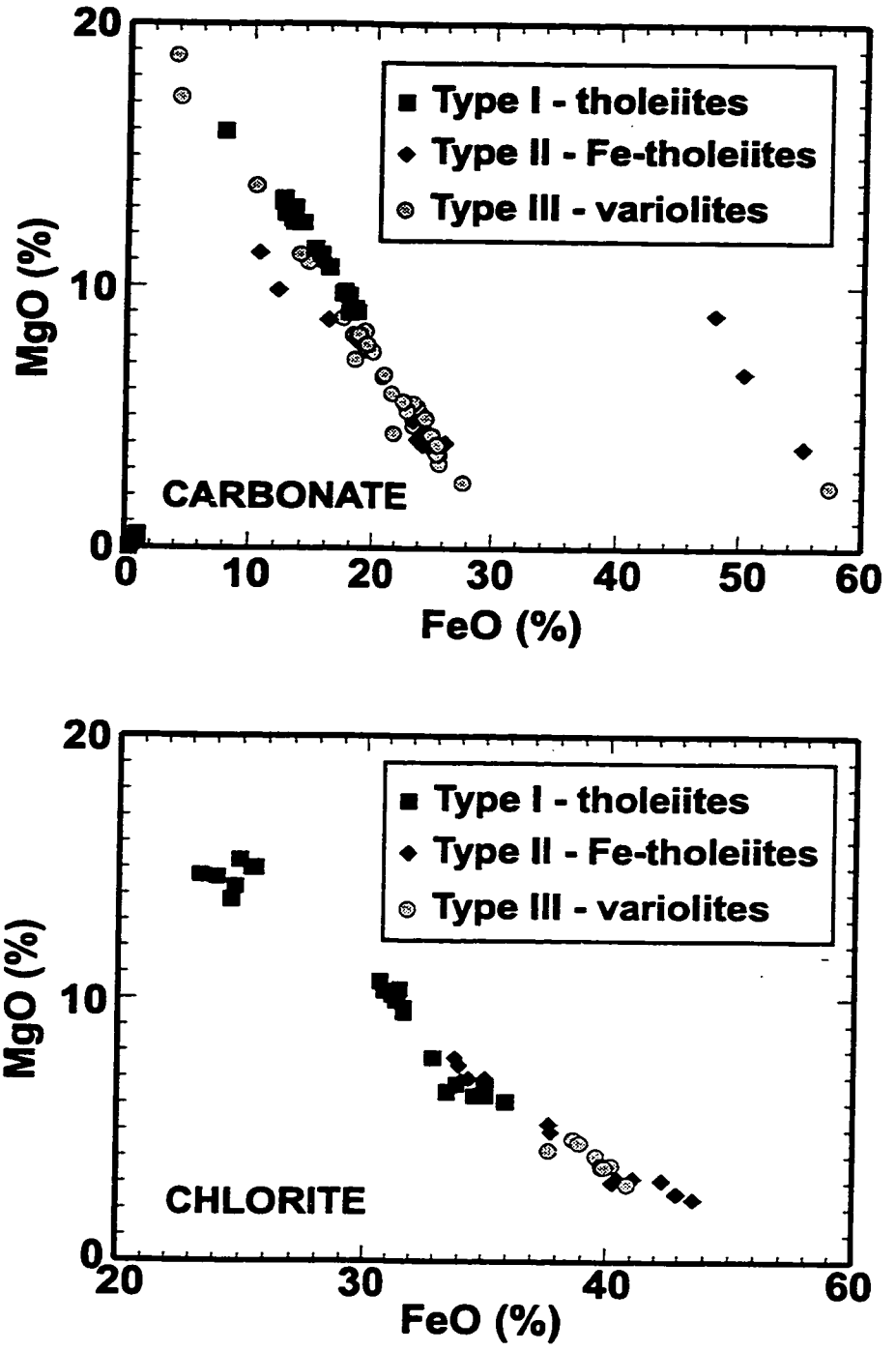

Figure 4.25: MgO versus FeO plot for carbonate and chlorite minerals from Holloway's meta-volcanic rocks. Carbonate and chlorite minerals from type I rocks are Mg-rich versus types II and III which are typically Fe-rich.

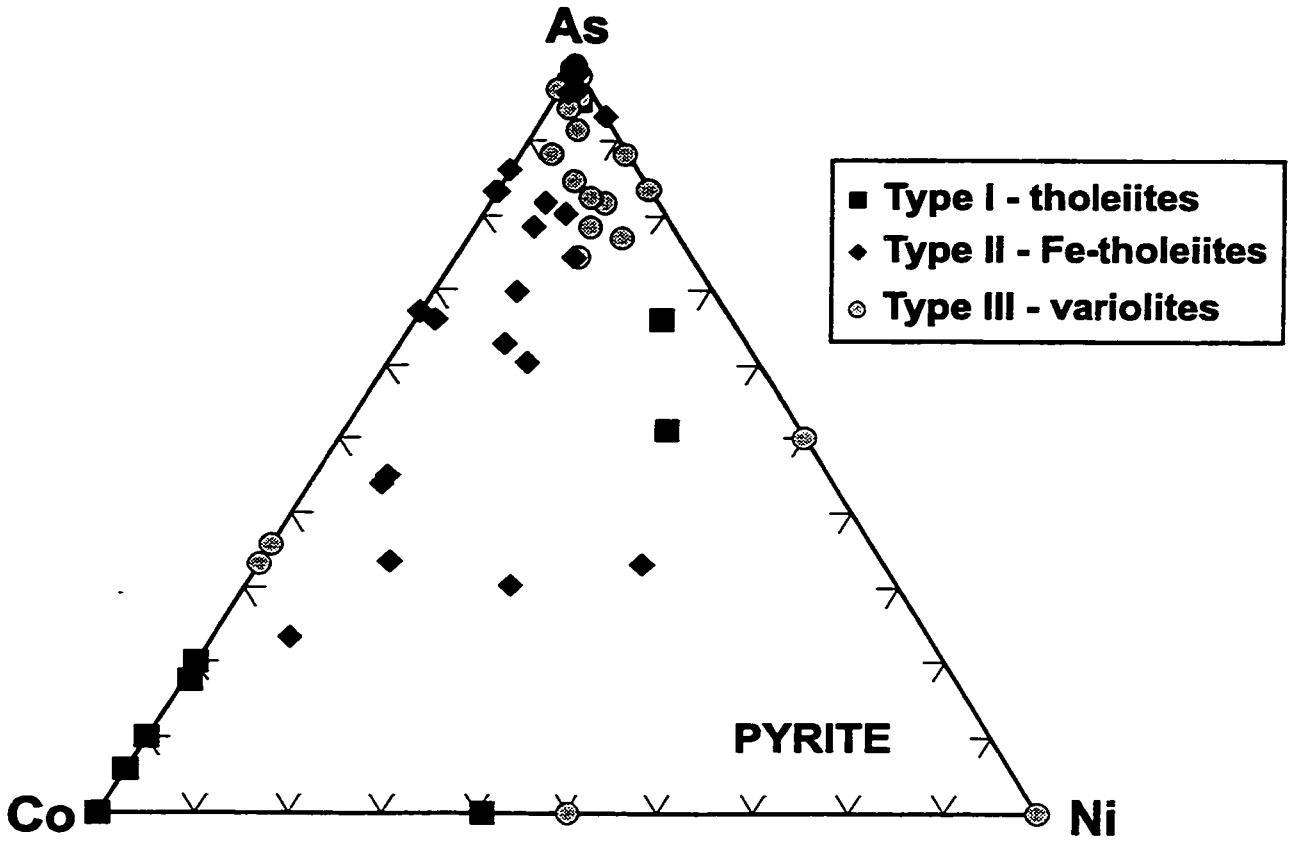

Figure 4.26: As-Co-Ni diagram for pyrite grains of Holloway's meta-volcanic rocks. Types II and III rocks tend to have more As-enriched pyrite grains.

Plate 17: Photomicrograph of different pyrite morphologies. Sample 520-127, CPL, field of view = 2 mm. The left side of the photomicrograph displays larger inclusion-rich pyrite grains, while a cluster of finer-grained euhedral pyrite grains is shown on the right side.

Plate 18: Photomicrograph of zoned pyrite grains. Sample 520-126, reflected light, field of view = 2 mm. Variable sized (μm to mm's) pyrite grains display zoning due to varying chemistry. Typically, zoned pyrite grains are euhedral and inclusion-rich.

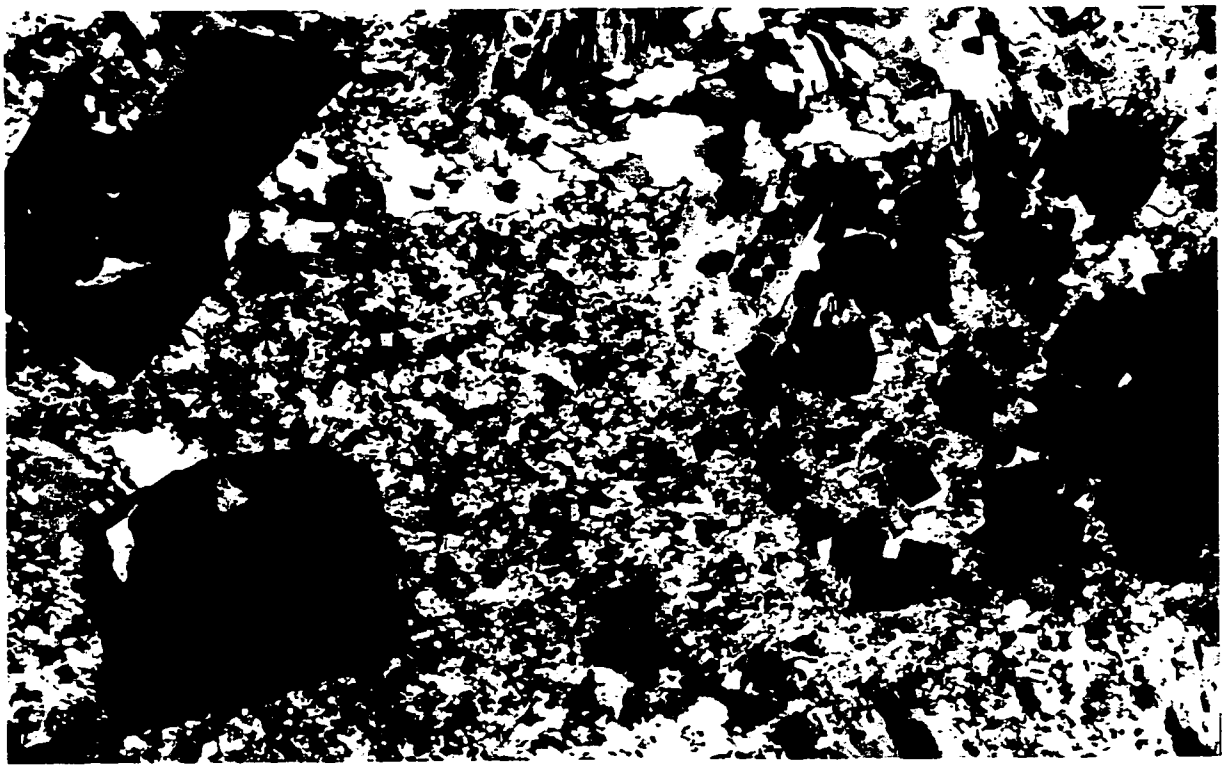

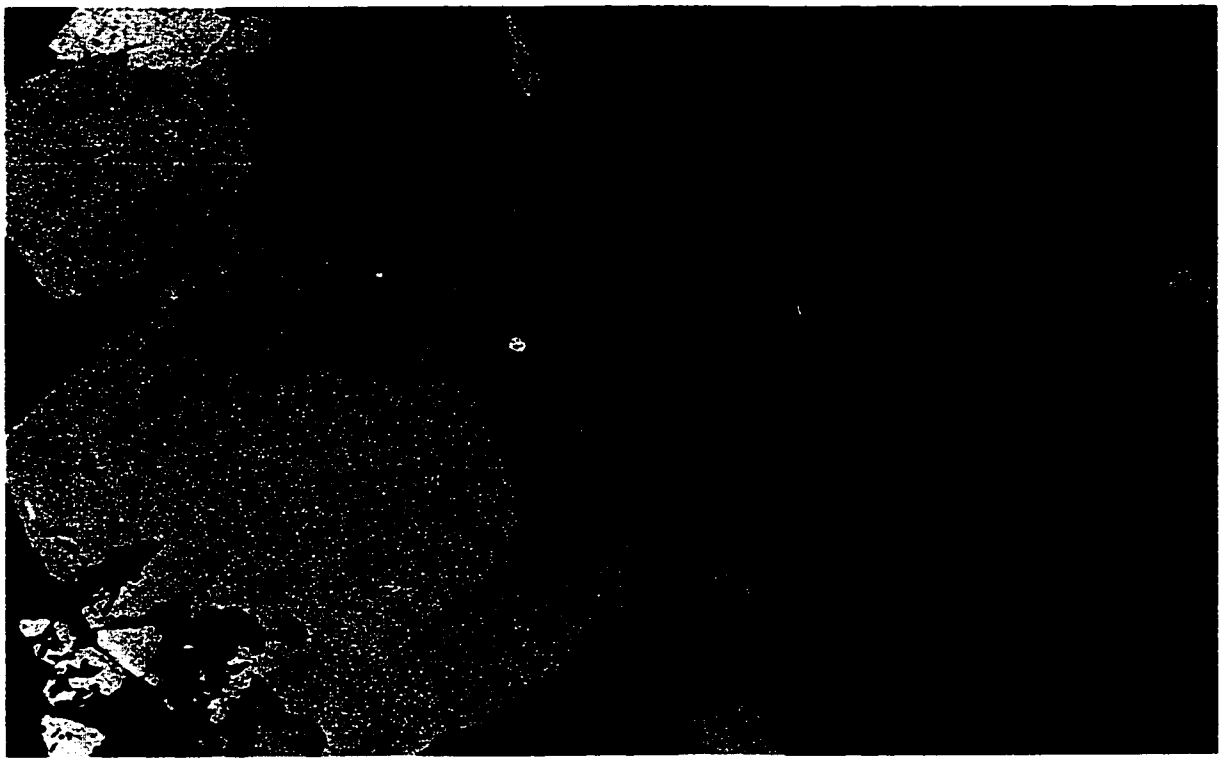

4.10 CHAPTER SUMMARY

Primary geochemical signatures were determined using REE and spider plots, basalt determination diagrams and differentiation trends. From this work it is established that meta-volcanic rocks from the Holloway deposit are comprised of a suite of tholeiitic rocks with differentiated geochemical signatures. This was an important breakthrough before an accurate alteration study could be completed. The meta-volcanic rocks are divided into three types.

Type I tholeiitic meta-volcanic rocks consist of pillowed and massive mafic meta-volcanic rocks having flat-lying REE patterns with concentrations approximately equal to 10 times chondrite. Immobile elements were identified using the Soma 1 software package and include Nb, Hf, Th, and Al_2O_3. Type I rocks have a Fe/Mg ratio equal to 2, corresponding to the results of the Jensen plot where the samples plot at the boundary between Mg- and Fe-tholeiitic rocks. Type I rocks are the least evolved type of meta-volcanic rocks at the Holloway deposit, correlating to N-type MORB, and have the lowest gold concentrations of 0.02 ±0.01 g/t.

Type II Fe-tholeiitic meta-volcanic rocks also consist of pillowed and massive tholeiitic meta-volcanic rocks, but have a more evolved flat-lying REE pattern with concentrations around 50 times chondrite. TiO_2, Al_2O_3, Hf and Th were identified as immobile elements for type II rocks. According to the TiO_2 versus Zr fractionation plot, type II rocks are equivalent to andesites in composition. Jones (1992) showed that more evolved variolitic rocks have Fe/Mg ratios greater than 4. An Fe/Mg ratio around 8 for type II rocks lends additional evidence that these rocks belong to a more evolved tholeiitic suite. Type II rocks are more auriferous than type I, having variable Au concentrations of 0.8 ±2.5 g/t. Vein-type gold mineralization, consisting of pyrite±arsenopyrite stringers with sericite alteration haloes, is hosted by type II Fe-tholeiitic meta-volcanic rocks.

Type III variolitic meta-volcanic rocks are the most evolved group having flat-lying REE patterns with concentrations around 100 times chondrite. Variolitic and hyaloclastite rock textures dominate this group, and their composition is equivalent to rhyolites on the TiO_2 versus Zr fractionation plot. Type III rocks have an Fe/Mg ratio around 8, which is in agreement with Jones' (1992) finding that variolitic rocks typically have Fe/Mg ratios greater than 4. Lightning Zone mineralization is hosted by type III variolitic meta-volcanic rocks and have gold grades of 5.0 ±9.8 g/t.

Meta-volcanic rocks of the Holloway deposit were generated by fractional crystallization of a N-MORB magma source. Type I rocks represent the least evolved magmatic source. Type II and III rocks are derived from a melt that has undergone 70-80% and 85-93% fractional crystallization respectively.

Upon determining immobile elements, isocon diagrams were plotted for sericite- and hematite-altered samples within types I and II meta-volcanic rocks. Isocon diagrams could not be generated for type III due to the lack of a least-altered and unmineralized sample. Results for sericite alteration showed that CO_2, K_2O, Rb, Ba, Cs, and Sb displayed elemental increases. Au frequently showed an elemental increase along with W and As. Hematized samples showed variable results on the isocon diagrams, but generally showed an elemental decrease in FeO, consistent with the oxidizing environment associated with hematization.

Factor analysis confirmed the chemistry of hydrothermal fluids as comprising of LILE (Cs, Rb, K, Ba, Sr, Tl). Au-bearing fluids were also recognized using the factor analysis technique. Gold was shown to have an elemental association with W, As, S, and CO_2. The composition of hydrothermal and Au-bearing fluids at the Holloway deposit are consistent with typical Archean lode gold deposits which show enrichments of precious metal (Au, Ag), associated trace elements (As, Sb, Se, Te, Bi, W, B), LILE (K, Rb, Ba, Cs, Tl), and volatiles (McCuaig and Kerrich, 1994).

Data from mineral chemistry confirms the tholeiitic Fe-enrichment trend as samples progress from type I to type III Host Iron-Tholeiites. Carbonate and chlorite mineral chemistry showed that types II and III meta-volcanic rocks host Fe-enriched minerals and type I meta-volcanic minerals were typically Mg-enriched. All of the plagioclase that was analyzed had an albite composition. Arsenic values within the Holloway deposit are enriched and pyrite grains reflect this by having arsenic weight percent concentrations up to 2.5%.

CHAPTER FIVE: SUMMARY AND CONCLUSIONS

Broughton *et al.* (1991) and Guy (1996) provided the foundation for this study. They described in detail the stratigraphy and structural geology of the Holloway deposit. Upon this base of information, the purpose of this study was to describe in detail the geochemistry of the meta-volcanic rocks which host gold mineralization at the Holloway deposit.

The objectives of this thesis (see italicized text) are reiterated and concisely addressed in this chapter. Full explanations of how the conclusions were derived can be found in the appropriate chapters. For the most part, this chapter has been divided into petrological observations, geochemical findings, and economic implications, although some overlap does occur. I once read that "gold is where you find it," but hopefully this study will shed some light on the elusive gold deposit.

6.1 PETROLOGICAL OBSERVATIONS

Petrological observations present the first clues in the search for a gold deposit. Certain rock types and especially the presence of alteration can lead to a major gold finding.

Characterize productive alteration types.

Carbonate alteration is the first indication that a gold deposit may be nearby, but carbonate alteration alone does not prove that a deposit exists! The productive alteration types at the Holloway deposit include a silicified-albitized core and the surrounding sericitized alteration halos. Hematite alteration also occurs at the Holloway deposit, but ore grades associated with this type of alteration are severely diminished.

Ore zones at the Holloway deposit are located at the lithologic boundary between the meta-komatiite footwall and tholeiitic meta-volcanic hanging wall. The contact is sheared, likely

serving as a conduit for hydrothermal fluids. Silicified-albitized variolitic meta-volcanic rocks host gold mineralization in the form of disseminated pyrite.

Describe the timing and relationship between alteration and mineralization types.

Two mineralizing events generated the economic gold deposit at the Holloway mine. The first mineralizing event, the Lightning Zone, is lithologically constrained to type III variolitic meta-volcanic rocks. Within the Lightning Zone, gold is proportionately associated with disseminated pyrite, such that 5% pyrite approximates 5 g/t of gold. Variolitic and hyaloclastite rock textures dominate this group, and their composition is equivalent to rhyolite on a TiO_2 versus Zr fractionation plot. The second mineralizing event is closely associated with sericite alteration. Within vein-type mineralization, gold occurs with pyrite±arsenopyrite stringers that are surrounded by sericite alteration halos. Sometimes vein-type mineralization overprints the Lightning Zone, significantly increasing ore grades.

The evolution of the Holloway gold deposit can be briefly summarized as follows. First, thick submarine volcanic piles were laid down. Tholeiitic volcanic rocks are likely the source of gold as hydrothermal solutions filtered through the rock concentrating Au-bearing CO_2-H_2O solutions over a range of metamorphic conditions and crustal depths. Type III rock units dominantly consist of hyaloclastites and variolites, their primary porosity was high allowing hydrothermal fluids to readily penetrate the unit. Early quartz-albite alteration hardened type III meta-volcanic rocks, causing them to be more brittle and easily fractured during subsequent deformational events. Gold is precipitated by oxidation of the solution, change in pH, decrease of temperature, or by lowering the activity of reduced sulphur by boiling, dilution, oxidation, or reaction with iron in the host rock to precipitate iron sulphide. In the case of the Holloway deposit, type III variolitic meta-volcanic rocks, with a high Fe/Mg, acted as the host rock providing the necessary iron to lower the activity of reduced sulphur in the solution. The fractures allowed Au-bearing solutions to percolate through the rocks, depositing gold as the fluid reacts with the wall rocks.

The timing of the first gold mineralizing event is constrained to be older than the radiometeric age of 2672 Ma of an unmineralized crosscutting dyke. A later vein-type mineralizing event occurred within type II Fe-tholeiitic meta-volcanic rocks. Type II rocks also have a high Fe/Mg (~8) making them favourable hosts for gold mineralization. Carbonate alteration represents the distal phases (*i.e.* lower temperatures) of a hydrothermal system. Several hydrothermal systems have influenced the alteration sequence at the Holloway deposit, creating a massive width of carbonate alteration. Carbonate alteration is pervasive at Holloway, created by several influxes of hydrothermal solutions over a relatively long period of time.

6.2 GEOCHEMICAL FINDINGS

Geochemical sampling and characterization of the Holloway deposit.

Meta-volcanic rocks from the Holloway deposit were sampled from underground workings such that a sequence from least altered to highly altered, mineralized rocks could be collected. Meta-volcanic rocks hosting the Holloway deposit belong to unit V of the Destor Porcupine Complex. The Destor Porcupine Complex is a fault-bounded block of komatiitic and tholeiitic meta-volcanic rocks with intermixed meta-sedimentary rocks. A large database of geochemical data was generated including: major elements (ICP-AES); trace elements (ICP-MS); S, CO_2, and H_2O (LECO®); FeO (titration); gold (INAA); and density (pycnometer). Appendix A presents data for the meta-volcanic rocks within the Holloway deposit; also, a disk that contains additional data from the mine are is included. A limited database of mineral chemical analyses was also acquired using an electron microprobe.

Investigation into the nature of the rocks prior to mineralization and their alteration.

An important finding of this thesis is that the rocks are not all basalts; they span the compositional range of tholeiitic basalt to rhyolite, and are shown to have been produced by

fractional crystallization. Three types of meta-volcanic rocks were isolated on the basis of trace element geochemistry. Type I tholeiitic meta-volcanic rocks are basaltic, having N-MORB composition, and flat-lying REE patterns of 10 times chondrite. Using the average chemistry of type I rocks and the Treuil method, it was determined that types II (Fe-tholeiitic) and III (variolitic) were derived by 70-80% and 85-93% fractional crystallization of a type I magma source. Type III variolitic meta-volcanic rocks are the most evolved group, having flat-lying REE patterns with concentrations around 100 times chondrite. Types II and III rocks have an Fe/Mg ratio around 8, creating a favourable environment for gold to precipitate.

6.3 Economic Implications

General gold deposit models suggest that fault zones and subsidiary shear zones are a good place to begin exploration for gold deposits. In addition, the presence of intrusions within fault zones increases the likelihood of finding an economical deposit. Detailed mapping where outcrop is available, and limited geochemical analysis of drill core will further substantiate whether an exploration camp has the appropriate characteristics to host a gold deposit. Alteration types are important indicators, such that high temperature magmatic fluid-related phases such as albitization and sericitization are more likely to host gold.

Statistical analysis of geochemical data from Holloway's altered meta-volcanic rocks demonstrated that Au was associated with increased As, W, S, and CO_2. These results are in agreement with typical enrichments associated with Archean lode gold deposits (*i.e.* As, Sb, Se, Te, Bi, W, and B)(McCuaig & Kerrich, 1994). The presence of arsenopyrite in mineral assemblages is consistent with elevated As values, and thus a good indicator of gold mineralization.

Determination of favourable lithologies for ore deposition.

The lithologies that are favoured for Holloway-type gold mineralization include type II and type III Host Iron-Tholeiitic meta-volcanic rocks. These type of rocks are able to initiate gold deposition because they have high Fe/Mg. Bohlke (1988) demonstrated that rocks with high Fe/Mg ratios are effective in scavenging gold from hydrothermal systems. Type I rocks have Fe/Mg=2, whereas types II and III rocks have Fe/Mg=8 making them favourable hosts for gold mineralization.

Type III rocks are relatively easy to identify in the field without conducting expensive geochemical analysis. Type III rocks consist of variolitic, flow-banded, and hyaloclastite textures. The primary porosity of these textures makes the units susceptible to alteration by hydrothermal fluids. Silicified and/or albitized type III rocks are brittle and during deformational events, secondary porosity may provide a conduit for Au-bearing fluids. Upon introduction of an Au-bearing fluid, the high Fe/Mg ratio of type III rocks will precipitate pyrite which in return scavenges gold from the fluid. Silicified-albitized type III rocks represent very good candidates for gold mineralization.

Least-altered type II rocks are indistinguishable from their type I counterparts. The presence of pyrite is the only visible indicator of mineralized type II rocks. In this case, geochemical determination of the Fe/Mg ratio is extremely useful for identifying potential gold-bearing host rocks. Jones demonstrated that rocks with a high Fe/Mg ratio (>4) represent potential hosts for gold mineralization. Therefore, type II meta-volcanic rocks having a Fe/Mg=8 are good potential hosts for gold mineralization, whereas type I rocks having a Fe/Mg=2 are not.

REFERENCES

ACTLABS, 1999. 1999 Fee Schedule, Activation Laboratories Ltd, Ancaster, Ontario, 22 pp.

Allègre, C.J., Treuil, M., Minster, J.-F., Minster, B., and Albarède, F., 1977. Systematic use of trace element in igneous process Part I: Fractional crystallization processes in volcanic suites. Contributions to Mineralogy and Petrology **60**: 57-75.

Appleyard, E.C., 1991. SOMA - a package of Fortran IV programs for calculating mass exchange in metasomatic and altered rocks (Revised and extended version for use at the University of Waterloo), 47 pp.

Ayer, J.A., Trowell, N.F., Amelin, Y., and Corfu, F., 1999. Geological compilation of the Abitibi greenstone belt in Ontario: toward a revised stratigraphy based on compilation and new geochronology results. In Summary of Field Work and Other Activities 1998, Ontario Geological Survey, Miscellaneous Paper 169, pp 14-24.

Berger, B., 1997. Geological investigations along Highway 101, east of Matheson In Summary of Field Work and Other Activities 1997, Ontario Geological Survey, Miscellaneous Paper 168, pp 20-22.

Berger, B., and Amelin, Y., 1999. Geological investigations along Highway 101; Guibord, Michaud and Garrison Townships In Summary of Field Work and Other Activities 1998, Ontario Geological survey, Miscellaneous Paper 169, pp 25-32.

Böhlke, J.K., 1988. Carbonate-sulphide equilibria and "stratabound" disseminated epigenetic gold mineralization: a proposal based on examples from Alleghany, California, U.S.A.. Applied Geochemistry **3**: 499-516.

Broughton, D., Green, K., and Cooper, P., 1991. Geology of the Holloway project, Volume 1 Technical Report. Noranda Exploration Company. 95 pp.

Chao, T.T., and Sanzolone, R.F., 1992. Decomposition techniques. Journal of Geochemical Exploration **44**: 65-106.

Corfu, F., 1993. The evolution of the southern Abitibi Greenstone Belt in light of precise U-Pb geochronology. Economic Geology **88**: 1323-1340.

Corfu, F., and Noble, S.R., 1992. Genesis of the southern Abitibi greenstone belt, Superior Province, Canada: Evidence from zircon Hf isotope analysis using a single filament technique. Geochimica et Cosmochimica Acta **56**: 2081-2097.

Corfu, F., Krogh, T.E., Kwok, Y.Y., and Jensen, L.S., 1989. U-Pb zircon geochronology in the southwestern Abitibi greenstone belt, Superior Province. Canadian Journal of Earth Sciences **28:** 1747-1763.

Couture, J.F., and Pilote, P., 1993. The geology and alteration patterns of a disseminated, shear zone-hosted mesothermal gold deposit: The Francoeur 3 Deposit, Rouyn-Noranda, Quebec. Economic Geology **88:** 1664-1684.

Couture, J.F., Pilote, P., Machado, N., and Desrochers, J.P., 1994. Timing of gold mineralization in the Val-d'Or district, southern Abitibi belt: evidence for two distinct mineralizing events. Economic Geology **89:** 1542-1551.

Couture, J.F., and Robert, F., 1997. Atypical gold deposits in the Abitibi belt, Field Trip B5, 21-25 May 1997, Geological Association of Canada, pp 29-51.

Cremer, M., and Schlocker, J., 1976. Lithium borate decomposition of rocks, minerals, and ores. American Mineralogist **61:** 318-321.

Davis, J.C., 1986. Statistics and Data Analysis in Geology 2nd edition, John Wiley and Sons, New York, 646 pp.

Dostal, J, and Mueller, W., 1996. An Archean oceanic felsic dyke swarm in a nascent arc: the Hunter Mine Group, Abitibi Greenstone Belt, Canada. Journal of Volcanology and Geothermal Research **72:** 37-57.

Ferrara, G., and Treuil, M., 1973. Petrological implications of trace element and Sr isotope distributions in basalt-pantellerite series. Bulletin Volcanologique **38:** 548-574.

Fleet, A.J., 1984. Aqueous and sedimentary geochemistry of the rare earth elements *In* Rare Earth Element Geochemistry *Edited by* P. Henderson, Elsevier, Amsterdam, pp 343-373.

Fowler, A.D., and Jensen, L.S., 1989. Quantitative trace-element modelling of the crystallization history of the Kinojevis and Blake River groups, Abitibi Greenstone Belt, Ontario. Canadian Journal of Earth Sciences **26:** 1356-1367

Gélinas, L., Brooks, C., and Trzcienski, W.E., 1976. Archean variolites - quenched immiscible liquids. Canadian Journal of Earth Science **13:** 210-230.

Grant, J.A., 1986. The isocon diagram - A simple solution to Gresens' equation for metasomatic alteration. Economic Geology **81:** 1976-1982.

Gresens, R.L., 1967. Composition-volume relationships of metasomatism. Chemical

Geology **2:** 47-65.

Grunsky, E.C., Easton, R.M., Thurston, P.C., and Jensen, L.S., 1992. Characterization and statistical classification of Archean volcanic rocks of the Superior Province using major element geochemistry *In* Geology of Ontario; OGS Special Volume 4, Part 2. *Edited by* P.C. Thurston, H.R. Williams, R.H. Sutcliffe, and G.M Stott. Ontario Geological Survey, Ontario, pp 1397-1438.

Guy, R.L., 1996. The geology of the Holloway gold deposit, Abitibi Greenstone Belt, Ontario. Unpublished M. Sc. Thesis, Queen's University, Kingston, Ontario, 270 pp.

Heather, K.B., 1998. New insights on the stratigraphy and structural geology of the southwestern Abitibi greenstone belt: Implications for the tectonic evolution and setting of mineral deposits in the Superior Province In The First Age of Giant Ore Formation: Stratigraphy, Tectonics, and Mineralization in the Late Archean and Early Proterozoic, papers presented at the Prospectors and Developers Association of Canada Annual Convention, Toronto, pp. 63-101.

Henderson, P., 1984. Rare Earth Element Geochemistry, Elsevier, Amsterdam, 510 pp.

Hodgson, C.J., 1993. Mesothermal lode-gold deposits. In Kirkham, R.V., Sinclair, W.D., Thorpe, R.I., and Duke, J.M., eds., Mineral Deposit Modeling: Geological Association of Canada, Special Paper 40, pp 635-678.

Hofmann, A.W., 1988. Chemical differentiation of the Earth: the relationship between mantle, continental crust, and oceanic crust. Earth and Planetary Science Letters **90:** 297-314.

Huanzhang, L., and Guoxiang, C., 1996. Geochemical characteristics of ore forming fluids in shear zone hosted Archean gold deposits. Earth Science Frontiers **3:** 19-38.

Irvine, T.N., and Baragar, W.R.A., 1971. A guide to the chemical classification of the common volcanic rocks. Canadian Journal of Earth Sciences **8:** 523-548.

Jackson, S.L., Fyon, J.A., and Corfu, F. 1994. Review of Archean supracrustal assemblages of the southern Abitibi greenstone belt in Ontario, Canada: products of microplate interaction within a large-scale plate-tectonic setting. Precambrian Research **65:** 183-205.

Jeffery, P.G., and Hutchinson, D., 1981. Chemical Methods of Rock Analysis, 3rd edition. Pergamon Press, Oxford, 379 pp.

Jensen, L.S., 1976. A New Cation Plot for Classifying Subalkalic Volcanic Rocks; Ontario

Division of Mines, Miscellaneous Paper 66, 22 pp.

Jensen, L.S., and Langford, F.F. 1985. Geology and Petrogenesis of the Archean Abitibi Belt in the Kirkland Lake Area, Ontario; Ontario Geological Survey, Miscellaneous Paper 123, 130pp. Accompanied by Maps P.2434 and P.2435, scale 1:63 360 or 1 inch to 1 mile and sheet of microfiche.

Jochum, K.P., Arndt, N.T., and Hofmann, A.W., 1991. Nb-Th-La in komatiites and basalts: constraints on komatiite petrogenesis and mantle evolution. Earth and Planetary Science Letters **107:** 272-289.

Johnson, W.M., and Maxwell, J.A., 1981. Rock and Mineral Analysis, 2nd edition. John Wiley and Sons, New York, xx pp.

Jones, M.I., 1992. Variolitic basalts: Relations to Archean epigenetic gold deposits in the Abitibi Greenstone belt. M. Sc. Thesis, Ottawa-Carleton Geoscience Centre, University of Ottawa, Ottawa, Ontario, 300 pp.

Kerrich, R., 1983. Geochemistry of gold deposits in the Abitibi Greenstone belt. The Canadian Institute of Mining and Metallurgy, Special Volume 27, 75 pp.

Kerrich, R., and Cassidy, K.F., 1994. Temporal relationships of lode gold mineralization to accretion, magmatism, metamorphism and deformation - Archean to present: A review. Ore Geology Reviews **9:** 263-310.

Kretz, R., 1985. Calculation and illustration of uncertainty in geochemical analyses. Journal of Geological Education 33: 40-44.

Lesher, C.M, Goodwin, A.M., Campbell, I.H., and Gorton, M.P., 1986. Trace-element geochemistry of ore-associated and barren, felsic metavolcanic rocks in the Superior Province, Canada. Canadian Journal of Earth Sciences **23:** 222-237.

Luinstra, B., 2000. Ph. D. thesis (in progress), Ottawa-Carleton Geoscience Centre, University of Ottawa, Ontario.

Maaløe, S., 1985. Principles of Igneous Petrology, Springer-Verlag, Berlin, 374 pp.

MacLean, W.H., and Barrett, T.J., 1993. Lithogeochemical techniques using immobile elements. Journal of Geochemical Exploration 48: 109-133.

McCuaig, T.C., and Kerrich, R., 1994. P-T-t-deformation-fluid characteristics of lode gold deposits: Evidence from alteration systematics, *In* Alteration and Alteration Processes Associated with Ore-Forming Systems. *Edited by* D.R. Lentz. Geological

Association of Canada, Short Course Notes, v. 11, pp 339-379.

Melnik-Proud, N., 1992. The geology and ore controls in and around the McIntyre mine at Timmins, Ontario, Canada. Ph. D. Thesis, Queen's University, Kingston, Ontario, 353 pp.

MERQ-OGS, 1983. Lithostratigraphic map of the Abitibi Subprovince; Ontario Geological Survey/Ministère de l'Énergie et des Resources, Québec; 1:500 000; Map 2482.

Meschede, M., 1986. A method of discriminating between different types of mid-ocean ridge basalts and continental tholeiites with the Nb-Zr-Y diagram. Chemical Geology **56:** 207-218.

Meyer, C., 1988. Ore deposits as guides to geological history of the Earth. Annual Reviews of Earth and Planetary Science 16: 147-171.

Michard, A., 1989. Rare earth element systematics in hydrothermal fluids. Geochimica et Comochimica Acta **53:** 745-750.

Mikucki, E.J., 1998. Hydrothermal transport and depositional processes in Archean lode-gold systems: A review. Ore Geology Reviews **13:** 307-321.

Mortensen, J.K., 1987. Preliminary U-Pb zircon ages for volcanic and plutonic rocks of the Noranda-Lac Abitibi area, Abitibi sub-province, Quebec. Geological Survey of Canada Paper, 87-1A, pp. 581-590.

Mueller, W.U., and Corcoran, P.L., 1998. Late-orogenic basins in the Archean Superior Province, Canada: characteristics and inferences. Sedimentary Geology **120:** 177-203.

Mueller, A.G., and Groves, D.I., 1991. The classification of Western Australian greenstone-hosted gold deposits according to wallrock-alteration assemblages. Ore Geology Reviews **6:** 291-332.

Pearce, J.A., 1983. Role of the sub-continental lithosphere in magma genesis at active continental margins *In* Continental Basalts and Mantle Xenoliths. *Edited by* C.J. Hawkesworth, and M.J. Norry, Shiva, Nantwich, pp.230-249.

Powell, W.G., Carmichael, D.M., Hodgson, C.J., 1995. Conditions and timing of metamorphism in the southern Abitibi greenstone belt, Quebec. Canadian Journal of Earth Sciences **32:** 787-805.

Roberts, R.G., 1988. Archean lode gold deposits. *In* Ore Deposit Models *Edited by* Roberts,

R.G. and Sheahan, P.A. Geoscience Canada reprint series 3, pp 1-19.

Rollinson, H.R., 1993. Using Geochemical Data: Evaluation, Presentation, Interpretation, Longman, Singapore, 352 pp.

Ryerson, F.J., and Hess, P.C., 1978. Implications of liquid-liquid distribution coefficients to mineral-liquid partitioning. Geochimica et Cosmochimica Acta **42:** 921-932.

Satterly, J., 1951. Geology of Harker Township. In 60th Annual Report of the Department of Mines Vol. 60, Part 7, 47 pp.

Seward, T.M., 1973. Thio complexes of gold and the transport of gold in hydrothermal ore solutions. Geochimica et Cosmochimica Acta **37:** 379-399.

Seward, T.M., 1984. The transport and deposition of gold in hydrothermal systems In Gold '82: The Geology, Geochemistry, and Genesis of Gold Deposits. Edited by R.P. Foster, Geological Society of Zimbabwe, Special Publication No. 1, pp. 165-181.

Sibson, R.H., Robert, F., and Poulsen, K.H., 1988. High-angle reverse faults, fluid-pressure cycling, and mesothermal gold-quartz deposits. Geology **16:** 551-555.

Staudigel, H., and Hart, S.R., 1983. Alteration of basaltic glass: Mechanisms and significance for the oceanic crust-seawater budget. Geochimica et Cosmochimica Acta **47:** 337-350.

Sun, S.S., and McDonough, W.F., 1989. Chemical and isotopic systematics of oceanic basalts: Implications for mantle composition and processes In Magmatism in the Ocean Basins. Edited by A.D. Saunders, and M.J. Norry, Geological Society Special Publication No. 42, pp.313-345.

Swan, A.R.H., and Sandilands, M., 1995. Introduction to Geological Data Analysis. Blackwell Science, Oxford University Press, Don Mills, 446 pp.

Talbot, D.A., 1998. Franco-Nevada and Greater Lenora Holloway Joint Venture Property, unpublished internal consultants report, 38 pp.

Thompson, R.N., 1982. British Tertiary volcanic province. Scottish Journal of Geology **18:** 49-107.

Thurston, P.C., 1991. Archean geology of Ontario: introduction *In* Geology of Ontario; OGS Special Volume 4, Part 1. *Edited by* P.C. Thurston, H.R. Williams, R.H. Sutcliffe, and G.M Stott. Ontario Geological Survey, Ontario, pp. 73-78.

Thurston, P.C., and Chivers, K.M., 1990. Secular variation in Greenstone sequence development emphasizing Superior Province, Canada. Precambrian Research **46:** 21-58.

Watson, B., 1976. Two-liquid partition co-efficients: experimental data and geochemical implications. Contributions to Mineralogy and Petrology **56:** 119-134.

Whipple, E.R., 1974. A study of Wilson's determination of ferrous iron in silicates. Chemical Geology **14:** 223-238.

Wilson, A.D., 1960. The micro-determination of ferrous iron in minerals by a volumetric and colorimetric method. Analyst **85:** 823-827.

APPENDIX A:DATA

SAMPLE	TECHNIQUE	415-01	415-02	415-03	415-04	415-05	415-06	415-07	415-08	415-09	415-10	415-11	415-12	415-13
type		thol	thol	thol	thol	thol	thol	thol	thol	thol	Fe-thol	var	var	sed
density	pycnometer	2.99	2.89	2.85	2.83	2.85	2.90	2.91	2.90	2.87	3.19	2.83	2.83	2.91
SiO_2	ICP	44.71	46.16	50.83	44.46	42.33	43.54	41.73	41.59	43.29	31.12	63.41	60.8	36.26
Al_2O_3	ICP	15.62	14.94	14.61	13.26	12.25	12.14	12.04	12.55	11.26	16.24	8.73	11.42	6.82
Fe_2O_3T	ICP	12.98	10.64	11.72	8.73	9.82	11.7	10.35	9.56	8.44	24.04	8.71	7.43	3.41
FeO	titration	11.21	8.47	9.61	4.59	7.47	9.91	9.15	8.24	7.57	21.63	12.57	9.06	3.83
Fe_{soln}	ICP	7.63	6.67	7.65	4.64	5.33	7.15	5.97	5.95	4.74	12.52	2.34	2.58	1.64
MnO	ICP	0.19	0.14	0.13	0.14	0.2	0.25	0.23	0.3	0.14	0.37	0.15	0.14	0.12
MgO	ICP	5.22	4.68	5.88	3.51	4.91	4.53	4.07	4.02	4.94	3.03	1.24	0.91	10.62
CaO	ICP	7.6	6.57	4.47	8.23	8.86	9.17	10.32	10.63	10.2	2.21	4.11	3.49	14.98
Na_2O	ICP	0.16	3.39	2.87	5.79	4.97	2.04	1.18	2.23	1.42	0.2	4.84	6.38	0.5
K_2O	ICP	1.9	1.61	0.11	1.14	0.61	0.72	1.66	1.01	2.33	3.98	0.21	0.27	1.87
TiO_2	ICP	1.4	1.08	1.22	1.08	1	1.09	1.09	1.14	0.95	2.18	0.45	0.5	0.36
P_2O_5	ICP	0.09	0.07	0.16	0.07	0.09	0.07	0.07	0.06	0.06	0.89	0.11	0.08	0.06
LOI	ICP	9.89	11.18	6.86	12.29	13.88	15.01	16.58	16.5	16.18	14.54	8.66	7.41	23.73
TOTAL	ICP	99.75	100.46	98.86	98.69	98.92	100.25	99.32	99.6	99.22	98.79	100.62	98.82	98.74
H_2O	LECO	4.8	2.9	4.8	0.6	1.3	2.5	2.1	1.9	1.5				1.5
CO_2	LECO	6.1	9.7	3.4	12.8	13.7	13.7	15.9	15.9	16.3	12.6	6	5.1	22.9
S	LECO	0.2	0.14	0.02	0.36	0.42	0.11	0.08	0.16	0.63	2.47	4.77	4.22	0.05
Sc	ICP	54	45	46	41	39	43	42	46	37	46	11	14	23
Be	ICP	2	1	1	1	1	1	1	2	2	2			1
V	ICP-MS	357	289	307	276	290	336	329	322	273	18	12	15	134
Cr	ICP-MS	86	147	115	89	94	78	81	110	109		21	373	1980
Co	ICP-MS	36	26	46	33	44	44	45	39	39	19	2.9	1.9	66
Ni	ICP-MS	58	73	91	134	73	68	69	39	71			59	794
Cu	ICP-MS	88	106	115	86	135	113	72	102	62	118	11		
Zn	ICP-MS	48	90	73	40	90	80	66	52	55	244	34	45	65
Ga	ICP-MS	16	17	17	14	16	16	15	15	15	39	20	21	10
Ge	ICP-MS	0.9	1.3	1.4	0.7	1.4	1.4	1.4	1.2	1	1.1	1.2	1	0.8
As	ICP-MS	19			13	6	7	109	8	215	1679	28	1566	1717
Rb	ICP-MS	45	43	3	27	20	21	42	32	57	90	5	6.3	44
Sr	ICP-MS	67.5	99.7	68	140	174	140	139	161	200	68.3	85.2	221	223
Y	ICP-MS	24	17	22	16	20	19	20	20	16	96	142	168	15
Zr	ICP-MS	50	46	57	51	44	41	41	45	40	200	457	531	24
Nb	ICP-MS	2.5	2.2	2.6	2.3	2.1	1.8	1.8	2	1.8	11	18	22	0.9
Mo	ICP-MS		0.4		3.3	0.7	0.2	0.3	0.3	0.2	0.4	9.8	4.2	0.2
Ag	ICP-MS					0.9								
In	ICP-MS										0.2	0.1	0.1	
Sn	ICP-MS		0.7	0.7			0.5				1.7	1.7	1.5	1.2
Sb	ICP-MS	3.65	7.19	2.16	8.09	12	8.84	8.32	8.17	6.7	3.97	2.76	1.97	9.93
Cs	ICP-MS	1.7	1.8	0.3	1.1	0.8	1	1.5	1.5	1.3	1.9	0.2	0.3	1.4
Ba	ICP-MS	321	156	11	88	72	81	102	103	334	590	43	75	169
La	ICP-MS	3.78	2.66	2.75	3.01	3	2.45	2.35	2.67	2.39	15.5	19.9	24.2	8.75
Ce	ICP-MS	9.53	6.8	7.36	7.62	7.78	6.71	6.76	7.14	6.26	42.6	57.7	68.4	19.4
Pr	ICP-MS	1.458	1.07	1.15	1.168	1.175	1.029	1.078	1.084	0.946	6.457	8.704	10.25	2.508
Nd	ICP-MS	8.07	5.79	6.46	6.39	6.86	5.91	6.37	6.34	5.55	37.1	48.8	56.8	12.5
Sm	ICP-MS	2.64	1.9	2.21	2.06	2.26	2.1	2.19	2.24	2.06	12.2	16.1	18.7	3.33
Eu	ICP-MS	0.925	0.762	0.821	0.831	0.816	0.785	0.789	0.798	0.714	3.544	3.421	3.917	0.93
Gd	ICP-MS	3.35	2.59	3.06	2.62	2.77	2.64	2.75	2.72	2.39	14.8	19	22.6	3.12
Tb	ICP-MS	0.68	0.5	0.62	0.51	0.55	0.54	0.56	0.57	0.49	2.87	3.89	4.68	0.52
Dy	ICP-MS	4.32	3.21	3.95	3.15	3.57	3.47	3.53	3.62	3.02	17.6	24.7	29.3	2.84
Ho	ICP-MS	0.93	0.67	0.87	0.64	0.76	0.75	0.79	0.79	0.66	3.74	5.47	6.34	0.57
Er	ICP-MS	2.75	1.96	2.66	1.92	2.26	2.23	2.33	2.36	1.96	10.9	16.6	19.4	1.59
Tm	ICP-MS	0.427	0.303	0.415	0.289	0.35	0.358	0.373	0.376	0.299	1.658	2.668	3.1	0.218
Yb	ICP-MS	2.83	1.93	2.77	1.88	2.25	2.33	2.41	2.46	2.01	10.6	17.3	20.1	1.37
Lu	ICP-MS	0.421	0.296	0.419	0.268	0.346	0.362	0.378	0.371	0.299	1.59	2.551	3.016	0.204
Hf	ICP-MS	1.6	1.4	1.8	1.6	1.3	1.3	1.3	1.4	1.2	6.3	14	16	0.7
Ta	ICP-MS	0.14	0.13	0.15	0.14	0.13	0.11	0.12	0.12	0.11	0.65	1.13	1.29	0.05
W	ICP-MS	3.8	1.3		2.2	1.9		0.7		23	38	256	29	4.3
Tl	ICP-MS	0.28	0.38		0.23	0.19	0.17	0.3	0.25	0.36	0.48	0.06		0.2
Pb	ICP-MS													
Bi	ICP-MS					0.1						0.43	0.06	
Th	ICP-MS	0.26	0.23	0.28	0.23	0.23	0.19	0.19	0.2	0.2	1.05	5.12	2.65	0.09
U	ICP-MS	0.08	0.06	0.08	0.08	0.07	0.06	0.06	0.07	0.05	0.31	1.62	0.75	
Au	INAA			26				15	25	45	1410	363	12500	43

SAMPLE	415-14	415-15	415-16	415-18	415-19	415-21	415W-101	430-10	430-11	430-12	430-13	430-14	430-15	430-16	430-17
type	u/m	var	Fe-thol	var	var	var	3D-CG	thol	thol	thol	thol	Fe-thol	Fe-thol	Fe-thol	Fe-thol
density	3.04	2.97	2.94	2.87	2.88	2.82	2.96	2.93	2.89	2.94	2.94	2.99	2.93	2.97	3.08
SiO_2	31.56	50.16	55.36	66.63	65.13	68.93	27.89	42.75	44.95	38.15	38.22	46.62	49.37	52.06	38.93
Al_2O_3	5.95	13.91	10.02	10.08	9.39	8.15	7.1	10.86	13.48	13.09	9.68	13.09	9.81	10.39	10.86
Fe_2O_3T	8.19	13.95	11.49	7.01	7.96	6.69	8.77	10.54	13.1	12.35	11.34	14.43	9.63	10.57	16.67
FeO	7.53	16.63	10.26	6.92	8	7.42	7.12	9.13	10.6	10.58	9.3	12.76	10.02	9.4	15.51
Fe_{sol}	4.04	1.60	6.70	4.25	3.90	2.32	5.27	5.86	7.88	7.51	6.96	8.41	5.13	6.24	9.32
MnO	0.2	0.07	0.25	0.13	0.14	0.11	0.26	0.17	0.25	0.37	0.2	0.24	0.19	0.17	0.35
MgO	13.21	0.58	1.4	0.9	1.19	1	13.6	5.22	3.87	5.55	6.2	2.51	1.83	1.95	2.11
CaO	11.94	1.79	4.29	3.19	4.38	2.93	14.84	10.04	8.14	9.6	12.79	5.07	8.25	6.21	8.13
Na_2O	0.26	7.87	3.05	3.34	4.35	4.56	1.12	1.48	3.03	1.52	1.07	1.87	4.54	3.46	0.82
K_2O	0.9	0.54	1.45	1.28	0.7	0.34	0.08	0.93	0.65	1.49	1.21	1.76	0.61	1.23	2.86
TiO_2	0.35	0.66	1.4	0.49	0.49	0.42	0.58	0.93	1.25	1.19	0.88	1.62	1.15	1.29	1.72
P_2O_5	0.03	0.12	0.6	0.09	0.1	0.08	0.16	0.08	0.09	0.07	0.08	0.57	1.09	0.46	0.74
LOI	26.4	9.07	9.92	6.4	7.12	5.97	24.44	16.29	11.96	15.25	18.91	11.36	12.04	10.97	15.49
TOTAL	98.99	98.71	99.22	99.53	100.95	99.17	98.84	99.29	100.75	98.62	100.57	99.12	98.51	98.76	98.67
H_2O	0.9		0.8	0.7			3	2.3	2.9	3	2			0.7	
CO_2	26.3	2.4	9.9	6.4	6.3	4.3	23	15	10.1	13.9	18.7	11	12.1	11.8	15.2
S	0.04	10.4	0.93	0.78	1.5	2.55	0.03	0.07	0.12	0.21	0.23	1.48	2.11	0.18	2.29
Sc	20	16	29	14	12	12	16	35	50	47	37	34	25	28	36
Be			1	1			1		2	2	1	1			2
V	124	16	13	7	12	14	84	250	358	360	243	41	29	31	50
Cr	1351	12	15	14	12	11	307	97	96	85	67	36	30	37	
Co	57	6.4	15	2.3	1.8	2	32	35	41	48	35	24	14	17	15
Ni	683	19					181	98	51	70	72				
Cu	11				15	34	10	100	81	109	140	21	17	17	22
Zn	52	66	40	56	58	33	34	81	54	70	66	97	64	85	81
Ga	8	29	21	25	22	15	10	14	15	17	13	25	18	20	27
Ge	0.8	0.9	1.2	1.4	1.5	1.1	1.2	1.6	0.9	1.3	1.4	1.6	1.2	1.2	1.1
As	1274	14	401	59	23	284		7	9	14	6	210	146	16	1473
Rb	27	8.8	31	30	10	6.4	1.7	30	14	49	29	48	17	33	64
Sr	323	145	83.7	78.5	82.3	118	381	1150	114	91.4	4093	154	184	147	190
Y	8.6	243	58	146	147	109	15	22	22	22	17	81	57	58	79
Zr	22	713	139	464	462	352	24	49	45	46	46	195	149	161	177
Nb	0.8	30	7.3	18	18	15	6.6	2.2	2.1	2	2	9.5	7.3	7.8	9.3
Mo	0.2	0.5	0.6	2.4	2.6	1.4		0.2		0.2	0.4	1.2	1.3	0.7	1.4
Ag															
In		0.1		0.1	0.2										
Sn		0.7	0.8	2	1.9	0.9				0.5		1.2	2.5	0.8	1.2
Sb	10.3	0.24	3.66	1.64	2.11	3.65	4.72	20.6	5.9	7.86	17.1	8.22	5.7	7.32	2.97
Cs	0.6	0.2	0.6	0.6	0.3	0.2	0.2	1.4	0.6	1.5	1.3	1.7	0.4	0.9	1.2
Ba	139	71	251	195	75	42	1,590	93	54	193	99	164	72	108	320
La	1.93	35.9	9.92	24.6	20.3	20.8	34.3	3.31	3.28	3.27	4.31	14.9	10.9	9.49	14
Ce	4.3	97.6	26	66.3	56.8	55.1	78.9	8.48	8.61	8.59	9.77	40	29.3	27	38.5
Pr	0.595	14.16	3.965	9.526	8.411	7.826	9.812	1.269	1.333	1.291	1.287	5.868	4.42	4.162	5.912
Nd	3.35	79.1	23.4	52.5	46.8	43.2	45	7.39	7.59	7.38	6.74	33.2	25.2	24.2	33.9
Sm	1.06	25.5	7.68	17.1	16	13.5	7.89	2.64	2.56	2.63	2.36	10.8	8.29	8.38	11.1
Eu	0.402	5.371	2.497	3.647	3.624	2.893	1.793	0.958	0.948	1.019	0.817	3.461	2.8	2.807	3.731
Gd	1.29	31.7	9.39	20.3	19.6	15.4	5.44	3.21	3.13	3.15	2.71	12.8	9.51	9.56	13
Tb	0.25	6.52	1.79	4.09	4.05	3.12	0.63	0.65	0.63	0.64	0.54	2.43	1.81	1.81	2.46
Dy	1.54	41.6	10.9	26.1	25.6	19.7	2.95	4	3.99	3.93	3.32	14.8	10.9	11.1	14.7
Ho	0.33	8.99	2.29	5.65	5.6	4.21	0.47	0.87	0.86	0.86	0.7	3.17	2.25	2.38	3.08
Er	0.99	27.3	6.59	17	16.8	12.8	1.3	2.6	2.62	2.53	2.04	9.16	6.65	6.87	9.17
Tm	0.151	4.334	0.994	2.745	2.62	2.042	0.151	0.407	0.401	0.4	0.317	1.41	1.032	1.052	1.374
Yb	0.98	27.8	6.48	17.8	16.7	13.2	0.88	2.67	2.61	2.54	2.14	9.04	6.46	6.88	8.6
Lu	0.147	4.14	0.975	2.668	2.483	1.948	0.123	0.403	0.389	0.393	0.316	1.365	0.948	1.037	1.304
Hf	0.7	21	4.2	14	14	10	0.7	1.5	1.4	1.4	1.4	5.7	4.3	4.7	5.2
Ta	0.05	1.73	0.43	1.16	1.11	0.86	0.52	0.14	0.12	0.12	0.12	0.54	0.42	0.44	0.54
W	3.9	140	17	18	12	16	1.8	0.7		4.7	1	28	13	51	49
Tl	0.16		0.15	0.16	0.07		0.05	0.22	0.08	0.37	0.19	0.22	0.09	0.21	0.27
Pb		8													
Bi	0.09				0.1	0.06				0.06		0.06	0.06		0.06
Th	0.14	3.6	0.68	2.43	2.45	1.67	3.5	0.22	0.2	0.19	0.22	0.88	0.66	0.71	0.78
U		1.51	0.21	0.72	1.96	0.47	0.48	0.06	0.08	0.06	0.06	0.26	0.19	0.21	0.23
Au	13	12500	995	181	170	10700	8	18			12	292	250	76	603

SAMPLE	430-18	430-19	430-20	430-21	430-22	430W-100	445-02	445-03	445-04	445-05	445-06	445-07	445-08	445-09	465-100
type	var	var	var	var	u/m	3D-CG	thol	thol	thol	thol	Fe-thol	Fe-thol	var	var	var
density	2.79	2.76	2.79	2.84	3.00	3.03	2.91	2.98	3.04	3.04	2.99	3.10	2.75	2.80	2.72
SiO_2	67.18	64.82	67.4	63.21	31.08	30.15	47.85	44.14	39.13	43.6	51.75	43.75	71.71	66.89	77.11
Al_2O_3	9.64	12.67	9.51	11.41	6.3	7.54	13.51	12.74	10.54	13.26	9.6	16.29	9.46	10.18	7.5
Fe_2O_3T	6.19	5.49	6.5	5.72	8.51	8.41	12.76	11.33	10.92	9.13	12.02	15.33	3.08	6.49	4.55
FeO	7.06	7.38	7.62	4.74	7.32	6.81	10.27	9.52	9.77	7.94	11.37	12.8	2.81	6.4	4.82
Fe_{soln}	2.23	1.60	1.92	3.17	3.26	4.88	8.16	7.07	6.83	4.94	7.89	9.66	2.05	3.57	2.58
MnO	0.12	0.03	0.11	0.09	0.15	0.17	0.19	0.27	0.27	0.19	0.27	0.16	0.08	0.13	0.08
MgO	0.66	1.8	0.68	1.38	17.71	11.04	4.76	4.95	4.61	4.92	1.54	1.96	1.18	0.98	0.52
CaO	3.04	2.84	2.83	4.39	8.36	15.84	6.22	8.24	11.73	9.07	6.28	6.45	3.27	3.34	2.4
Na_2O	5.64	4.22	5.6	0.45	0.29	0.21	3.91	2.74	1.33	1.58	2.23	0.38	3.14	5.44	4.18
K_2O	0.11	1.41	0.08	4.04	0.9	1.43	0.05	0.95	0.68	1.24	1.49	3.5	1.16	0.09	0.23
TiO_2	0.44	0.58	0.41	0.49	0.34	0.99	1.21	1.13	1	1.1	1.3	2.21	0.45	0.41	0.31
P_2O_5	0.07	0.07	0.15	0.09	0.02	0.37	0.1	0.07	0.06	0.08	0.56	0.96	0.08	0.07	0.09
LOI	5.83	5.29	5.62	7.44	26.95	23.82	9.17	13.32	18.49	16.58	12.16	9.37	4.98	5.35	3.8
TOTAL	98.92	99.21	98.9	98.71	100.6	99.98	99.74	99.89	98.74	100.74	99.21	100.37	98.58	99.37	100.77
H_2O				1.5	1.3	2.1	3.4	2.6	2	2.1	0.9	3.6	0.8	0.7	0.3
CO_2	4.6	4	4.1	6.6	26.3	23.4	7.2	12.3	17.8	15.2	12.8	7.5	4.7	4.8	3.9
S	2.41	2.39	3.12	0.41	0.02	0.1	0.03	0.05	0.14	0.53	0.05	0.4	0.05	0.99	0.56
Sc	12	17	13	13	22	25	47	46	40	45	26	45	13	13	7
Be		2		2	1	1	1	2	1	2	1	2			
V	10	33	13		114	203	353	321	281	282	11	18	6	8	23
Cr	22		18		1429	338	81	80	159	109			12	77	
Co	2.1	2	1.1	2.3	58	41	48	36	39	34	13	14	1.3	1.2	4.1
Ni					688	262	66	62	553	80	27				
Cu	15		34	15	43	16	90	102	72	73	32	189	26	16	
Zn	47	52	48	55	53	88	86	56	64	41	114	155	10	50	49
Ga	20	38	20	32	9	13	15	14	13	14	17	40	21	25	21
Ge	1.3	1.7	1.2	1.6	0.9	1.6	1.5	1.3	1.4	1.4	1.5	2.4	1.4	1.2	2.6
As	755	303	4118	59	1135	9			10	9	18	145	7	135	27
Rb	2.7	36	1.6	84	25	41	0.9	31	21	33	38	81	27	2.1	5.7
Sr	183	61	197	78.4	289	806	104	89.9	231	193	90.5	132	61	151	120
Y	163	200	148	173	8.1	17	21	19	18	22	60	96	137	144	107
Zr	522	687	468	556	22	80	44	40	36	51	128	212	436	459	324
Nb	20	27	18	22	0.9	11	2.1	1.9	1.9	2.3	6.9	11	17	18	15
Mo	2	1.8	1.4	1.3	0.1		0.2	0.2	1	0.1	0.8	0.6	0.9	0.8	6.9
Ag		0.6		0.5									0.6	0.7	
In		0.1		0.2								0.2	0.1	0.2	
Sn	1.7	3	1.5	3.8			0.5				1.8	2.9	2.6	2.1	1.6
Sb	3.47	4.84	3.2	3.3	26.1	10.2	7.16	7.96	18.5	8.5	8.95	5.35	1.49	2.05	5.74
Cs	0.1	0.8	0.1	1.5	0.6	1.6	0.1	1.8	1	1.2	0.8	1.6	0.4	0.2	0.2
Ba	37	247	36	532	63	308	4.4	84	74	100	138	399	132	30	70
La	29.3	38.2	27.2	38	2.28	50.6	3.14	3.1	2.01	2.98	10.4	14.2	25.4	26.7	23.2
Ce	78.6	101	73.4	95.5	5.15	106	8.15	7.84	5.82	8.23	27.9	39.3	68.4	71.3	58.4
Pr	11.18	14.17	10.59	13.18	0.713	14.1	1.231	1.187	0.983	1.298	4.28	6.105	9.827	10.29	8.203
Nd	60.5	77.3	57.3	71.8	3.67	57.4	6.96	6.5	6.11	7.5	24.5	34.9	52.4	54.6	43.5
Sm	19.3	24.1	18.4	22	1.1	9.88	2.41	2.17	2.21	2.56	7.92	13	16.3	17.2	13
Eu	4.011	4.987	3.82	4.637	0.344	2.412	0.843	0.827	0.854	0.962	2.551	3.998	3.482	3.596	2.429
Gd	22.2	27.1	21.1	24.4	1.19	6.79	2.82	2.65	2.49	3.05	9	15.6	18.8	19.6	13.8
Tb	4.49	5.63	4.26	4.95	0.23	0.67	0.56	0.54	0.49	0.61	1.69	2.83	3.72	3.87	2.67
Dy	28.1	35.9	26.5	31.1	1.44	3.22	3.63	3.43	3.19	3.87	10.4	17.3	23.8	24.8	16.9
Ho	6.16	7.75	5.73	6.74	0.31	0.52	0.77	0.72	0.67	0.85	2.15	3.55	5.17	5.35	3.45
Er	18.7	23.4	17.4	20.7	0.91	1.34	2.32	2.14	2.04	2.5	6.29	10.4	15.6	16.2	11.7
Tm	2.971	3.76	2.762	3.323	0.14	0.147	0.37	0.356	0.323	0.395	0.94	1.545	2.495	2.559	1.921
Yb	19	24.2	17.3	21.3	0.93	0.95	2.37	2.23	2.14	2.58	5.9	9.86	16	16.6	11.9
Lu	2.816	3.558	2.587	3.121	0.139	0.15	0.357	0.327	0.321	0.387	0.879	1.481	2.379	2.476	1.796
Hf	15	20	14	16	0.6	2.2	1.3	1.2	1.1	1.5	3.8	6.2	12	13	9.6
Ta	1.2	1.65	1.09	1.31	0.05	1.11	0.12	0.11	0.1	0.13	0.38	0.63	1.03	1.05	1.74
W	23	37	383	5.9	6.7	13	0.6	0.9	0.5	1.2	3.1	21	8.6	113	20
Tl		0.15		0.46	0.13	0.24		0.22	0.17	0.19	0.27	0.51	0.15		
Pb						8									6
Bi	0.1	0.08	0.07	0.05	0.09	0.08					0.06				0.11
Th	2.31	3.08	2.08	2.5	0.18	5.71	0.2	0.19	0.17	0.25	0.63	1.02	2.16	2.29	1.91
U	0.69	0.88	0.58	0.7		0.9	0.05		0.06	0.07	0.18	0.33	0.55	0.66	0.67
Au	1930	2350	4370	11	23	111					8	27		465	122

SAMPLE	465-102	465-103	465-110	485-101	485-102	485-103	485-105	485-108	485-112	485-113	485-115	485-117	485-119
type	dyke	dyke	var	Fe-thol	Fe-thol	Fe-thol	var	Fe-thol	dyke	var	3D-CG	Fe-thol	sed
density	2.91	2.88	2.85	3.05	2.78	2.98	2.79	2.89		2.80	2.93	2.92	3.03
SiO_2	23.84	33.05	64.56	52.46	53.72	43.71	63.29	59.27	33	62.42	43.94	48.09	18.29
Al_2O_3	12.65	9.75	9.82	11.35	12.16	10.58	11.32	10.69	8.71	9.17	10.08	10.3	13.8
Fe_2O_3T	8.54	8.59	7.7	13.39	10.32	14.81	7.8	9.71	7.53	8.44	10.5	18.18	10.51
FeO	6.95	7.16	8.24	11.4	3.24	13.02	8.59	8.31	6.43	8.94	9	14.71	9.14
Fe_{soln}	4.95	4.92	2.60	8.28	4.94	8.51	2.48	6.00	4.00	3.35	6.40	10.79	6.42
MnO	0.18	0.22	0.19	0.35	0.23	0.32	0.14	0.19	0.18	0.18	0.2	0.31	0.25
MgO	8.26	8.61	0.72	0.73	1.68	1.28	0.72	0.72	9.98	1.17	5.11	2.04	7.13
CaO	16.34	14.23	3.81	4.68	6.01	8.76	2.99	4.87	12.7	4.78	9.44	6.96	17.97
Na_2O	0.95	2.83	5.26	2.73	7.05	6.14	5.25	2.57	0.36	5.2	2.37	2.82	0.52
K_2O	3.98	1.21	0.36	1.87	0.06	0.08	0.89	1.8	2.78	0.08	1.12	0.06	3.34
TiO_2	0.78	0.65	0.55	1.51	1.67	1.36	0.46	1.38	0.58	0.45	0.98	1.35	0.98
P_2O_5	0.14	0.34	0.17	0.75	0.72	0.6	0.08	0.69	0.24	0.1	0.42	0.62	0.57
LOI	24.81	21.18	6.67	9.85	6.4	12.93	6.49	8.52	23.05	8.12	15.14	9.96	25.77
TOTAL	100.47	100.65	99.81	99.67	100.03	100.58	99.45	100.41	99.11	100.09	99.31	100.67	99.13
H_2O	1.8	1.6		1	0.3	0.3		1	1.7		1.8	2.8	1.9
CO_2	24.5	21.1	5.4	10.6	6.4	14.3	4.4	8.6	22.4	6.9	15	9	26.2
S	0.01	0.15	3.13	0.15	0.36	0.99	3.6	0.17	0.22	2.71	0.05	0.38	0.01
Sc	24	17	16	32	29	30	12	29	22	14	27	30	35
Be	4	4			1		1	1	4		1		2
V	135	146	15	11	12	16	12	9	127	16	107	10	182
Cr	268	235							322	40	237		764
Co	33	30	0.8	19	8.5	11	0.8	12	33	1.1	18	17	42
Ni	121	124							123		66		242
Cu	50	80	12	51	29	28		19	76	12	38	28	22
Zn	84	78	39	305	53	58	32	46	61	43	44	186	63
Ga	23	11	19	20	22	17	24	18	10	17	14	19	20
Ge	1.3	0.8	0.9	1.2	0.8	0.8	1	1	0.8	0.9	0.8	1.3	1.3
As	176	59	5,050	49	15	339	762	19	152	402	32	42	349
Rb	97	44	8.1	47	1.4	1.1	19	44	75	1.7	30	1.4	77
Sr	725	743	149	78.2	179	248	137	76	780	149	264	158	425
Y	17	15	159	71	79	69	180	73	18	127	54	74	23
Zr	55	71	413	149	168	134	514	156	57	339	139	146	114
Nb	14	20	17	7.9	8.4	6.5	19	7.5	21	14	6.6	6.9	7.3
Mo			1.4	0.5	1.4	1.2	0.7	0.2		5		0.2	
Ag													
In				0.1	0.1								
Sn	1.1		2.5	2.1	0.8	0.6	2.4	0.8		1.3	0.9	1.2	1.4
Sb	9.53	6.39	6.56	4.15	3.15	3.92	5.02	3.95	26	3.51	1.89	2.05	8.2
Cs	2.3	2.2	0.2	1.2	0.1		0.5	1.3	2.2		0.7	0.1	2.8
Ba	1,090	359	121	173	43	96	217	147	418	37	217	18	554
La	28.4	35.5	23.4	11.1	13.5	9.82	27.4	10.1	54.8	15.5	20.8	9.55	44.6
Ce	65.4	78.6	63.3	29.6	36.9	28	77	29.1	99.4	45.2	48.4	26.2	95.4
Pr	8.158	9.552	8.956	4.319	5.316	4.145	10.75	4.477	11.92	6.761	5.96	3.9	11.24
Nd	33.9	38.2	47.4	25.3	29.4	22.9	54.4	23.7	48.3	34.7	27.8	22.6	45.6
Sm	6.44	6.32	16	8.48	10.4	8.02	17.9	8.18	7.63	11	7.52	7.97	9.14
Eu	1.657	1.628	3.459	2.645	3.351	2.579	3.748	2.833	1.757	2.542	2.046	2.658	2.336
Gd	4.52	4.58	18.1	9.55	11.5	9.1	21.2	9.83	6.78	14.5	7.67	9.07	6.06
Tb	0.56	0.51	3.62	1.84	2.16	1.69	4.01	1.74	0.69	2.76	1.22	1.66	0.76
Dy	3.02	2.57	25	11.8	14.2	11	27.1	10.9	3.21	17.8	7.93	11.3	3.98
Ho	0.58	0.48	5.23	2.36	2.84	2.28	6.09	2.34	0.58	4.03	1.64	2.36	0.71
Er	1.67	1.38	16.5	7.34	8.59	7.15	19.2	7.19	1.66	13.4	5.06	7.2	2.05
Tm	0.206	0.185	2.436	1.096	1.193	1.031	2.871	0.989	0.213	1.957	0.731	1.046	0.256
Yb	1.34	1.17	16.8	7.04	7.74	6.88	18.7	6.35	1.27	12.3	5.06	7.15	1.71
Lu	0.24	0.196	2.613	1.072	1.17	1.042	3.017	1.012	0.202	1.963	0.785	1.09	0.252
Hf	1.8	1.8	13	4.8	5.6	4.2	16	4.6	1.4	10	4	4.4	2.9
Ta	0.72	0.71	1.05	0.52	0.67	0.53	1.25	0.52	0.56	0.88	0.38	0.43	0.4
W	23	0.8	41	20	4.2	43	21	3.4	4.5	26	3	3.1	14
Tl	0.56	0.25		0.3			0.08	0.26	0.28		0.1		0.46
Pb	7	6				7							7
Bi	0.06	0.16	0.26	0.21	0.27	0.13	0.21	0.1		0.1	0.1	0.1	0.08
Th	1.58	2.12	2.33	0.84	1	0.79	2.79	0.8	2.27	1.72	2.54	0.76	7.2
U	0.21	0.14	0.61	0.23	0.25	0.21	0.92	0.22	0.37	0.51	0.7	0.2	1.89
Au	5		1530	10	7	128	2250	7		1870	5	7	

SAMPLE	505-100	505-101	505-103	505-105	505-105B	505-106	505-107	505-108	505-109	505-110	505-112	505-113	520-101
type	dyke	var	Fe-thol	var	var	Fe-thol	Fe-thol	Fe-thol	Fe-thol	Fe-thol	var	var	Fe-thol
density	2.95	2.83	2.90		2.91	2.89	2.96	2.85	2.85	2.95	2.81	3.20	2.92
SiO_2	23.61	67.5	49.38	46.06	60.49	48.73	49.89	52.91	56.94	51.58	68.28	46.6	51.75
Al_2O_3	9.32	8.79	11.36	19.63	12.02	9.44	11.61	12.54	10.33	11.71	9.49	7.94	11.09
Fe_2O_3T	8.22	6.89	11.66	10.16	9.38	14.17	12.95	10.69	8.79	16.92	6.61	22.59	16.76
FeO	7.5	7.84	10.55	7.88	7.78	7.1	10.71	9.16	9.11	10.46	8.51	26.44	13.65
Fe_{soln}	4.82	2.89	3.19	5.19	5.73	7.61	7.58	5.88	4.65	10.21	1.87	2.13	9.98
MnO	0.2	0.16	0.2	0.12	0.18	0.33	0.2	0.14	0.14	0.18	0.14	0.16	0.3
MgO	9.37	0.98	1.46	1.32	1.05	1.13	1.27	1.53	1.03	2.42	0.73	0.94	1.75
CaO	18.15	3.65	6.68	3.51	3.56	9.86	6.12	4.91	5.56	4.45	2.8	2.95	5.66
Na_2O	0.87	4.28	6.71	4.15	0.32	5.04	2.19	6.52	6.25	5.28	5.77	4.7	3.52
K_2O	2.69	0.61	0.16	4.58	3.62	0.05	2.16	0.05	0.06	0.08	0.11	0.17	0.04
TiO_2	0.62	0.46	1.76	1.13	0.63	1.2	1.52	1.69	1.24	1.55	0.39	0.37	1.43
P_2O_5	0.15	0.09	0.72	0.17	0.19	0.54	0.71	0.87	0.51	0.6	0.19	0.21	0.64
LOI	27.06	6.9	9.03	9.34	8.19	10.15	11.59	7.48	8.65	6.04	5.62	14.04	7.9
TOTAL	100.26	100.31	99.12	100.18	99.62	100.64	100.21	99.33	99.51	100.79	100.13	100.66	100.82
H_2O	1.3				1.6	0.7	1.2	1		1.7			2.6
CO_2	27.6	5.6	5.3	4.7	8	10.2	11.7	7	8.9	5.4	3.9	4.2	7.4
S	0.02	2.25	3.56	1.17	0.27	0.81	0.14	0.76	1.1	0.5	3.74	16.6	0.09
Sc	22	12	28	27	17	29	30	31	23	33	11	11	32
Be	2			4	3		1			1			
V	98	14	32	22	6	11	14	13	16	16	19	11	13
Cr	332								22		15		
Co	32	1.5	12	2.7	2.6	14	17	23	11	20	0.9	6.9	19
Ni	136				21		77	10					
Cu	45		19	13	15	28	29	29	17	25	11		22
Zn	61	45	96	85	106	83	71	195	121	137	38	33	176
Ga	13	18	19	57	32	18	25	27	19	24	23	16	23
Ge	0.9	1.1	0.8	1.4	1.9	1	0.9	1	1	1.9	1.2		1.6
As	243	710	560	52	40	24	57	16	37	36	784	2,040	37
Rb	74	15	8.4	100	86	1.2	70	1.1	1.6	5.4	0.9	4.3	1.4
Sr	870	146	206	147	84	345	119	168	183	238	125	109	233
Y	18	157	73	276	193	63	75	78	66	75	156	157	72
Zr	48	427	209	997	521	140	167	215	153	154	480	401	163
Nb	18	17	12	38	24	7.6	11	13	8.5	9.6	22	19	10
Mo		4.4	0.3	1.3	1.1	1.2		1.4	1.2	1	6.1		0.5
Ag				1									
In				0.3	0.2			0.1					
Sn	0.7	2.1	0.8	4	3.4	0.7	1.1	1.5	0.7	0.6	1.6		1.3
Sb	10.7	5.93	4.98	5.7	6.92	3.52	3.87	4.68	4.68	4.28	5.71	0.85	1.96
Cs	1.6	0.4	0.3	1.9	1.8	0.1	1.9	0.1		0.2		0.1	0.2
Ba	740	147	61	1,070	986	40	255	39	33	25	52	30	13
La	33.5	18	11.2	50.6	28.8	7.82	10.8	11.7	8.69	9.61	22.1	21.8	10.2
Ce	68	51	29.5	127	74.7	22.5	28.9	33.2	24.6	26.9	58.6	59.4	27
Pr	8.732	7.478	4.481	18.5	10.08	3.337	4.483	5.047	3.657	3.901	8.351	8.204	4.23
Nd	36	38.4	26.2	97.1	59.5	19.1	26.7	29.8	21.2	23.2	46.9	45	25.7
Sm	5.92	13.5	7.56	29.1	18.8	6.04	7.98	8.86	6.29	7.51	13.7	14	7.85
Eu	1.384	2.922	2.397	6.488	3.836	2.203	3.049	3.073	2.288	2.733	2.825	2.945	2.673
Gd	4.24	16.8	10.9	32.8	23.9	8.29	11.1	12	8.82	10	19.5	19.5	10.5
Tb	0.57	3.16	1.96	6.5	4.64	1.54	2.04	2.08	1.57	1.82	3.83	3.69	2
Dy	2.89	20.9	11.8	43.1	30.4	9.53	12.1	12.3	9.66	11.7	22.6	23.7	11.9
Ho	0.52	4.78	2.43	9.38	6.21	2.04	2.53	2.57	2.12	2.43	4.88	5.41	2.46
Er	1.6	15.1	7.71	29.1	19	6.29	8.06	8.12	6.28	7.29	16.4	16.5	7.9
Tm	0.219	2.149	1.143	4.735	3.229	0.957	1.175	1.166	0.892	1.051	2.587	2.554	1.171
Yb	1.33	14.4	6.54	29.6	20.3	5.94	6.69	6.87	5.39	6.87	15.5	16.1	7.24
Lu	0.196	2.313	1.058	4.584	3.044	1	1.091	1.105	0.873	1.096	2.475	2.62	1.135
Hf	1.4	11	5.8	25	14	3.7	4.6	5.9	3.8	4.2	13	12	4.7
Ta	1.1	1.75	0.71	2.14	1.46	0.67	0.57	0.7	0.41	0.5	1.21	1.06	0.7
W	16	26	73	26	11	8.2	4	7.4	21	4.3	23	23	3.9
Tl	0.29	0.06		0.53	0.46		0.26						
Pb	6					6					6		
Bi	0.07	0.11	0.06		0.08	0.07	0.06		0.08	0.07	0.11	0.08	0.05
Th	1.65	2.12	0.9	4.37	2.47	0.63	0.79	0.94	0.65	0.74	2.17	2.01	0.75
U	0.29	0.56	0.29	1.18	0.65	0.17	0.24	0.28	0.22	0.2	0.65	0.57	0.21
Au		4210	11700	109	21		9	10	44		2490	46000	29

SAMPLE	520-102	520-114	520-116	520-117	520-118	520-126	520-127	520-128	520-129	520-131	520-132	550-100	550-101
type	Fe-thol	u/m	Fe-thol	Fe-thol	Fe-thol	var	var	u/m	u/m	3D-CG	Fe-thol	var	var
density	3.14		2.91	2.91	2.92	2.86	2.93			2.86	2.96	2.86	2.77
SiO_2	44.81	21.06	57.96	50.77	52.53	58.58	62.29	30.33	33.12	51.45	48.04	57.98	69.09
Al_2O_3	12.25	5.03	10.96	12.13	12.44	10.43	10.37	6.58	5.18	12.42	10.64	14.92	9.54
Fe_2O_3T	17.94	10.12	12.56	10.85	9.62	8.88	9.14	8.92	8.04	9.85	19.07	7.21	7.86
FeO	16.75	10.16	11.09	9.71	8.57	10.22	10.68	8.69	7.71	8.1	14.89	6.3	2.82
Fe_{sch}	7.83	4.91	7.95	6.55	6.17	2.47	1.95	4.84	4.02	5.42	11.15	3.25	4.67
MnO	0.3	0.14	0.15	0.28	0.19	0.25	0.17	0.23	0.15	0.15	0.33	0.11	0.16
MgO	1.8	24.08	1.14	1.06	1.52	1.47	0.73	13.07	20.97	6.87	3.08	1.03	0.55
CaO	4.1	3.18	4.44	7.09	5.73	4.51	2.74	11.35	6.55	6.35	6.04	3.81	3.1
Na_2O	0.38	0.54	2.58	2.64	1.93	6.07	6.1	0.07	0.06	3.33	1.46	2.91	5.79
K_2O	3.67	1.26	0.64	2.35	2.8	0.24	0.22	2.3	0.04	0.06	0.48	3.47	0.05
TiO_2	1.55	0.28	1.44	1.61	1.63	0.63	0.55	0.36	0.26	0.89	1.37	0.75	0.43
P_2O_5	0.64		0.62	0.76	0.75	0.13	0.16	0.09	2.29	0.32	0.74	0.11	0.08
LOI	13.49	32.35	6.31	10.81	10.19	8.92	6.78	26.27	24.26	8.35	9.08	7.75	3.89
TOTAL	100.92	98.04	98.81	100.32	99.35	100.11	99.26	99.58	100.9	100.04	100.32	100.05	100.53
H_2O		0.9	2.5	1.2	1.4			1.1	3.4	3.9	3.8		0.1
CO_2	10.6	33.1	5.2	11.2	9.9	6.5	3.9	27.1	22.4	5.4	7.3	5.8	4.3
S	4.82	0.07	0.15	0.18	0.14	4.75	5.36	0.03	0.03	0.2	0.25	1.72	0.14
Sc	34	21	27	32	33	17	17	23	20	29	29	17	10
Be	1	1		1	1			1		1		3	
V	21	133	12	14	15	27	20	130	103	164	15	7	6
Cr		2,290						1,410	1,870	285			30
Co	19	66	9	16	12	0.5	1.1	61	69	29	20	1.4	2.6
Ni		1,040						734	1,750	148	24		
Cu	29		23	33	29	11	12	48	44	66	44	13	28
Zn	111	33	53	143	61	105	81	43	40	142	163	54	150
Ga	28	13	18	24	24	21	22	9	5	19	21	46	19
Ge	0.9	0.8	0.7	1.1	1	0.9	1	1	0.9	1.3	1.1	1.4	1
As	348	1,860	17	45	29	390	2,130	816	529	19	22	70	10
Rb	88	41	16	55	69	5.6	4.7	63	0.8	1.2	13	89	0.9
Sr	103	142	58.5	105	94.5	148	129	398	193	215	150	138	215
Y	81	7.7	69	76	75	168	149	12	6.8	42	74	220	142
Zr	169	9.8	145	170	175	479	458	21	12	155	129	744	447
Nb	10	0.7	8.3	9.5	10	23	20	1.1		7.8	7.8	28	16
Mo	1.1			0.4	0.2	5.7	0.2			0.6	0.2	0.4	1.4
Ag							0.5					0.7	
In	0.1											0.2	0.1
Sn	1.2	1.3		1.2	0.8	1				0.8	0.6	2.7	2.3
Sb	1.24	4.31	2.1	2.94	3.09	6.25	3.02	14.2	16.4	7.69	4.64	3.4	3.4
Cs	2	0.9	0.5	1.5	1.7	0.1	0.1	1.2	0.1	0.4	0.5	1.8	0.1
Ba	583	353	74	203	260	69	74	482	5.1	18	88	707	233
La	12	0.55	11.3	11.5	11.1	28.2	23	1.22	0.49	28	12	38.2	26.1
Ce	31.8	1.35	31.2	32.6	31.3	72	61.4	3.04	1.29	63.3	30.8	94.6	64.9
Pr	4.674	0.207	4.619	4.73	4.719	9.866	8.993	0.439	0.201	7.412	4.273	13.87	9.69
Nd	28.4	1.43	27.2	28.9	27.7	57.1	51.1	2.81	1.36	35.4	25.9	71.3	49.4
Sm	9.08	0.49	8.2	9.08	8.44	17.7	14.7	0.99	0.56	7.6	8.04	21.8	15.2
Eu	2.586	0.122	2.773	3.104	2.978	3.638	3.153	0.441	0.215	1.968	2.727	4.571	3.184
Gd	11.2	0.8	11	11.7	11.7	22.8	19.8	1.44	0.77	8.3	10.6	25.7	17.5
Tb	2.15	0.19	1.91	2.1	2.01	4.46	3.74	0.28	0.16	1.26	1.93	5.19	3.39
Dy	14	1.31	11.6	13.1	12.1	29	23.4	1.83	1.19	7.25	12.7	33.4	21.7
Ho	2.75	0.28	2.45	2.62	2.56	5.92	5	0.39	0.24	1.52	2.59	7.26	4.7
Er	8.24	0.85	7.33	7.64	7.61	18.6	16.7	1.21	0.71	4.64	7.6	22.6	14.2
Tm	1.272	0.133	0.998	1.07	1.034	2.903	2.526	0.185	0.11	0.654	1.116	3.655	2.288
Yb	8.48	0.88	6.21	7.12	6.57	18.6	15.4	1.14	0.7	4.04	6.87	23	14.3
Lu	1.268	0.123	0.998	1.085	1.026	2.859	2.513	0.183	0.116	0.684	1.095	3.524	2.216
Hf	5	0.4	4.3	4.9	4.9	14	13	0.7	0.4	4.5	3.8	20	12
Ta	0.58	0.04	0.5	0.57	0.55	1.37	1.38	0.07		0.46	0.46	1.61	0.95
W	35	7.8	1.3	7.5	6	40	29	7.7	1.3	0.6	1.3	14	6.6
Tl	0.28	0.11		0.34	0.7			0.22			0.07	0.31	0.05
Pb				5						6			
Bi	0.22	0.15	0.13	0.15	0.22	0.12	0.07	0.11	0.06	0.25	0.1		
Th	0.82	0.07	0.7	0.8	0.82	2.21	2.15	0.14		3.42	0.68	3.29	2.02
U	0.22		0.2	0.22	0.22	0.72	0.95			0.94	0.19	0.9	0.53
Au	2800	65	24	39	54	9760	3790	11	20	15	15	720	